frontiers | Frontiers in Nuclear Engineering

TYPE Review
PUBLISHED 18 July 2024
DOI 10.3389/fnuen.2024.1404739

OPEN ACCESS

EDITED BY
Bernd Grambow,
UMR6457 Laboratoire de Physique Subatomique et des Technologies Associées (SUBATECH), France

REVIEWED BY
Markus Olin,
VTT Technical Research Centre of Finland Ltd., Finland
Tadeja Kosec,
Slovenian National Building and Civil Engineering Institute, Slovenia

*CORRESPONDENCE
Nikitas Diomidis,
nikitas.diomidis@nagra.ch

RECEIVED 21 March 2024
ACCEPTED 10 June 2024
PUBLISHED 18 July 2024

CITATION
Muñoz AG, Abdelouas A, Alonso U, Fernández AM, Bernier-Latmani R, Cherkouk A, Gaggiano R, Hesketh J, Smart N, Padovani C, Mijnendonckx K, Montoya V, Idiart A, Pont A, Riba O, Finck N, Singh AR, King F and Diomidis N (2024), WP15 ConCorD state-of-the-art report (container corrosion under disposal conditions). *Front. Nucl. Eng.* 3:1404739.
doi: 10.3389/fnuen.2024.1404739

WP15 ConCorD state-of-the-art report (container corrosion under disposal conditions)

Andrés G. Muñoz[1], Abdesselam Abdelouas[2], Ursula Alonso[3], Ana María Fernández[3], Rizlan Bernier-Latmani[4], Andrea Cherkouk[5], Roberto Gaggiano[6], James Hesketh[7], Nick Smart[7], Cristiano Padovani[7], Kristel Mijnendonckx[8], Vanessa Montoya[8], Andrés Idiart[9], Arnau Pont[9], Olga Riba[9], Nicolas Finck[10], Ashutosh R. Singh[10], Fraser King[11] and Nikitas Diomidis[12]*

[1]GRS, Braunschweig, Germany, [2]SUBATECH, Nantes, France, [3]CIEMAT, Madrid, Spain, [4]Environmental Microbiology Laboratory, EPFL, Lausanne, Switzerland, [5]HZDR, Rossendorf, Dresden, Germany, [6]Ondraf/Niras, Brussels, Belgium, [7]Jacobs, Oxford, United Kingdom, [8]SCK CEN, Mol, Belgium, [9]Amphos 21, Barcelona, Spain, [10]KIT-INE, Karlsruhe, Germany, [11]Integrity Corrosion Consulting Ltd., Nanaimo, BC, Canada, [12]Nagra, Wettingen, Switzerland

A sealed container for the geological disposal of spent nuclear fuel and vitrified high-level waste is the only component of a deep geological repository that provides complete containment of radionuclides. As such, attention is focused on its lifetime. The lifetime of the container is influenced by material degradation processes during disposal and is typically of the order of several millennia and, for some container materials, up to one million years. Designing, manufacturing, and predicting the performance of containers over such long periods requires an in-depth understanding of their material properties, fabrication processes, and degradation mechanisms. Scientific and technological progress can improve both the performance of containers and the robustness of lifetime predictions. Optimization of these aspects is of primary importance for many national radioactive waste disposal programs. In this article, the state of the art of complex coupled degradation processes, as well as the optimization potential of novel container materials, is presented. Furthermore, the existing tools allowing the prediction of long-term barrier integrity are discussed.

KEYWORDS

nuclear waste containers, disposal canisters, corrosion, radiation, microbiologically influenced corrosion, lifetime prediction

1 Introduction

A sealed container (or canister) for the disposal of high-level radioactive waste (HLW) and spent fuels (SF) is a key component of all deep geological repository programs. The container constitutes the only barrier within the overall multi-barrier disposal system that provides complete confinement of radionuclides. Therefore, attention is frequently focused on the performance of the canister, especially concerning the length of time during which the material stability and, thus, the barrier function can be guaranteed.

Preestablished lifetime requirements can vary significantly between the different national programs. They are typically linked to the type of waste, the selected canister

TABLE 1 Canister concepts and illustrative environmental conditions for various WMO repository designs.

WMO	Canister concept	Estimated or target lifetime (a)	Nominal buffer dry density (g/cm^3)	Max canister temperature (°C)	Time to full near-field saturation (a)	Maximum surface absorbed dose rate (Gy/h)	Expected mechanical loads (MPa)
SKB (SE)	Copper–cast iron	>10^6	1.6	95	Few tens to a few thousand	0.2	15 50 (glacial)
Posiva (FI)	Copper–cast iron	>10^6	1.55	95	Few tens to a few thousand	0.3	14 50 (glacial)
Andra (FR)	Carbon steel	>500	No buffer	90		10	
Ondraf-Niras (BE)	Carbon steel	Several thousand	Cementitious buffer	100	5–10 up to a few thousand	25	8
Nagra (CH)	Carbon steel	10^4	>1.45	~120	A few centuries	0.2	22–29 max
SURAO (CZ)	Carbon steel	10^4	1.4	95	100	0.3	20
NWMO (CA)	Copper-coated steel	>10^6	1.6	85	50–5,000, depending on host rock type	0.8	15 45 (glacial)
NUMO (JP)	Carbon steel	>10^3	1.6	100	<1,000 Host-rock dependent	0.006–0.011	11 (hard rock)

material(s) and disposal concept, and the characteristics of the near-field and the geological environment. The failure of canisters is typically expected after the environmentally induced degradation of the materials exceeds a permissible threshold, which typically depends on the mechanical stress. In such a case, the possibility of the release of radionuclides in the near-field can no longer be excluded.

The source of stress during disposal can be residual, lithostatic, and hydrostatic pressures, the swelling of the bentonite buffer, or rock displacements. The hydrostatic loads are essentially isotropic. The other types of canister loads, on the other hand, can be unevenly distributed, generating anisotropic stress fields and shear forces. The generated stresses in the canister wall, lid, and base, including the seal joint region, must remain under the failure limit for the expected canister lifetime by an adequate margin. This is typically demonstrated by structural assessments that consider the strength and fracture toughness of the canister material(s), the maximum conceivable size of manufacturing defects, and the evolving disposal environment.

The reduction of the wall thickness by environmentally induced corrosion is an important input to the structural analysis for some canister concepts. As the thickness reaches a critical value, stresses can lead to plastic collapse. The intrinsic material properties can also be altered by hydrogen uptake, neutron embrittlement, or preferential leaching/dissolution, which often leads to a reduction of the fracture toughness and a larger risk of mechanical failure.

An overview of the currently planned container concepts by various waste management organizations (WMO) and their expected exposure conditions is shown in Table 1. Copper (e.g., Sweden, Finland, Canada, Korea, Taiwan) and carbon steels (e.g., Belgium, France, Switzerland, Czechia, Japan, Slovakia, Hungary) are the container materials that have been traditionally considered for the disposal of SF/HLW in countries with advanced disposal programs. The feasibility of containers made from these materials has been demonstrated, and the required manufacturing technology is available and mature.

The required prediction of the degradation rate needs a precise knowledge of the corrosion mechanism under the environmental conditions created in the canister's near-field environment after sealing the disposal area. This includes the long-term alteration of the physicochemical properties of the environment caused by chemical-geological activity, radiolysis, and microbial activity.

While steels provide a strong solution for this application, corrosion under anoxic conditions yields hydrogen gas, which moves away from the canister surface by mass-transport processes through both the engineered barriers of the repository and the geological barrier. If the rate of generation is higher than the rate of mass transport, the gas can accumulate to the point of creating overpressure. In order to provide alternative solutions to the use of steels for containers and thus limit the production of hydrogen in the long term, alternative materials to non-alloy steels have been studied in recent years in different countries. One of the difficulties lies in achieving equivalent or better properties than steels to meet the requirements for the concerned components.

As is the case for traditional canister materials, alternative materials for nuclear waste containers should guarantee sufficient resistance to localized corrosion (e.g., stress corrosion cracking of welds). In this context, the choice of the material and the production route for the canister are very important. Chemical compatibility with all other components, including waste, must also be part of the formulation/manufacturing requirements. Recent developments

(e.g., copper coatings) considered in Canada and investigated in Switzerland (Holdsworth et al., 2018), France, and Japan have demonstrated that container optimization is indeed possible. Further alternative and novel container materials are also under consideration (e.g., steels with more controlled composition, Cu-based alloys and composites, ceramics, and Zr alloys) (Holdsworth, 2013; Baroux and Martin, 2016).

The aim of this article is to summarize the state of the art on the research targets of EURAD WP15 ConCorD, which were based on a previous review (Padovani et al., 2017). These targets are:

- to assess the corrosion mechanisms of traditional canister materials (i.e., carbon steel and copper) in complex disposal scenarios where the corroding environment is under the influence of irradiation (Section 2), temporal changes of the near-field environment (Section 3), or microbial activity (Section 4)
- to assess the potential of novel materials for optimization of the canister performance (Section 5), and
- to integrate experimental evidence on canister degradation into the prediction of container corrosion and lifetime assessment (Section 6).

2 Effects of irradiation

2.1 Effects of irradiation on the corrosion of carbon steel containers

The corrosion rate of carbon steel under disposal conditions depends on several factors, such as temperature, pH, the composition of solution and gas phases, and irradiation. The nature of the oxide phases formed on the surface can be influenced by changes in the corrosion potential (E_{corr}) due to water radiolysis products. Most of the studies concerning corrosion under irradiation found in the literature report the formation of a passivating film constituted of magnetite and hematite. Some other phases, such as lepidocrocite and goethite, are also reported, likely due to local oxidizing conditions related to radiolysis radicals and species. The corrosion rate often increases under radiation, which is ascribed to the presence of water radiolysis products. However, quite high dose rates in the kGy h^{-1} range are necessary to show corrosion enhancement. Several studies report that the corrosion rate, after an initial increase, returns to the same value as measured in unirradiated experiments (Nelson et al., 1983; Smart et al., 2008). This can be explained in terms of the formation of a protective corrosion film.

2.1.1 Effect of steel composition and microstructure

In their review of radiation effects on the corrosion of candidate container materials for the disposal of HLW, Shoesmith and King (1999) compared the results of corrosion experiments using several types of steel. They concluded that, except for low chromium and low molybdenum steels, the composition and microstructure of the steel do not seem to affect the corrosion rate under irradiation. The presence of impurities or welding induces localized corrosion (Ahn and Soo, 1995).

2.1.2 Effect of temperature

Temperature can play a major role by increasing the corrosion rate in aqueous media. An increase in temperature increases the rate of chemical and electrochemical reactions involved in the corrosion process. Moreover, temperature modifies the rate of diffusion processes and the solubility of the corrosion products (Kursten et al., 2003; Konovalova, 2021).

Gray (1987) observed an increase in the corrosion rate with temperature when studying the corrosion of mild steel in salt brines under gamma radiation at 75°C and 150°C. These results, however, do not distinguish between the contributions of temperature and irradiation.

Winsley et al. (2011) studied the corrosion of carbon steel in a deaerated alkaline solution (pH ~13.4, $[O_2]$ < 10 ppm) under gamma radiation at a dose rate of 25 Gy h^{-1}. The initial corrosion rate at 80°C is higher than at 25°C but decreases more rapidly at 80°C than at 25°C. The appearance of the oxide formed on the samples changes between 25°C and 80°C (magnetite). The irradiation, however, does not appear to modify the appearance or the composition of the corrosion products formed.

Daub et al. (2011) and Daub et al. (2019) studied the effect of temperature (25°C–150°C) on the corrosion of steel immersed in deaerated water with $pH_{25°C}$–7 or adjusted to 10.6 with LiOH ($[O_2]$ < 1,000 ppm). They used a ^{60}Co gamma source with a dose rate of 6.2 kGy $h^{-1,}$ and samples were irradiated for 20 h or 66 h (~12–41 kGy). They showed that, compared to irradiation, the temperature has little influence on the corrosion potential and, hence, on the nature of the corrosion products formed. It may, however, determine the amount of corrosion products and the oxide layer thickness. These results are in line with the study by Čuba et al. (2011), who irradiated carbon steel plates immersed in deaerated deionized Millipore water or synthetic granitic water (pH of ~6.3 and ~6.9 respectively) at 25°C, 50°C, and 70°C. The dose rate was 0.22 kGy h^{-1}, and the total dose ranged from 0 kGy to 120 kGy. They observed an increased quantity of dissolved iron in solution with increasing temperature, indicating a higher dissolution rate of iron.

2.1.3 Effect of the composition of test solution

Upon exposure to radiation, the vapor or aqueous phase decomposes into oxidizing and reducing species that can influence the corrosion processes. The nature and concentration of the radiolytically produced species (radicals or molecular products) depend on the environment. Beyond the iron ions, various inorganic ions present in groundwater, such as carbonates, magnesium, calcium, or chlorides, can act as scavengers for radiolysis products. The solution composition might, therefore, impact the corrosion behavior of steel under irradiation. Marsh and Taylor (1988), for instance, measured a higher corrosion rate in seawater than in granitic water.

Smart et al. (2008) studied the anaerobic corrosion of carbon steel in two synthetic waters (modified Allard groundwater and bentonite-equilibrated groundwater) and observed in both cases an increase of the corrosion rate with radiation: 30 times higher for the Allard water and 10 to 20 times higher for the bentonite water than unirradiated controls. In contrast to the Allard groundwater with pH 8.8, the bentonite groundwater (pH 10.4) has a simpler composition but has a high concentration of chloride and

sodium and also contains carbonates. The lower increase in the corrosion rate for the bentonite groundwater was attributed to its higher ionic strength and initial pH.

Daub et al. (2011) studied the effect of gamma radiation (6.2 kGy h^{-1}, total doses of ~12–41 kGy) on the corrosion of carbon steel as a function of the pH. They observed that when the carbon steel samples were irradiated at 150°C in either LiOH ($pH_{25°C}$ 10.6) solution or distilled water ($pH_{25°C}$ ~7), pH had no impact on the nature of the formed oxides but did affect their crystallinity. At mildly basic pH, the layer formed is uniform and compact. This contrasts with the layer formed at neutral pH, which is non-uniform and porous. The authors attributed this to the influence of the pH on the iron solubility, which can alter the rates of the reactions forming the oxide, thereby affecting its crystallinity and overall protective ability.

Among the radiolytic species produced by water radiolysis, H_2O_2 plays a key role in controlling carbon steel corrosion under radiation. Daub et al. (2010) also compared the gamma radiation effect on corrosion with that of the addition of H_2O_2. They demonstrated that the H_2O_2 concentration can change the nature of the corrosion products formed. While irradiation transforms maghemite into magnetite, the reaction is reversed toward maghemite with $[H_2O_2] < 10^{-3}$ mol L^{-1}. At H_2O_2 concentrations higher than 10^{-3} mol L^{-1}, however, magnetite and maghemite transform into lepidocrocite. This study indicated that under the experimental conditions (i.e., room temperature and pH of 10.6), the corrosion rate of carbon steel in a γ-radiation environment can be predicted from the dependence of the corrosion potential on $[H_2O_2]$.

Vandenborre et al. (2013) also pointed out the role of hydrogen peroxide in the corrosion of carbon steel by showing similar results in the corrosion induced by the $^4He^{2+}$ water radiolysis (22 kGy) and by addition of H_2O_2 by comparable volumetric concentration (10^{-4} mol L^{-1}), which resulted in the formation of lepidocrocite among other products. An inhibition effect of H_2 in the corrosion process is also underlined, as well as a potential role of O_2 species.

2.1.4 Effect of relative humidity

With regards to the impact of the gas phase radiolysis on carbon steel, Brehm (1990) showed that, in an air/steam mixture, the irradiation effect on the corrosion rate of low-carbon steel at 150°C is very limited but increases significantly (factor of ~10) at 250°C.

Lapuerta et al. (2006) and Lapuerta et al. (2008) studied atmospheric iron corrosion under proton irradiation (3 MeV, 10 nA) as a function of the relative humidity (RH) and under several gas phases (N_2 with O_2 or H_2O or both). Their results indicate that, in their experimental conditions, the coupled action of H_2O and O_2 is necessary for the formation of an iron oxide layer because no iron oxidation was observed in the absence of one of the species. Moreover, corrosion starts at lower RH values (<20%) under irradiation than without (60%). A maximal corrosion rate was observed for a RH of 45% against 95% or higher without irradiation. A layer of water on the surface of the iron is necessary to induce atmospheric corrosion. It forms from an RH of 40%–60% without radiation. Irradiation allows this layer to form at lower RH, particularly via the formation of $H^+(H_2O)_n$ clusters.

2.1.5 Effect of the radiation source

The main effect of the radiation source is to change the radiolysis products. The production of the primary products relies on the type of radiation, while their concentration depends on the linear energy transfer (LET). This concept corresponds to the energy loss by unit length in the irradiated medium and depends on the energy and type of radiation. High LET radiation (heavy ion radiation) has a high production of molecules and a low production of radicals, while low LET radiation (ionizing radiation) tends to produce more radicals (Mendoza, 2017).

2.1.6 Effect of the total dose and dose rate

There appears to be some correlation between steel corrosion rates and the dose rate, but this effect is limited in time, and corrosion rates often evolve toward those of unirradiated steel coupons after a few months.

Gray (1987) observed that at 75°C, the corrosion potential and corrosion rate of mild steel in salt brines increase as the dose rate increases. After 3 weeks of irradiation, the corrosion rate for a dose rate of 2.6 kGy h^{-1} was three times larger than that measured for a dose rate of 240 Gy h^{-1} (from 73 μm a^{-1} to 220 μm a^{-1}).

Marsh and Taylor (1988) observed a similar tendency while irradiating carbon steel in synthetic seawater at dose rates of 3 Gy h^{-1}, 35 Gy h^{-1}, and 1,000–1,500 Gy h^{-1} at 90°C. The corrosion was accelerated when the radiation dose rate was increased: at 35 Gy h^{-1}, the measured corrosion rate was ~8 times higher than that for a non-irradiated sample and ~20 times greater for the highest dose rate applied. For a dose rate of 1,000–1,500 Gy h^{-1} and after a period of 100 days, a stabilization or even a decrease of the corrosion rate was observed. It is interesting to note that a negligible increase in the corrosion rate at a dose rate of 3 Gy h^{-1} was observed (Marsh and Taylor, 1988). A similar effect was observed by Crusset et al. (2017) for 20 Gy h^{-1} dose rate irradiation in anoxic conditions.

The variation of the corrosion rate under irradiation with time was also reported by Smart et al. (2008), who compared the corrosion of carbon steel at dose rates of 11 Gy h^{-1} and 300 Gy h^{-1} in anoxic Allard water at 30°C and bentonite-equilibrated water at 50°C. In both media, gamma radiation increases the anaerobic corrosion rate of steel. At 11 Gy h^{-1}, the corrosion rate decreased after about 1,000 h to finally reach the same value as for unirradiated conditions (roughly between 2,000 h and 4,000 h, Figure 1A). At 300 Gy h^{-1}, the corrosion increase lasted longer and may even have been continuous. Interestingly, the initial increase in corrosion rate seems to be less important at 300 Gy h^{-1} than at 11 Gy h^{-1}.

Westerman et al. (1983) studied the corrosion of ferrous materials at 150°C in an anoxic brine. The corrosion rates observed at 1,000 Gy h^{-1} were considerably higher than those obtained under non-irradiated conditions (by a factor of ~6). On the other hand, the corrosion rates determined at 150°C and 20 Gy h^{-1} showed an increase of the corrosion rate by a factor of 1.5–2.0 after 1 month, but no significant increase over values measured under non-irradiated conditions was observed after 3 months of exposure. Similar results were observed at dose rates of 13,000 Gy h^{-1} (Ahn and Soo, 1995) and 35,000 Gy h^{-1} (Nelson et al., 1983) in basaltic water (Figure 1B).

2.1.7 Buffer-container system

There are only a few reports on buffer-container systems under irradiation. Pusch et al. (1992) studied MX-80 bentonite in conditions close to those found in a repository. They enclosed bentonite saturated in Allard water (low salinity) in contact with carbon steel plates in the presence of both a temperature and a radiation (^{60}Co source) gradient

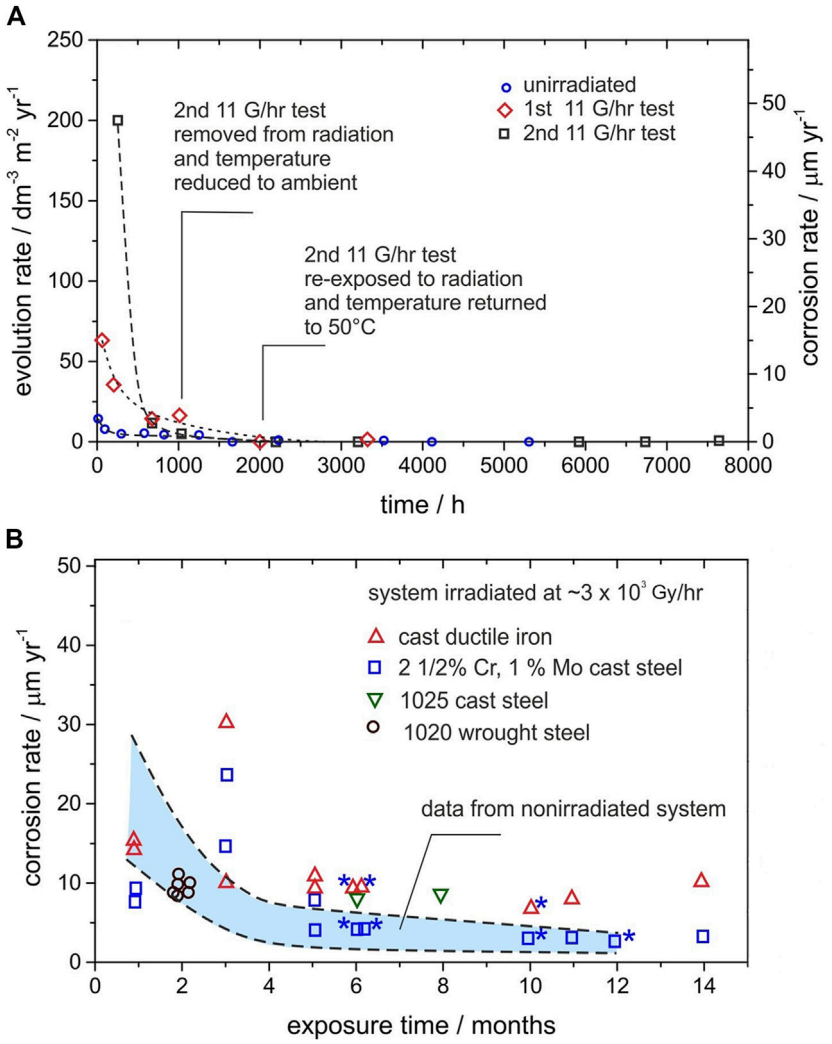

FIGURE 1
(A) Hydrogen evolution and corrosion rates of carbon steel in anoxic bentonite-equilibrated water at 50°C at 0 Gy h^{-1} and 11 Gy h^{-1}. Adapted from Smart et al. (2008). **(B)** Corrosion rates of iron-based alloys exposed to synthetic Hanford Grande Ronde basalt water at 250°C at 3 × 10^3 Gy h^{-1}. Adapted from Nelson et al. (1983).

for 1 year. The temperature ranged from 130°C in the clay area in contact with the carbon steel (highest radiation dose rate: 3.97 kGy h^{-1}) to 90°C at the opposite side in contact with stainless steel and where the irradiation dose rate was ten times lower (0.46 kGy h^{-1}). They replicated the experiment with no radiation source and extensively analyzed the clay to determine if the bentonite properties were affected by the environmental conditions. The main conclusion is that the combined effect of gamma radiation and heating causes only insignificant modifications of the smectite properties. MX-80 bentonite is mainly composed of Na-montmorillonite and, as accessory minerals, quartz, feldspars, and low amounts of calcite and opal. For the two experiments, the structure of the clay remained almost intact after 1 year. The major mineralogical alterations were the disappearance of feldspars, the formation of calcium and magnesium-bearing sulfates in the hotter part of the samples, and a slight dissolution and transformation of a 10-Å-thick sheet of minerals. A slight cementation of the clay associated with the precipitation of silicious compounds was also reported. Physical properties such as hydraulic conductivity and rheological behavior underwent only small changes, indicating that cementation effects were not very important and that the swelling capacity did not decrease significantly.

Extensive pitting corrosion was observed in steel plates after experiments with and without radiation (Pusch et al., 1992). Irradiation increased the corrosion process. An average corrosion depth of 80 µm was measured in the irradiated sample, while a depth of 18 µm could be determined in the non-irradiated steel. The pitting depth was found to be 480 µm and 160 µm for the irradiated and non-irradiated systems, respectively. Iron was released from the steel and diffused into the clay to about 10 mm depth. This iron may have participated in the cementation of the clay and in the formation of new phases.

Radiation-enhanced corrosion was also observed by Debruyn (1988), who summarized results obtained on the corrosion of several candidate container materials, including carbon steel and cast iron, under clay repository conditions. In some of the tests, samples were in direct contact with the clay, while others were in contact with interstitial clay water, a humid clay atmosphere (up to

170°C), or Antwerpian groundwater. Some tests were performed under gamma radiation (^{60}Co) with dose rates of 1 kGy h^{-1} in an inert or oxidizing atmosphere. Furthermore, they performed experiments on carbon steel in interstitial clay water and clay/clay–water mixtures at 90°C for exposure times ranging from 50 h to 1,000 h. After 40 days of irradiation, the pH of the clay remained almost unchanged, but a slight acidification was observed in oxic conditions. H_2 was produced with a yield close to the one calculated for the radiolysis of water. Concerning the steel corrosion mechanism, pitting was observed in both irradiated and non-irradiated samples with a similar penetration depth in both cases. A maximum corrosion rate of 150 μm a^{-1} was measured without radiation, whereas a value of 300 μm a^{-1} was determined under radiation in oxic conditions.

In more recent work, Liu et al. (2017) studied the corrosion of low-carbon steel in bentonite containing 17 wt.% of Beishan groundwater (Na-Cl-SO_4 type) and irradiated with a ^{60}Co gamma source with a dose rate of 2.98 kGy h^{-1} for 1,007 h (total dose 3 MGy). The same experiment was performed without radiation. Finally, samples were thermally aged at 90°C for 2,880 h. The corrosion products formed were mainly magnetite, hematite, and goethite, with the formation of two new phases under irradiation: siderite and maghemite. The distribution of these corrosion products on the surface was not uniform, and two corrosion layers were clearly observed on the samples, an inner and an outer layer, which is consistent with aerobic corrosion. Pitting was the main corrosion form observed in these experiments, with deeper pits appearing in the irradiated sample. Irradiation was indeed shown to accelerate the corrosion rate of steel by ~33%, the corrosion rate being 24 μm a^{-1} in the non-irradiated samples and 32 μm a^{-1} in the irradiated samples.

2.2 Effect of irradiation on the corrosion of copper containers

The recent literature on the effect of irradiation on the corrosion behavior of copper has been reviewed in Posiva (2021a), from which the following text is taken.

2.2.1 Radiolysis effects on copper corrosion

Because of the general lack of oxidizing species for copper in the repository, the generation of additional radiolytic oxidants is an important consideration. Figure 2 shows the enhancement factor for the rate of general corrosion for oxygen-free copper based on the results of seven different irradiation studies from various nuclear waste management programs. Under saturated conditions (i.e., in bulk solution or in saturated buffer material), an increase in the corrosion rate is only observed for absorbed dose rates greater than 20 Gy/h (Figure 2A). At lower dose rates, the observed corrosion rate is typically lower in the presence of radiation. Neither the initial degree of aeration of the solutions nor the exposure period appears to have any significant impact on the enhancement factor. Alternatively, plotting the data in terms of the total dose, Figure 2B suggests an increase in the degree of enhancement with increasing dose, with no apparent increase for absorbed doses <10 kGy. However, caution should be used in interpreting the data in Figure 2, as the various studies were not all conducted to the same total dose or for the same period of time. In addition, the absence of an observed increase in the corrosion rate may simply reflect the sensitivity of the corrosion rate measurements, although the consistent observation of a decrease in the corrosion rate for irradiation at low dose rates or low total doses does suggest the absence of any increase under these conditions.

Björkbacka and co-workers investigated the mechanism of the radiation-induced corrosion of oxygen-free, phosphorus-doped (OFP) copper in deaerated, high-purity water (Björkbacka et al., 2012; Björkbacka et al., 2013; Björkbacka et al., 2015; Björkbacka et al., 2016). Experiments were conducted at relatively high absorbed dose rates (80–770 Gy/h) and total absorbed doses similar to those predicted for a KBS-3 style canister for times up to 100 years (of the order of 100 kGy). Based on the early studies, Björkbacka et al., 2012, Björkbacka et al., 2013 reported three unexplained observations:

- the total amount of corrosion (as both precipitated oxide and dissolved copper in solution) far exceeded that predicted based on a homogeneous radiolysis/surface kinetic model,
- the dissolved copper concentrations exceeded the solubility of either Cu_2O or CuO,
- and there was evidence for localized attack in the form of circular corrosion features (local depth of penetration of 0.8 μm).

Subsequent investigations have resolved these unexplained observations (Björkbacka et al., 2016; Soroka et al., 2021). Furthermore, even though the extent of corrosion was described by the authors as significant, the maximum predicted depth of penetration for repository-relevant total absorbed doses was only of the order of 1–2 μm.

Perhaps the most significant issue of those listed above was the discrepancy between the observed extent of corrosion and the amount predicted by radiolysis modeling. For a time, this unexplained discrepancy led the investigators to suggest that an unknown process other than the radiolytic production of oxidants was responsible for the radiation-induced corrosion (Björkbacka et al., 2013; Björkbacka et al., 2015; Björkbacka et al., 2016). Experiments were conducted at relatively high absorbed dose rates (80–770 Gy/h) and total absorbance. The initial modeling attempt was based on coupling a homogeneous radiolysis model to predict the time-dependent concentrations of various radiolysis products to a kinetic expression for the rate of corrosion as a function of oxidant concentration. The only two oxidants considered were H_2O_2 and hydroxyl radicals OH•, with the latter considered to be the primary oxidant (Björkbacka et al., 2016). However, this modeling approach, which had proved successful in predicting the rate of oxidative dissolution of UO_2 (Ekeroth et al., 2006), could only account for a fraction (as little as one thousandth) of the observed corrosion. This led the investigators to suggest that the presence of a semi-conducting oxide, which was found to increase the extent of radiation-induced corrosion (Björkbacka et al., 2016), played a key role. It was suggested that irradiation of the oxide could lead to the formation of electron-hole pairs, which would lead to an increased potential difference between the (cathodic) oxide and (anodic) underlying copper. Alternatively, it was speculated that the yield (G-value) of OH• was much greater in the presence of the oxide than was assumed for the homogeneous radiolysis model. This increased yield of oxidants, along with the large effective surface area of the oxide, would result in a greater predicted degree of corrosion (Björkbacka et al., 2016).

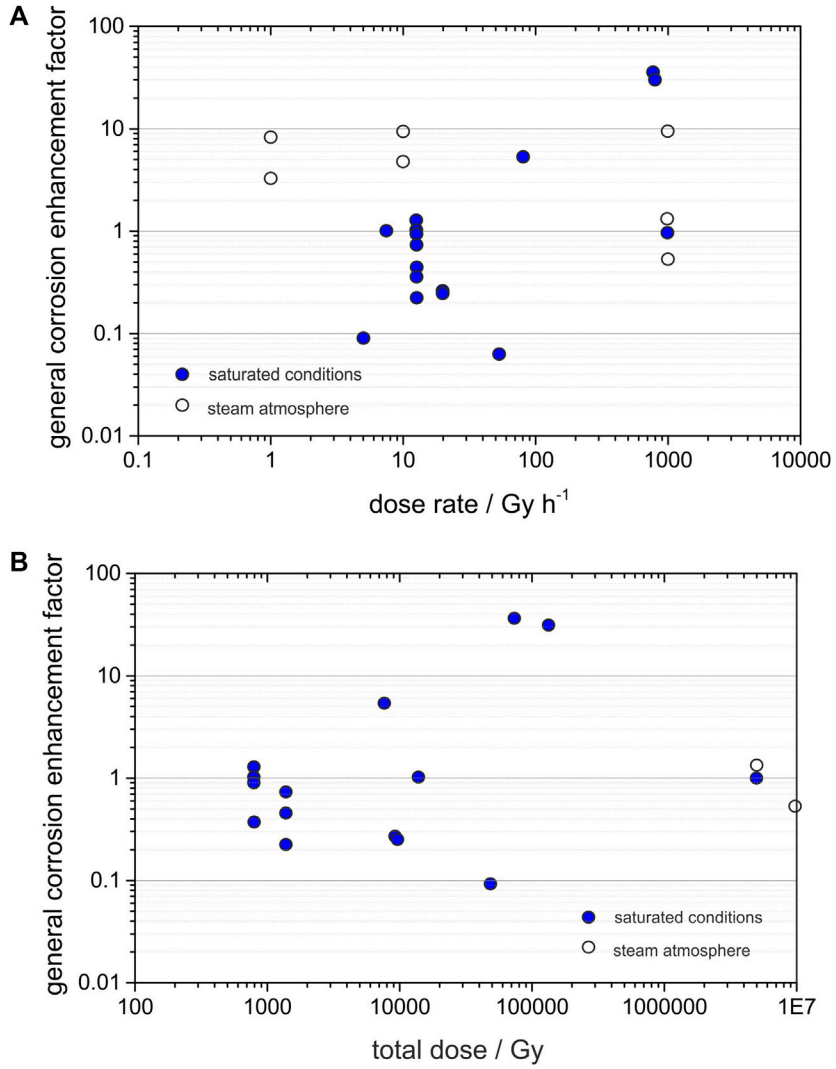

FIGURE 2
Effect of gamma irradiation on the enhancement factor of the rate of uniform corrosion of oxygen-free copper as a function of **(A)** dose rate and **(B)** total dose. Adapted from King and Behazin (2021).

Subsequently, however, Soroka et al. (2021) resolved this discrepancy by modifying the radiolysis model. A series of experiments was performed in which copper coupons were exposed to H_2O_2-containing anoxic water, and the oxide film thickness was measured for different exposure conditions and durations. Corrosion was found to continue long after the added H_2O_2 had been completely consumed (either by electrochemical reduction to support corrosion or through heterogeneous decomposition to O_2 and H_2O), from which Soroka et al. (2021) concluded that O_2 rather than either H_2O_2 or OH• was the oxidant under irradiated conditions. A radiolysis model was developed that included the H_2O_2 decomposition reaction (see Eq. 1):

$$2H_2O_2 \rightarrow O_2 + 2\,H_2O \quad (1)$$

as well as the subsequent reaction between O_2 and Cu. In this initial model, these two interfacial processes were treated as homogeneous reactions with rate constants characteristic of diffusion-controlled reactions. With these modifications, Soroka et al. (2021) were able to account for the oxide film thickness previously reported by Björkbacka et al. (2013). Thus, the apparent discrepancy between the observed and predicted corrosion was the result of an incomplete radiolysis model rather than an additional non-radiolytic process.

Björkbacka et al. (2016) also resolved another early unexplained observation related to the concentration of dissolved copper. Following irradiation, the amount of copper measured in solution was 30 times higher than that predicted based on the solubility of Cu_2O and three times higher than the solubility of CuO. However, the concentration of "dissolved" species decreased when the solution was filtered with a 20-nm pore filter, suggesting that the solution contained nanoparticulate copper in addition to dissolved copper (Björkbacka et al., 2016). Bessho et al. (2015) previously reported the formation of colloids during the irradiation-induced corrosion of copper.

Several irradiation studies have been conducted in humid air because the period of the highest radiation field will correspond with the early unsaturated phase in the repository. In an unsaturated system, the ratio of the surface area of copper (but also of other

solids, such as bentonite) to the volume of the aqueous phase will be relatively high. The SA:V ratio will affect the relative influence of interfacial and homogenous processes. Björkbacka et al. (2017) found that the extent of corrosion was 7–9 times higher in humid air or humid argon (60% or 100% RH) in the presence of radiation (470–500 Gy/h, total absorbed dose 45–48 kGy) than in unirradiated systems. The similarity of the enhancement factor in air and Ar led the authors to conclude that, although nitrate-containing corrosion products were observed in irradiated humid air, the radiolytically produced HNO_3 did not play a direct role in the increased corrosion. The extent of corrosion in these irradiated unsaturated systems (as measured by the mean film thickness) was higher than that in an equivalent experiment in bulk anoxic water. This was explained on the basis of the understanding at that time that the primary oxidant in irradiated systems is OH•. In a bulk water system, there is more opportunity for the more-stable, longer-lived H_2O_2 to scavenge the HO• radical prior to it reacting with the surface than there is in a thin-layer, high SA:V ratio unsaturated system. This explanation may have to be reconsidered now that molecular O_2 rather than the HO• radical is considered to be the primary oxidant (Soroka et al., 2021), although it is possible that the nature of the primary oxidant is different in saturated and unsaturated systems.

Björkbacka et al. (2017) speculated that radiation-induced corrosion could render the surface more reactive to other species present in the repository, but their own data show that this is not the case. After irradiation in humid air (60% RH) for a period of 96 h at 500 Gy/h (total dose 48 kGy), no additional corrosion occurred if the irradiated sample was then placed in anoxic water. Thus, irradiation does not "activate" the copper surface and makes it more reactive.

Ibrahim et al. (2018) also studied the radiation-induced corrosion of copper in humid air (70%–85% RH, 75°C). In the absence of radiation, the surface was covered by a thin water layer along with larger isolated water droplets. The surface under the thin water layer was passivated due to the formation of a duplex Cu_2O/CuO layer, with thicker deposits under the droplets where the surface films appeared to remain porous and non-passivating. Irradiation at a dose rate characteristic of the canister (0.35 Gy/h) had relatively little impact. The oxide thickness under the thin water layer was the same as in the absence of radiation. Irradiation did increase the number and rate of secondary spreading of the condensed water droplets, but corrosion did not extend any deeper. Lateral spreading of the droplets was thought to result from the deliquescence of nitrate species formed from the radiolytically produced HNO_3, although no nitrate phases were found on the surface. In general, the rate of depth-wise penetration was relatively minor compared with the rate of lateral spreading of the droplets. Consequently, irradiation resulted in superficial, rather than deeply penetrating, corrosion. After 1 year of exposure to unirradiated conditions, the maximum thickness of the porous corrosion products in the droplet regions was 10 μm. No quantitative measure of the depth of penetration into the copper surface was given, but it would be expected to be a factor of 2–3 lower due to the difference in molar volumes of Cu and Cu_2O/CuO and due to the porosity of the corrosion products.

Irradiation has not been found to lead to the environmentally assisted cracking of copper. There was no evidence for the occurrence of stress corrosion cracking on various types of stressed samples exposed to irradiated environments at dose rates between 19 Gy/h and 4.9 kGy/h, for total doses up to 10 MGy, for exposure periods up to 5 years, and for temperatures up to 150°C (Yunker and Glass, 1986; Yunker, 1990; Johnson et al., 1996).

Lousada et al. (2016) reported an increase in the hydrogen content of 99.98 wt.% copper following irradiation in anoxic pure water at a dose rate of 490 Gy/h and total doses of between 35 kGy and 70 kGy. The lack of correlation between the two sets of data was used as evidence that the source of the absorbed H was not the dissociative adsorption of H_2O (Lousada et al., 2016).

2.2.2 Effect of irradiation on material properties

The creation of radiation damage in materials, including copper (Li and Zinkle, 2012), is generally associated with in-reactor exposure and high neutron flux. Radiation damage has been shown to affect the mechanical properties of copper alloys, including an increase in yield strength (radiation hardening), reduction in fracture toughness, and in-reactor creep (Li and Zinkle, 2012). In contrast to these effects observed at high doses, the neutron- and γ-dose rates for the canister are considerably lower, and radiation damage of the copper corrosion barrier has always been considered to be negligible (Guinan, 2001; SKB, 2010a).

Yang et al. (2019) confirmed earlier estimates of Guinan (2001) that the damage from neutron- and gamma-irradiation over the lifetime of the canister will be between 10^{-7} and 10^{-6} displacements per atom (dpa). Thus, any effects of radiation hardening are immeasurable below 10^{-4} dpa (Li and Zinkle, 2012). Recent experiments on gamma-irradiation of 99.999% copper at a dose rate of 1 kGy h^{-1} to a total dose of 100 kGy did not show any microstructural changes or changes to the population or nature of defects. (Padovani et al., 2019; SKB, 2019; Yang et al., 2019).

3 Corrosion under environmental transients

3.1 Nature of environmental transients

An understanding of the evolution of the environment surrounding the canister in the repository over long periods of time is essential for a reliable analysis of the corrosion of canister materials.

There are two important aspects of the disposal environment impacting the corrosion behavior of the canister (King and Padovani, 2011): i) the changes in the corrosive nature of the environment in the geological disposal repository (GDR) and ii) the type of canister material.

The evolution of the chemistry of the environment after repository closure depends on the engineered barriers and the composition of the groundwater. Other important factors include (King and Padovani, 2011):

(i) The maximum canister surface temperature: typically ~100°C.
(ii) The engineered barriers: compacted bentonite, cement, or concrete.
(iii) The pore water in contact with the canister: its properties will likely change over time and, initially at least, differ from those of the ground water.

(iv) The amount of available O_2, which is limited in deep geological formations to that trapped after sealing of the GDR.
(v) The magnitude of the gamma (and neutron) radiation fields at the outer surface of the canister and the amounts of oxidizing (and reducing) radiolysis products formed.
(vi) The time for the GDR to saturate with ground water following closure, typically a few decades or hundreds of years.
(vii) The rate of mass transport of reactants to, and of corrosion products away from, the canister, which is largely determined by the nature of the barriers.
(viii) The possibility of microbial activity at and away from the canister surface.
(ix) The magnitude of residual and applied stress.
(x) The permeability of the host rock and its transport capacity for any H_2 that may be produced by the anaerobic corrosion of the canister.
(xi) The mineral content of the rock; the oxidation of pyrite can lead to the formation of thiosulphate and other oxidized forms of sulfur that can be deleterious for some candidate canister materials.

The corrosion of container materials has been extensively studied under constant conditions, commonly those reflecting the long-term period of the repository. The experimental results that have been extrapolated to the evolving chemical, mechanical, and redox conditions of the early post-closure period must be verified and complemented. Conceptually, four phases are identified for the temperature-relative humidity (RH) and for aerobic/anaerobic conditions at the canister surface from the time of emplacement up to one million years (see Landolt et al., 2009 for the specific case of the Nagra concept):

- Phase 1—initial dry phase (oxic and dry conditions)
- Phase 2—aerobic unsaturated phase (oxic and unsaturated conditions)
- Phase 3—anaerobic unsaturated phase (anoxic unsaturated conditions)
- Phase 4—long-term cool, anoxic phase (long-term anoxic and fully saturated conditions).

Establishing anoxic conditions after an initial oxidic period is a key consideration. The corrosion behavior in steady-state conditions after the consumption of oxygen has been the focus of EC research projects (e.g., NF-PRO[1] and PEBS[2]) as well as several independent studies (Arcos et al., 2005; Carlson et al., 2006; Arcos et al., 2008). The role of the "dry" period preceding resaturation (not corrosive or slightly corrosive) and the transient period during resaturation (potentially corrosive) should also be regarded. After facility closure, the saturation of the bentonite barrier during the thermal phase of the repository leads to swelling and the development of mechanical stresses on the container. Such transient effects can be further influenced by attempts at repository footprint optimization (e.g., increased container heat production). Considering the time span of the processes, we can presume that the characteristic timescales of the various environmental transients are oxygen consumption < saturation < chemical < temperature.

3.2 Redox transients

The redox conditions in the engineered barrier system (EBS) constitute an important factor in determining corrosion and the behavior of radionuclide transport in the near-field (Giroud, 2014). A redox system may involve gases (O_2, N_2, H_2, CH_4, CO_2), dissolved components (NO_3^-, NH_4^+, CH_2O (TOC), Fe^{2+}, Mn^{2+}, SO_4^{2-}, HS^-, H^+), solids (FeOOH, MnO_2, $FeCO_3$, $MnCO_3$), and components (Fe^{2+}, Mn^{2+}, NH_4^+) associated with the solids by ion exchange (Christensen et al., 2000). The most important species that undergo redox reactions contain carbon, iron, sulfur, and nitrogen. Thus, the knowledge of the kinetics and reactivity of the redox-active species involved is important for the determination of the redox conditions.

In the case of an SF/HLW repository, the redox conditions will be determined by the inventory of O_2 trapped during closure and by the radiolysis of the pore water. The different processes that *a priori* can have a larger influence on the short and long-term redox evolution of the repository are a) metal corrosion, b) organic matter degradation, and c) microbial activity.

The corrosion evolutionary path (CEP) defines the time-dependent corrosion behavior of the canister and is closely tied to the evolution of environmental conditions. A useful indicator of this evolution of the corrosion behavior is the time dependence of the corrosion potential (E_{corr}) of the canister (Figure 3). During the early aerobic phase, E_{corr} is relatively noble (positive) because of the cathodic reduction of O_2. At longer times, the corrosion potential falls to a value determined by the relative rates of Fe dissolution and the reduction of H_2O, resulting in E_{corr} values close to the H_2/H_2O equilibrium potential during the long-term anaerobic phase. Between these two periods, the value of E_{corr} undergoes a transition, during which Fe(III) corrosion products formed during the aerobic phase are reductively dissolved to Fe(II) species (Johnson and King, 2008). Although H_2O is also an oxidant for some canister materials, the rate of corrosion processes in anoxic conditions is typically less severe than in aerobic environments (Shoesmith, 2006). The redox potential of the repository (Eh) will be determined by the most dominant redox couple. In aerobic systems, the Eh will be determined by the O_2/H_2O couple, whereas equilibrium between Fe^{2+} and $Fe(OH)_3$ or involving pyrite may determine the redox potential under anaerobic conditions. Certainly, in systems where sulfide is present (either naturally in the ground water or produced by the action of sulfate-reducing bacteria (SRB)), the Eh of the repository will become reduced. The expected near-field redox conditions have been investigated in different EU Projects

1 https://cordis.europa.eu/project/id/2389

2 https://cordis.europa.eu/project/id/249681/reporting/es

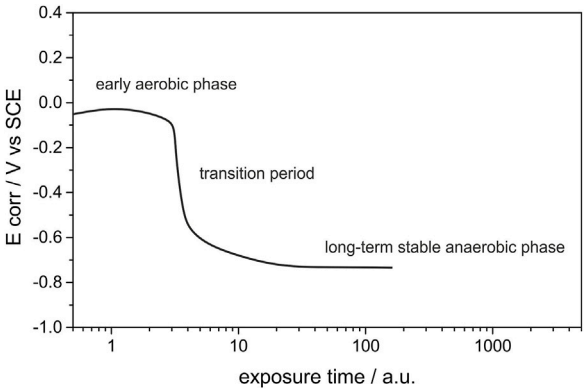

FIGURE 3
Schematic representation of the evolution of the open circuit potential of carbon steel during the aerobic–anaerobic transition. Potentials are given with respect to the SCE scale, which is +242 mV, versus the normal hydrogen electrode (NHE). Adapted from Johnson and King (2008), King (2008a), and Diomidis and Johnson (2014).

(NF-PRO, RECOSY[3]) (Carlsson and Muurinen, 2008; Duro et al., 2014). Wersin et al. (2021) proposed a conceptual model of corrosion, the redox evolution, and Fe-clay interaction processes in the ABM2 *in situ* test, and Hadi et al. (2019) proposed a model in the FEBEX[4] *in situ* test.

The establishment of anoxic conditions after an initial oxic period is a key consideration for the evaluation of conditions for corrosion processes. Apart from the oxygen trapped in the pore spaces, the radiolysis of humid air or water also produces oxidizing species, such as H_2O_2, resulting in an increase in the general corrosion rates of metals or localized corrosion (Crusset et al., 2017). The effect of the radiolysis of water on corrosion, however, can be significantly attenuated in the absence of oxygen (Lapuerta et al., 2008).

Oxygen can be consumed by corrosion of the canister and of the steel mesh stabilizing the tunnel wall (for clay rock, see Landolt et al., 2009), oxidation of Fe minerals in the bentonite (Wersin et al., 1994; Puigdomenech et al., 2001; Grandia et al., 2006; Giroud et al., 2018), or by microbial activity in bentonite (Kotelnikova and Pedersen, 1998; Giroud et al., 2018). Corrosion conditions during Phase 1 support a uniform dry oxidation yielding trivalent iron oxide. Oxidation of sulfides in the backfill may contribute to oxygen consumption and would produce sulfate and thiosulfate (Landolt et al., 2009). All the oxygen is presumed to be consumed during Phase 2.

Wersin et al. (1994) and Wersin et al. (2017) proposed two ways for the $O_2(g)$ consumption in the buffer: i) diffusion into surrounding rock and ii) reaction with mineral phases existing in the buffer and backfill materials. They predicted that anoxic conditions would be re-established in the buffer after a period ranging between 7 years and 290 years (Wersin et al., 2017) depending on the value taken for the most uncertain parameter: the pyrite reactive surface area. Giroud et al. (2018) considered gas exchange with bentonite pore water and adsorption on mineral surfaces as the most important processes controlling O_2 in the drift of the FE experiment, which was fully consumed after only a few months. According to Grandia et al. (2006), aerobic conditions can prevail for more than 5,000 years in the absence of geochemical processes (consumption of O_2 in the buffer).

Other authors (Kotelnikova and Pedersen, 1998) determined that the period of consumption of O_2 by microorganisms was in the range of 9 days to 4 years. Puigdomenech et al. (2001) also confirmed the short-term consumption of O_2 due to microbial involvement.

The Swedish research program studied the consumption of O_2 trapped in the repository, reacting with rock minerals in tunnels and deposition holes in more detail. Malmström et al. (1995) studied the kinetics of dissolution of Fe(II)-bearing silicate minerals (biotite and chlorite) and presented a simple calculation of the time needed for oxygen consumption in fractured granite due to the oxidation of the Fe(II) contained in the silicates. Periods of time ranging from 50 years to 300 years were estimated, depending on the type of mineral and on whether oxygen was considered to be depleted by direct consumption on the mineral surface or by oxidation of the Fe(II) previously released from the mineral.

During Phase 2, the environment is still aerated, and atmospheric corrosion takes place as the moisture starts to condense on the iron surface. Atmospheric corrosion is an electrochemical phenomenon that leads to various corrosion products: in addition to Fe_3O_4 and Fe_2O_3, hydrated ferric species, including different forms of FeOOH and green rust, can be formed. Corrosion during Phase 2 may be influenced by the deliquescence of salts and by the presence of particulates on the surface in a process that is not necessarily uniform (Landolt et al., 2009). Droplets of water can form by deliquescence of individual salt crystals or collections of crystals, with surrounding areas either dry or wetted by microdroplets or thin layers of moisture. If O_2 is still present in the bentonite at this time, the regions around the deliquesced droplets will tend to become cathodic because of the greater access of O_2. The droplets themselves will tend to become O_2 depleted. Some degree of localized attack can be expected during this period (Johnson and King, 2008; Diomidis and Johnson, 2014).

3.3 Saturation transients

The time-dependent degree of saturation of a repository will determine when and how corrosion will occur (King, 2006; King, 2013a). Initially, the system may remain sufficiently dry to hinder aqueous corrosion. As the system cools and the RH increases, the surface of the canister becomes wet, and aqueous corrosion is possible.

The time for complete saturation of a repository is estimated to be in the range of 100–1,000 years (Johnson and King, 2008), although it may take tens of thousands of years in certain low-permeability sedimentary host rocks. According to estimations

3 https://cordis.europa.eu/project/id/212287

4 https://grimsel.com/gts-projects/archive-of-previous-gts-projects-1997-to-2004/febex/febex-i-introduction

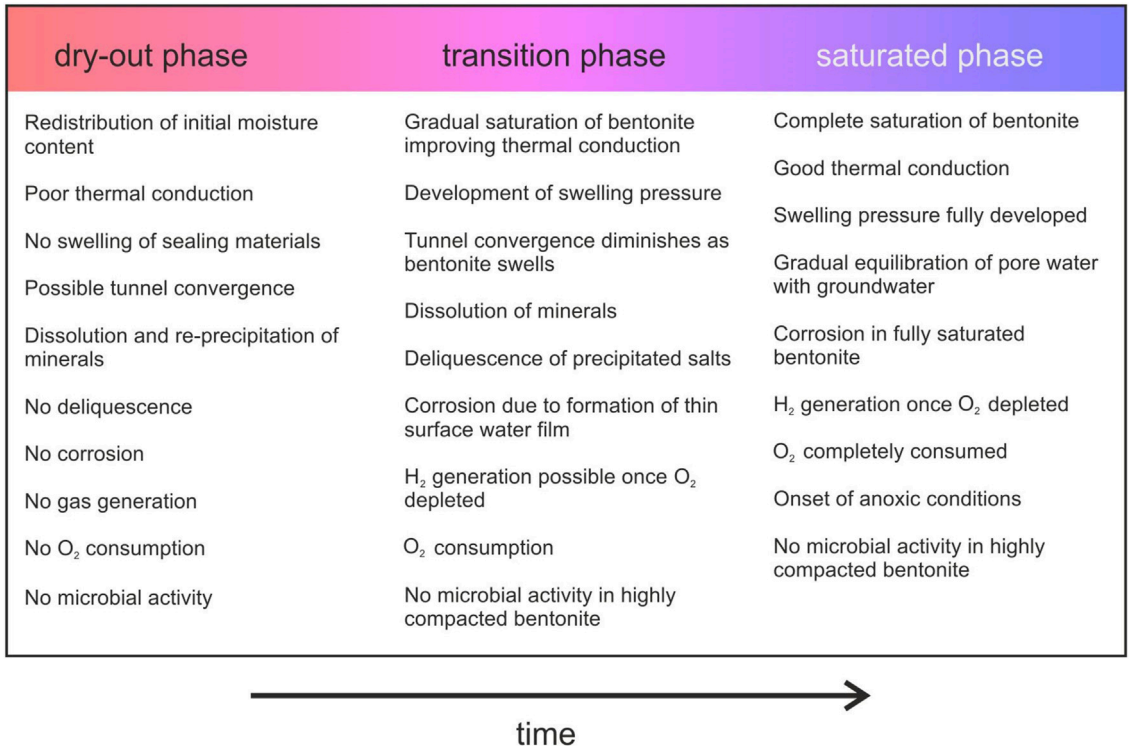

FIGURE 4
Evolution of environmental conditions in a deep geological repository characterized in terms of the stages of saturation. Adapted from King (2005).

using standard multi-phase flow process models, complete resaturation occurs in 3–4 years in a permeable, fully saturated host rock (Rutqvist and Tsang, 2008). Different *in situ* experiments, such as the FEBEX experiment at Grimsel or the HE and FE Experiments at Mont Terri, provide information about the saturation behavior of the bentonite barrier (Villar et al., 2020).

The typical assumption applied to bentonite resaturation is that ground water is available in the host rock. Due to the high chemical suction in partially saturated bentonite (SKB, 2006a), water is drawn in from the surrounding host rock into the bentonite. The rate at which resaturation can occur will be controlled by the intrinsic permeability and water saturation state of the surrounding host rock.

The application of a thermal load on the inner (nominally "dry") side of a bentonite buffer has a significant impact in terms of accelerating the generation and diffusion of water vapor. The water vapor migration is implicitly related to water suction, and both vapor and liquid water are driven in proportion to the suction pressure. Therefore, water vapor mobilizes at the canister boundary and drives water away from the canister. Moving away from the heat source, some of this vapor returns to the liquid state. The condensate migrates back toward the low water saturation, high-suction inner surface, creating a local water circulation pattern. However, if the availability of water from the host rock is low or the heat source is relatively large, it is possible to dry large sections of the bentonite and induce relatively high temperatures in the inner annulus (Wilson et al., 2011).

These fluid processes would also lead to an accumulation of chloride and sulfate salts near the hot canister surface while driving away dissolved silica. This induces canister corrosion and a radial variation of clay density, resulting in changes in porosity (Couture, 1985).

The processes observed during the evolution of the environmental conditions in a deep geological repository (DGR) are summarized in Figure 4. Before saturation, localized corrosion is possible because surface salts wet (deliquesce) before the development of full saturation, leading to spatial separation of anodic and cathodic sites (King, 2013a; King, 2017). With increasing RH, the surface of the canister becomes progressively wetter until it is uniformly wetted. The rate of supply of gaseous reactants (e.g., O_2) will be higher under unsaturated conditions, but the rate of removal of dissolved corrosion products will diminish, increasing the propensity for the formation of protective corrosion product films.

Aqueous corrosion requires an adsorbed water film on the metal surface that is able to sustain electrochemical reactions. Initially, corrosion may not occur if the relative humidity is lower than the critical relative humidity (CRH). This is a threshold value above which vapor can condense and form aqueous films on the metallic surface. In the case of a discontinuous adsorbed water film, a localized corrosive attack of the canister surface may occur. Such adsorbed films form when the surface temperature of the canister decreases below 100°C and the relative humidity rises to about 60%–80%. However, an adsorbed water film can also form at a relative humidity as low as 30% if particularly hygroscopic salts (such as $MgCl_2$ or $CaCl_2.xH_2O$) are deposited on the surface (King, 2006).

Various studies have been performed on the corrosion of steel with time, as a function of RH, oxygen content, and temperature, and how adsorption of water affects corrosion rates of different metals at different temperatures (Dante and Kelly, 1993; Lee and Staehle, 1997; Ben Lagha et al., 2007).

If the bentonite barrier is composed of compacted blocks and granular material, the blocks beneath the canister have a moisture content of 16%, while the granular material on top has a moisture content of about 5% at the time of emplacement. Consequently, moisture initially flows from the partially saturated bentonite blocks beneath the canister into the less moist granular material. While the bentonite close to the canister will not swell, the redistribution of water to locations away from the surface could lead to the development of swelling pressure around the periphery of the tunnel.

Dry conditions persist until cooling, and an increasing level of saturation of bentonite causes the relative humidity to rise above the critical level for the formation of thin films of moisture on the metal surface. The resulting thin electrolyte layer can support aqueous corrosion and the formation of electrochemical corrosion cells. Wetting may also be facilitated by the deliquescence of salts. Progressive saturation by water inflow will cause swelling of the bentonite starting from the periphery of the tunnel and gradually progressing toward the center (Landolt et al., 2009).

Swelling of bentonite continues during Phase 3. In the long-term anoxic Phase 4, bentonite is completely saturated, and all oxidized corrosion products formed at the canister surface and the support structures have been degraded. Once complete saturation has been achieved, the groundwater pressure in the bentonite will slowly increase as the hydrostatic head is restored. Equilibration of the bentonite pore water with that in the surrounding host rock will take place over a longer period until the pore water chemistry reaches a steady state.

3.4 Thermal transients

In deep geological repositories, the engineered barriers are exposed to two separate heat sources. One is the increase in ambient temperature with depth (temperature increases by 25°C–30°C/km for dry rock formations, depending on geographical position). The second source is the heat released due to the decay of radionuclides. The heat dissipates into the nearby engineered structures and the host formation.

The temperature evolution within the bentonite barrier and the surrounding host rock depends on the reference concept for waste disposal in each country. It is a critical factor, as it may alter the properties of the multi-barrier system by accelerating the corrosion of the waste form and of metal components of the containment systems. Further, high temperatures may degrade the bentonite or cement used as backfill materials, as well as argillaceous host rocks (King et al., 2017a; Finsterle et al., 2019). Temperature variations may also create driving forces that affect the migration of radionuclides in the near-field of the repository. Chemical thermodynamics, kinetics, and diffusion processes are temperature dependent. Thus, the maximum allowable temperature must be determined by analyzing the acceptable impact on barrier functions.

The evolution of temperature is determined by thermal simulations (e.g., Finsterle et al., 2019). Heat generation from radioactive decay of the SF/HLW results in an initial period of elevated temperature (sometimes referred to as the "thermal pulse"), followed by a period of slow cooling as the heat release from the waste decreases. The temperature evolution during the thermal pulse has been extensively studied for various disposal systems using both laboratory and field experiments as well as numerical analyses (Payer et al., 2019).

Large-scale, long-term heater tests for mined repositories in the saturated zone have been conducted in underground rock laboratories dedicated to nuclear waste research (HE-E Experiment: T > 100°C, EB Experiment: isothermal, FEBEX *in situ* test: T_{max} = 100°C, FE Experiment: T < 120°C (see Villar et al., 2020)). These studies reveal the importance of heat generation as it induces coupled thermal-hydrologic (TH) effects. Strong thermal perturbations also affect the geochemical conditions and corrosion products, as well as the geo-mechanical properties and stress state of the repository components, with complex feedback mechanisms to thermal and hydrologic processes (Nguyen et al., 2005; Gens et al., 2009; Zheng et al., 2011; Sánchez et al., 2012; Kumpulainen et al., 2016; Finsterle et al., 2019). An important thermally induced effect in low-permeability media is the pore water pressurization that occurs upon heating (Delage, 2010; Mohajerani et al., 2012). Such strong THM couplings were clearly demonstrated from both *in situ* experiments and laboratory tests performed in the TIMODAZ Project.

Most reported corrosion studies have been performed under defined and constant temperatures. An increase in the corrosion rate with temperature is usually observed (e.g., Smart et al., 2002a). Only a few studies have been performed under fluctuating temperature conditions. The effect of decreasing temperature in iron–bentonite interaction experiments was investigated by Pignatelli et al. (2013) and Pignatelli et al. (2014), with a focus on the nature of formed corrosion products. In these experiments, Callovo-Oxfordian claystone was contacted with metallic iron (present both as coupon and as powder) in autoclaves and heated to 90°C for 6 months before the temperature was reduced by 10°C every month until it reached 40°C. The pH measured after cooling to 25°C did not change considerably. Unfortunately, neither the oxidation–reduction potential nor the value of the iron corrosion rate have been reported. Magnetite, cronstedtite, and greenalite were detected in all samples. These studies also indicated that cronstedtite may not be stable below 50°C. In all cases, the formation of these iron silicates was directly linked to the dissolution of silicates present in the argillite, and the solubility was dependent on the temperature.

3.5 Chemical (pore water) transients

In the early, non-isothermal, and unsaturated periods, thermal and hydraulic gradients influence the properties and performance of the bentonite barrier. The bentonite pore water can be modified over time due to changes in the initial physicochemical conditions under different types of perturbations: a) interaction with groundwater (saturation phase), b) desaturation phase due to heating, c)

perturbations linked to the interactions between the bentonite and the engineered solid materials (concrete, iron, steel, organics, etc.), and d) interactions with different gases produced and consumed in the system (CO_2, H_2, CH_4, etc.), due to mineral dissolution/precipitation, microbiological reactions, and corrosion processes.

The impact of the different perturbations can be described in terms of a) modifications in the pore water chemistry and redox conditions that may affect the smectite structural stability and speciation of dissolved ions, b) mineralogical alteration: dissolution and redistribution of primary mineral phases and precipitation/neoformation of secondary minerals, c) clay mineral stability and alteration of the clay mineral properties (especially cation exchange capacity, cation exchange population, crystallo-chemical structure, layer charge, and swelling ability), and d) modification of transport properties through modifications of porosity, permeability, and tortuosity by cementation processes. The perturbation processes may change the physical, hydraulic, and mechanical properties of the bentonite system.

The scientific challenge of predicting the long-term clay barrier behavior consists of analyzing the results from experiments conducted in underground research laboratories (URL) in real scales and conditions (Tournassat et al., 2015). Most of the bentonite barrier experiments described in the literature have been carried out under laboratory conditions (e.g., Cuevas et al., 1997; Fernández and Villar, 2010, and references therein) to study the chemical evolution of the pore water and the alterations of the bentonite barrier. There are only a few large experiments, such as LOT, ABM, FEBEX, and FE *in situ* experiments (Karnland et al., 2009; Svensson et al., 2011; Müller et al., 2017; Villar et al., 2017). Several articles have reported results of geochemical and reactive-transport modeling for long-term analysis and near-field evolution (Bradbury and Baeyens, 2002; Wersin, 2003; Fernández et al., 2004; Wersin et al., 2004; De Combarieu et al., 2007; Itälä, 2009; Savage et al., 2010; Curti, 2011; Zheng et al., 2015; Červinka and Vasicek, 2018; Jenni et al., 2019; Zheng et al., 2020).

After repository closure, gradual saturation of the bentonite may lead to some redistribution of the water, density, and salts during Phase 1. Precipitation of salts close to the canister surface may also occur, assisted by the desiccation of the bentonite (Landolt et al., 2009). Progressive saturation by water inflow causes the re-dissolution of precipitated salts, and the bentonite pore water equilibrates with the incoming water from the host rock. During Phase 3, Fe(III)-rich corrosion products formed during the previous periods can be reduced (Diomidis and Johnson, 2014). Equilibration of the bentonite pore water with that in the surrounding host rock will continue until a steady state has been reached. Steady-state conditions for the chemical composition of the pore water, however, have not been achieved before 10.5 years in the EB experiment (Fernández, 2019a) or before 18 years in the FEBEX *in situ* test (Fernández et al., 2018) and during the ABM5 experiment (Fernández et al., 2022). In different tests, it has been observed that the most important parameter for pore water chemistry is the bentonite composition, independent of groundwater chemistry (deliverable D2.6 WP ACED) (Havlová et al., 2020). However, this is true if the infiltrating ground water is diluted granitic pore water. Modifications in the pore water chemistry and in the cation exchange composition of the bentonites have been observed in the ABM5 experiment after the interaction of saline granitic groundwater with Na- and Ca-bentonites during 4.4 years (Figure 5), indicating the influence of the type of the infiltrating water and the type of bentonite (main cation at exchange sites) on the evolution of the pore water chemistry of the bentonite barrier (Fernández et al., 2022).

Concrete structures are needed for supporting galleries in the case of waste disposal concepts in clay formations. In this context, the pore water pH will evolve as the alkaline mineral phases are leached out over time (see De Windt et al., 2020; Deissmann et al., 2021). There will be an interface between cement-based materials and metal supporting structures. Highly alkaline pH values during the thermal phase keep the carbon steel canister passivated, thus limiting corrosion.

3.6 Mechanical transients

Canisters are exposed to residual and applied stresses, and hence, environmentally assisted cracking is a possibility (Shoesmith, 2006). The magnitude of the applied stress (~20–50 MPa) depends on the repository design, the depth, and the host rock formation. The external load will comprise the swelling pressure of the backfill (if used), the hydrostatic pressure, and the lithostatic load (the latter only for non-self-supporting rock, such as salt domes and sedimentary deposits).

For a bentonite-backfilled repository, the pressure on the canister depends on (Hasal et al., 2019):

1. the hydrostatic water pressure in the rock, which is transferred to the canister through almost fully saturated bentonite,
2. the swelling pressure of bentonite (Raiko et al., 2010),
3. the increase of temperature of the bentonite and surrounding rocks,
4. degradation of the canister and influence of corrosion products on the bentonite (if the Pilling–Bedworth ratio is > 1),
5. the increase in pore pressure due to gas release,
6. chemical changes of materials, namely bentonite, and
7. deposition hole deformation (Raiko et al., 2010).

The mechanical load on the canister develops with the continuing saturation of the bentonite. The buffer swelling pressure increases with increasing bentonite dry density (Figure 6A), decreasing temperature (Figure 6B), and decreasing bentonite pore water salinity (Figure 6C). After the bentonite barrier is completely saturated, the total pressure comprises the sum of the bentonite swelling pressure and the water pressure. While the water pressure is isostatic, bentonite density variations in combination with imperfections in the deposition hole/disposal tunnel can impose an asymmetric pressure on the outer surface of the canister, which may be permanent and may yield an over-stress affecting the canister integrity (Jonsson et al., 2018).

In the last few years, considerable research has been carried out to evaluate the behavior of compacted clay-based buffer material in the framework of coupled thermo-hydromechanical (THM) processes in nuclear waste repositories (Villar et al., 2020). An important issue is the total time for saturation of the bentonite, the changes in dry density and porosity of the bentonite barrier, and the pressure exerted on the canisters. The time-dependent degree of

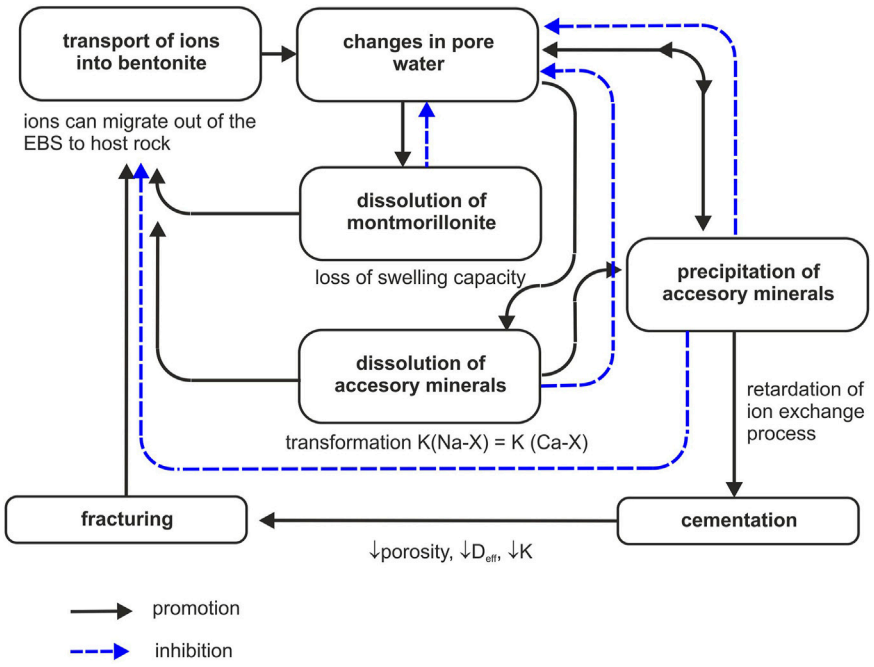

FIGURE 5
Water–bentonite interaction processes and possible buffer alterations. Adapted from Takase (2004).

saturation of the repository is an important factor in determining when and in what form corrosion can occur (King, 2006). The process of hydration depends on the hydraulic permeability and thermal conductivity of the bentonite and the host rock, the salinity, and temperature. In addition, hydration triggers the swelling of interlayer space in the clay particles and transforms the material from an initial heterogeneous to a homogeneous one, changing the local volume constraint conditions. The changes in macroscopic volume due to clay–water interactions are associated with the evolution of the microstructure and its interaction with the macrostructure and are described by dual-porosity models and water retention behavior. The changes in pore size distribution domains in terms of micro- to macro-porosity fractions are highly sensitive to the physicochemical processes involved in the applied loading paths (Schanz, 2016).

3.7 Influence of transients on the corrosion process

The surface damage resulting from dry oxidation due to oxygen entrapped upon closure is expected to be very limited. Typical corrosion products are Fe_3O_4 and Fe_2O_3 (Terlain et al., 2001). The oxygen will be consumed after a certain time, and the environment will become anoxic. This modification of the geochemical conditions influences metallic corrosion as the reduction of higher oxides becomes the main cathodic reaction before water reduction starts to dominate the cathodic process during the anaerobic phase (Johnson and King, 2008).

Several studies on the effect of changing oxidic/anoxic conditions have been published. For example, the effect of fluctuating redox conditions on the corrosion mechanism has been investigated by Saheb et al. (2011) using archaeological artifacts. In that study, a nail that was exposed to an aerated unsaturated soil for several hundred years was reburied and exposed to anoxic and saturated conditions. Goethite and smaller amounts of magnetite and maghemite formed under aerobic and unsaturated conditions, while ferrous carbonates were detected in the corrosion layer after subsequent exposure to anoxic and saturated conditions. Based on experimental findings and aided with geochemical modeling, the authors concluded that phase transformation occurred rather than metallic corrosion progressing by direct formation of new phases. In the same study, an experiment was also conducted by applying the reverse sequence of changing conditions: a nail that had been exposed to anoxic and saturated conditions for several hundred years was immersed in an aerated carbonated solution for 5 weeks. Ferrous carbonate and iron oxides (magnetite, maghemite) formed as corrosion products upon exposure to anoxic water-saturated conditions, and the subsequent exposure to aerated conditions resulted in the formation of an external goethite layer on the external part of the corrosion layer. In this last experiment (i.e., the transition from anoxic to oxidic conditions), the authors also concluded that the presence of the ferric phase resulted from the transformation of the corrosion layer.

El Hajj et al. (2013) investigated sequential aerobic and anaerobic microbiologically induced corrosion of carbon steel. They found that the corrosion rate under anaerobic conditions is lower when specimens experienced a prior phase of aerobic corrosion. This outcome was attributed to the nature of the formed corrosion products and their adherence to the steel surface. The transition from aerobic to anaerobic conditions

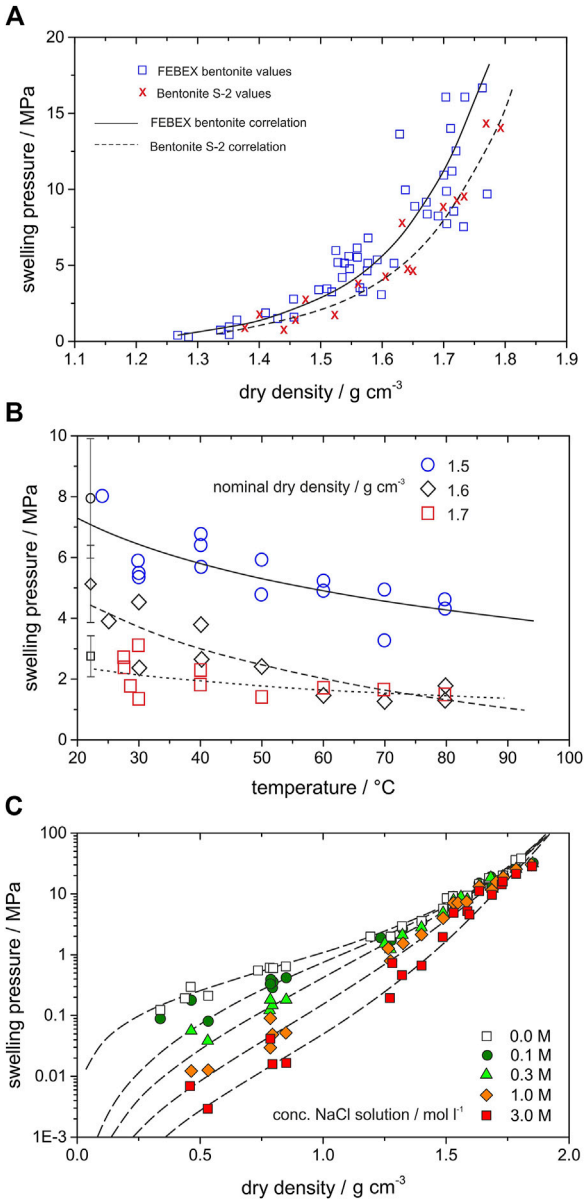

FIGURE 6
Dependence of the swelling pressure on **(A)** dry density [adapted from Huertas et al., 2005], **(B)** temperature [adapted from Villar and Gómez-Espina (2009)], and **(C)** porewater salinity [adapted from SKB (2006b)].

resulted in the formation of pyrrhotite as a single phase, while nanocrystalline mackinawite formed during direct anaerobic steel corrosion. The different results observed in this study were attributed to the stimulation of the activity of SRB and the hydrogen sulfide production upon transition from aerobic to anaerobic conditions.

Experiments performed at 85°C under *in situ* conditions showed that transient oxidic conditions can have substantial effects on steel corrosion. Fe^{2+}-bearing compounds in clay rock (e.g., pyrite) oxidize in the presence of oxygen (ingress due to loss of tightness), resulting in a decrease in the pH of the porewater (Necib et al., 2016). These transient acidic conditions had, in turn, a relatively important impact on the corrosion rate owing to the positioning of spatially decoupled anodic and cathodic areas (Schlegel et al., 2016). Galvanic coupling between areas exposed to different concentrations of O_2 in (sub)oxidic conditions can result in the formation of pits (Sherar et al., 2011; Refait et al., 2016). Areas more easily accessed by oxygen become cathodic, while those less exposed may become anodic. The coupling is sustained by the precipitation of corrosion products, and the driving force is the large difference in electrochemical potentials between O_2 reduction and Fe oxidation (Schlegel et al., 2018).

Romaine et al. (2015) showed that the reactions are, in fact, more complex and highly dependent on the mineralogical composition of the used argillite. Coupling of a bare electrode under argillite (anode) with a pre-corroded electrode covered by a bilayer of corrosion products (magnetite/siderite) under argillite (cathode) resulted in the formation of heterogeneous layers of corrosion products. The heterogeneity of these layers resulted from the variation of the galvanic effect along the surface of the initially bare electrode due to the variation of the distance from the initially covered electrode. Such variation of galvanic effects may also be assimilated to transient conditions affecting corrosion processes.

In anoxic groundwaters, anaerobic steel corrosion generates hydrogen, which results in a decrease in the E_h. However, with increasing reaction time, corrosion products will form a protective layer, which will result in a progressive lowering of the corrosion rate and, thus, of the hydrogen production (Smart et al., 2002a; Turnbull, 2009). The evolution of hydrogen is thus expected to decrease with time until reaching a lower constant value in the long term (Smart et al., 2002a).

Several studies have reported the effect of hydrogen on selected reactions (Truche et al., 2009; Truche et al., 2010; Truche et al., 2013). Under elevated temperature and calcite-buffered conditions, pyrite can be reduced by hydrogen through a coupled dissolution-precipitation mechanism that generates H_2S (Truche et al., 2010; Truche et al., 2013). Similarly, aqueous sulfate can also be reduced by hydrogen (Truche et al., 2009), but this reaction is kinetically slow under expected disposal conditions. Experimental findings reported by El Mendili et al. (2015) indeed showed the formation of a continuous iron sulfide layer covering carbon steel contacting Callovo-Oxfordian argillite in experiments performed at 90°C. The origin of this layer was attributed to the presence at the corroding interface of H_2S formed by the reduction of pyrite by hydrogen. Iron sulfide was likewise detected in experiments performed at 30°C, but the corrosion layer was thinner than in experiments performed at 90°C. At this lower temperature, the origin was attributed to the activity of SRB (consumption of hydrogen and release of hydrogen sulfide).

In the absence of argillite, Smart et al. (2002a) and Smart et al. (2002b) reported experiments performed in the presence of a hydrogen overpressure. Their studies could not detect any significant effect of this parameter on the anaerobic corrosion of carbon steel and cast iron in artificial groundwaters.

Reported studies showed that evolving redox conditions at the steel–bentonite interface can have a substantial impact on canister corrosion by changing the corrosion rate and mechanism. Among them, the presence of oxygen plays an important role and involves an increase in corrosion rate. Similarly, the presence of hydrogen may have an impact on the geochemical conditions of the canister near-field, such as the dissolution of selected minerals and the

formation of dissolved species, which in turn influence steel corrosion. The presence of hydrogen does not seem to directly modify the corrosion of steel (e.g., no decrease in corrosion rate).

Geochemical conditions in a repository are also expected to evolve due to the metallic corrosion itself, which produces corrosion products and generates hydrogen. The accumulation of corrosion products at the steel–bentonite interface may influence the nature of the electrochemical reactions. For instance, the presence of magnetite at the steel–bentonite interface results in an increase in steel corrosion by acting as an external cathode coupled to the steel surface (Kojima et al., 1995; Taniguchi, 2003). It was shown that the observed increase in corrosion rates was caused by the reduction of Fe_3O_4 itself. Consequently, because magnetite dissolves, such corrosion products may not necessarily play any role in the long term, but magnetite may influence corrosion processes between its formation and its dissolution.

Only a few studies on Cu corrosion under transient conditions have been reported. Smith et al. (2006) reported electrochemical experiments on the effect of pre-oxidation on the surface attack of Cu by sulfides in 0.1 mol/L NaCl under anoxic conditions. Cu was pre-oxidized to mimic the formation of corrosion products during the warm oxic period. Depending on the extent of pre-oxidation, the surface was covered either with a thin film made of Cu_2O or Cu_2O covered by $CuO/Cu(OH)_2$ for longer reaction times. Samples were subsequently immersed in a sulfide-containing solution (30 μmol L^{-1}), and the evolution of the corrosion potential (E_{corr}) was recorded. For all samples, E_{corr} stabilized at a value slightly more negative than observed in the absence of sulfide, then decreased to a value between −0.5 V and −0.6 V (SCE) before a sudden decrease to the equilibrium potential for the Cu/Cu_2S redox reaction. The time needed during the first decrease in E_{corr} increased with the extent of pre-oxidation and probably reflects the penetration of SH^- (the predominant species) to the Cu metal surface. The second drop was comparable for all samples and indicates that the redox conditions are dominated by the Cu/Cu_2S redox couple. Overall, outcomes pointed out a beneficial effect of Cu pre-oxidation, indicating that deposits could impede the reaction of Cu with aqueous sulfide.

More recently, Senior et al. (2019) reported corrosion rates of copper in anoxic NaCl solutions at various temperatures by measuring the rate of hydrogen release. Copper exposed to 0.25 mol kg^{-1} NaCl at 30°C or 50°C produced negligible amounts of H_2 below the detection limit. At 75°C, the H_2 release was in agreement with a corrosion rate of about 10 nm a^{-1}. When the temperature was returned to 50°C, the H_2 production immediately fell below the detection limit. Comparable findings were obtained for experiments performed in solutions containing up to 5 mol kg^{-1} NaCl. These results may suggest that the corrosion rate of copper in NaCl solutions up to 5 mol kg^{-1} is very low and decreases with temperature.

Smart et al. (2005) used electrochemical techniques to investigate the galvanic corrosion of the copper–cast iron couple in artificial groundwaters while changing the oxygen content. The context was an unlikely event of the outer copper canister being breached, followed by water entering the annulus between the inner and the outer canisters. In the presence of oxygen, copper was the cathode in the galvanic couple. In deaerated conditions, potentials were considerably more negative than in aerated conditions: the potential of the copper in deaerated conditions was within the thermodynamic domain of stability of copper, while that of iron suggested that the hydrogen evolution by anaerobic corrosion of iron was thermodynamically possible. Accordingly, copper plating was observed on the surface of iron in the experiment where conditions evolved from aerobic to anaerobic.

4 Microbial effects

4.1 Microbial corrosion in the context of nuclear waste disposal

In the literature, microbially influenced corrosion (MIC), the process by which microorganisms directly or indirectly impact the corrosion of a metal, is categorized into two broad groups: chemical MIC (CMIC) that relies on corrosive chemical by-products of microbial metabolism and electrical MIC (EMIC) that entails the transfer of electrons from the metal to the bacterium (directly or indirectly) (Venzlaff et al., 2013; Enning and Garrelfs, 2014). The latter is presumed to require biofilm formation (Jia et al., 2019; Little et al., 2020), which, for nuclear waste, is only relevant in the absence of a bentonite backfill.

In the context of nuclear waste disposal, the major concern is the corrosion of the waste canisters, whether made of steel or copper. Here, we are exclusively concerned with anoxic corrosion and will not discuss MIC under oxic conditions. Furthermore, the text hereafter is focused on steel, but corrosion of copper due to sulfide is also a concern. Anoxic corrosion will take place regardless of microbial activity, with an anodic and a cathodic half-reaction (Féron and Crusset, 2014), as shown in Eqs 2, 3:

$$\text{Anodic reaction: } Fe^0 \leftrightarrow Fe^{2+} + 2e^- \quad (2)$$

$$\text{Cathodic reaction: } 2H_2O + 2e^- \leftrightarrow H_2 + 2OH^- \quad (3)$$

The mechanism by which microbial activity accelerates this process was long attributed to cathodic depolarization, by which microbial activity can consume H_2 and thus accelerate the process, but this theory has since been invalidated (Costello, 1974).

The major form of CMIC is through the production of corrosive by-products of microbial metabolism. A diversity of metabolisms has been identified in metal-corroding biofilms, including SRB, sulfide-oxidizing bacteria, manganese-oxidizing bacteria, iron-oxidizing bacteria, iron-reducing bacteria, and microorganisms producing acidic compounds (Amendola and Acharjee, 2022). Reductive metabolisms, such as sulfate reduction, iron reduction, acetogenesis, and methanogenesis, are expected in the repository if the appropriate electron donor (e.g., H_2) and acceptor (i.e., sulfate, ferric iron, and CO_2) are available.

Of the potential microbes in the repository, SRB are considered the most relevant for MIC because, through dissimilatory sulfate reduction (DSR), they utilize sulfate as an electron acceptor and produce the corrosive compounds, hydrogen sulfide (H_2S) or the bisulfide ion (HS^-), depending on the pH of the environment. Methane is not corrosive but could facilitate MIC through EMIC (Mand et al., 2016). Acetogens produce acetate that is acidic and can fuel sulfate reduction, and they likely also corrode via EMIC (Mand

et al., 2016). Here, we will focus on SRB as they are the major players in CMIC.

DSR stoichiometry depends on the electron donor that is available (either H_2 or organic carbon) (Eqs 4, 5, respectively):

$$4H_2 + SO_4^{2-} + 2\,H^+ \rightarrow H_2S + 4H_2O \quad (4)$$

$$2CH_2O + SO_4^{2-} + 2H^+ \rightarrow H_2S + 2CO_2 + 2H_2O \quad (5)$$

Sulfide reacts chemically with zerovalent Fe (Fe^0) to produce mackinawite and H_2 (Eq. 6).

$$Fe^0 + H_2S \rightarrow FeS + H_2 \quad (6)$$

The overall reactions (with H_2 or organic carbon as the electron donor) become Eqs 7, 8, respectively:

$$3H_2 + SO_4^{2-} + Fe^0 + 2H^+ \rightarrow FeS + 4H_2O \quad (7)$$

$$2CH_2O + SO_4^{2-} + Fe^0 + 2H^+ \rightarrow FeS + 2CO_2 + H_2 + 2H_2O \quad (8)$$

Thus, sulfide-driven CMIC generates a layer of FeS that ultimately covers the surface of metallic iron, resulting in the formation of a film of FeS that serves as a protective layer (a passivation layer), precluding the diffusion of Fe^{2+} from the metal anode (Enning and Garrelfs, 2014). Thus, in the absence of other processes, the rate of sulfide-dependent CMIC is expected to decelerate over time. However, if the FeS film is interrupted, the corrosion rate will increase (Lv and Du, 2018). CMIC can take place in the absence of a biofilm as long as there exists a diffusion path for H_2S (or HS^-) to the metal surface.

EMIC depends on the transfer of electrons from metallic iron to SRB (or other microorganisms). Thus, iron serves as the electron donor for DSR (Eq. 9), and the ferrous iron generated precipitates with sulfide as mackinawite (Eq. 10) or, for instance, with carbonate as siderite (Eq. 11) due to the production of CO_2 in heterotrophic sulfate reduction (Eq. 5):

$$4Fe^0 + SO_4^{2-} + 10\,H^+ \rightarrow 4Fe^{2+} + H_2S + 4\,H_2O \quad (9)$$

$$Fe^{2+} + H_2S \leftrightarrow FeS + 2\,H^+ \quad (10)$$

$$Fe^{2+} + CO_3^{2-} \leftrightarrow FeCO_3 \quad (11)$$

However, because of the stoichiometry of the reaction, there is a single sulfide produced per four ferrous ions produced, which means that the production of mackinawite will be threefold lower than that of siderite (Eq. 12):

$$4Fe^0 + SO_4^{2-} + 3CO_3^{2-} + 8H^+ \rightarrow 3FeCO_3 + FeS + 4H_2O \quad (12)$$

The different mineral products detected during EMIC and CMIC can be used to decipher which of the two mechanisms takes place or even the relative contribution of each MIC mechanism in the presence of carbonate (Enning et al., 2012).

SRB can carry out both forms of MIC (Figure 7), depending on the species considered. EMIC strains such as *Desulfovibrio ferrophilus* (Chatterjee et al., 2021) or *Desulfopila corrodens* (Beese-Vasbender et al., 2015) are currently a minority. This is likely due to the use of organic carbon in the isolation of most SRB. In order to capture EMIC-specific SRB, it is necessary to consider a lithotrophic medium that requires metallic Fe to be the only electron donor and thus favors EMIC-SRB. The mechanism of electron transfer from the metal surface to the bacterium remains a matter of discussion (Liang et al., 2021). SRB are the most relevant organisms for CMIC, but other sulfide-producing microorganisms such as thiosulphate-reducing bacteria or SRB or sulfate-reducing archaea are also important. Furthermore, other organisms, such as nitrate-reducing bacteria and methanogenic archaea, are likely to be capable of carrying out EMIC via the abstraction of electrons from the iron metal surface. There is increasing evidence of microbially-mediated electron transfer from mineral surfaces, and this phenomenon of electrochemistry is likely to be underestimated to date.

In the context of nuclear waste disposal, particularly those concepts that require a bentonite backfill in direct contact with the waste canister, it is unlikely that biofilms will develop on canister surfaces. Thus, the main mechanism of concern is the formation of corrosive by-products of microbial metabolic activity (CMIC). If information about biofilm formation on metal surfaces were to emerge, EMIC would become an important consideration.

Several studies have considered the corrosion of steel by exposing steel coupons to a solution representative of repository conditions (Rajala et al., 2015; Diler et al., 2021; Shrestha et al., 2021).

The study by Shrestha et al. (2021) was based on the exposure of metal coupons to a solution of synthetic bentonite porewater (sterilized) that was inoculated with groundwater from the Josef Underground Research Center. Pitting corrosion and the formation of mackinawite and magnetite were observed on the steel only in the biotic sample, while the abiotic sample exhibited a uniform layer of magnetite. The biofilm that formed on the surface of the steel coupon included SRB but also nitrate-reducing organisms such as *Pseudomonas, Methyloversatilis*, and *Acidovorax*, which is consistent with the presence of 10 mM nitrate in the water. A combination of CMIC and EMIC probably occurred here due to the absence of a solid phase and the formation of a biofilm. This type of study is only relevant to the French concept in which there is a gap between the carbon steel tunnel casing and the canister overpack, which will become filled with groundwater (Diler et al., 2021).

Similarly, Rajala et al. (2015) evaluated the corrosion of carbon steel in the presence of Olkiluoto groundwater (at RT and at 6°C) and found that pitting corrosion occurred after 3 months and 8 months, and a biofilm developed at the surface of the coupons. Betaproteobacteria appeared to thrive in the presence of carbon steel, perhaps through the utilization of H_2 as an electron donor (as they are known as hydrogenotrophic bacteria). Additionally, iron oxidizers and reducers were observed, suggesting iron cycling. The electron acceptor for iron oxidation was not identified in this anoxic environment, and it is presumed that H_2 drove iron reduction. SRB were also observed in the biofilm, and some genera (e.g., *Desulfopila*) were presumed to use elemental iron as an electron donor for sulfate reduction.

Also relevant to the French concept, the iron corrosion (IC) experiment (Necib et al., 2017) was performed at the Mont Terri Underground Laboratory. It consisted of test chambers placed within a core of Opalinus clay confined in stainless steel screens and introduced into a borehole within the same rock formation. The test chamber contained four steel electrodes, electrically insulated from each other with alumina, and mounted on a central tubing.

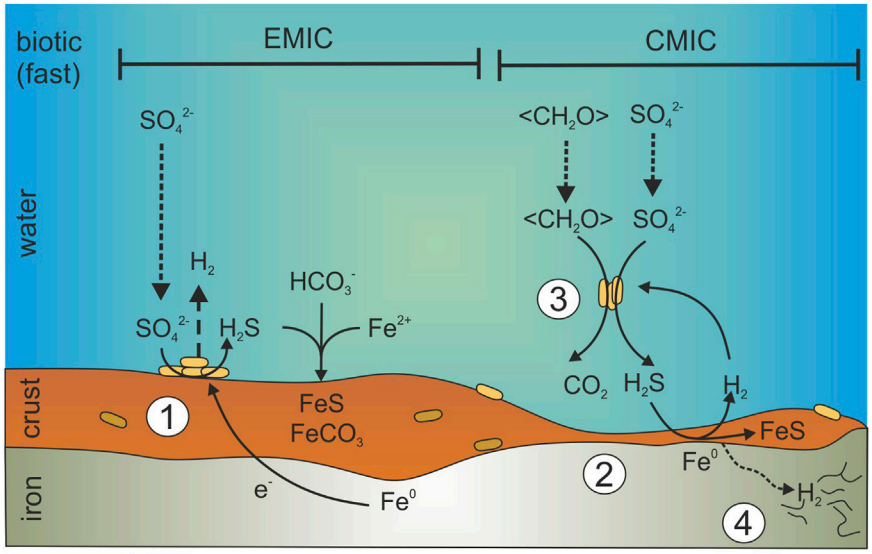

Electrical microbially influenced corrosion (EMIC)

1: $4\ Fe^0 + SO_4^{2-} + 3\ HCO_3^- + 5\ H^+ \rightarrow FeS + 3\ FeCO_3 + 4\ H_2O$

Chemical microbially influenced corrosion (CMIC)

2: $H_2S + Fe^0 \rightarrow H_2 + FeS$

3: $3\ <CH_2O> + 2\ Fe^0 + 2\ SO_4^{2-} + H^+ \rightarrow 3\ HCO_3^- + 2\ FeS + 2\ H_2O$

4: $2\ H_{abs} \rightarrow H_2$

FIGURE 7
Microbially influenced corrosion pathways. Modified from Enning and Garrelfs (2014).

Thus, the electrodes were close (~1 mm) to the Opalinus clay. A synthetic solution representative of Opalinus clay porewater was injected into the test chamber. The water flow rate was manually set to ensure circulation between the metallic electrodes and the Opalinus clay core. Electrochemical measurement on the electrodes allowed an estimation of the corrosion rate. After a total period of 7 years, the equipment was dismantled, and the iron was characterized. Inspection of the metal surface/Opalinus clay interface revealed several layers of corrosion products. Various iron-bearing minerals such as magnetite, goethite, lepidocrocite, akageneite, chukanovite, and siderite were observed. Various oxidation states of Fe sulfide, as well as elemental sulfur, were also observed, and the original surface had been replaced by iron sulfide, likely pointing to MIC.

However, for the bentonite-backfilled repository environment, CMIC in the clay buffer is the more relevant question. A study by Grousset et al. (2020) investigated the sulfur isotopic fractionation during the exposure of steel embedded in Toarcian argillite to sulfate-rich water inoculated with an SRB isolate and an iron-reducing bacterium. The novelty of the study was the use of a NanoSIMS to spatially delineate the S isotope signature. Mackinawite was detected at the surface of the steel coupon, but it was not possible to conclusively determine whether its formation resulted from microbial processes due to the poor constraints on the isotopic signature of the sulfate source.

One study probed the corrosion of steel by exposing coupons to a solution representative of the Callovo-Oxfordian (Cox) rock formation in contact with cement–bentonite with or without uncompacted representative solid phases (Cox or Cox + cement/bentonite) and with or without Cox-derived microbial amendments (Diler et al., 2021). Corrosion was observed in the systems in which microorganisms were amended in comparison to the control systems that were left unamended (but not sterile). However, in the presence of a cement–bentonite mix, the extent of corrosion decreased considerably for 47 days. In addition, the embedding of the Cox clay rock in the cement–bentonite mix further decreased the extent of corrosion. These results are in line with expectations, as alkaline conditions are inhibitory to sulfate reduction. The microbial community was dominated by Firmicutes, including SRB in the incubations with cement–bentonite and Cox, as well as the incubation with Cox alone.

Another experiment (IC-A) carried out at the Mont Terri rock laboratory was designed to measure the *in situ* rate of iron corrosion. Metal coupons (carbon steel of various types) embedded in bentonite were deployed in a borehole by using stainless steel modules. The modules included holes and a sintered stainless steel filter to allow for the exchange of pore water with the host rock. The bentonite (MX-80) varied in its formulation (compacted or granular) and in its dry density. Modules were retrieved at various time intervals, and the corrosion was evaluated along with the microbial community within the bentonite. This is an ongoing

experiment. Findings do not point to any detectable microbial impact on corrosion (Smart et al., 2017). However, it was also suggested that SRB did not grow within the bentonite due to the persistence of O_2 (Burzan, 2021). Thus, this would suggest that longer deployment times are needed to reach conditions representative of a repository, that is, to allow the consumption of O_2 and the potential growth of SRB. Another scenario is that bentonite is fully saturated at the point in time at which O_2 is depleted, precluding SRB growth. The latter scenario would ensure the inhibition of SRB growth during saturation, providing excellent protection against MIC. This experiment presents strong evidence that the borehole water microbial community did not colonize the bentonite significantly but that the bentonite microbial community grew initially and persisted.

The evidence presented above indicates the absence of CMIC in the bentonite backfill. However, the question remains as to whether the experiments conducted so far were carried out long enough to show that SRB do not grow within bentonite after depletion of the adsorbed O_2. In order to put to rest the question of whether the inhibition of SRB growth would persist in the absence of O_2, experiments should be conducted with bentonite from which O_2 was stripped. The bentonite, embedded with carbon steel coupons, would receive H_2 as an electron donor, and steel corrosion should be monitored over time.

4.2 Impact of irradiation on microbial viability in the context of nuclear waste disposal

Microorganisms can cope with ionizing radiation to some extent. This depends on the type of microorganism. In the context of the safe long-term disposal of high-level radioactive waste, the impact of the ionizing radiation on the microbial community structure, viability, and activity is of concern because it affects the possible microbial processes. The expected radiation doses depend on various factors such as the disposal concept. The latter includes the radionuclide inventory, the distance from the source, the engineered barriers, especially the container material, and the half-life of radionuclides and daughters (Černá and Bartak, 2019). In the case of the Swedish KBS-3 repository concept, a maximum dose outside the container of less than 500 mGy h^{-1} was calculated. The dose is dominated by Cs-137 (SKB, 2006b). The gamma and neutron radiation are expected to be significant for approximately 1,000 years post deposition (SKB, 2006b). Lundgren (2004) calculated an average dose rate outside the copper container of 100–150 mGy h^{-1}. In contrast, the latest Canadian and Belgian HLW concepts predict a maximum surface dose rate of 1 Gy h^{-1} and 25 Gy h^{-1}, respectively (Kursten et al., 2017; King and Behazin, 2021). Therefore, a low ionizing radiation is expected for a longer period.

Radiation, independent of its source, affects biomolecules like nucleic acids, proteins, and lipids directly or indirectly (Jung et al., 2017). The ionizing particles can directly damage DNA. The indirect effect considers the impact of secondary reactive species produced by ionizing radiation. The indirect effect concerns the aqueous solution chemistry of water radiolysis products, which produces reactive oxygen species (ROS)—hydroxyl radicals ($^{\bullet}OH$), ionized water (H_2O^+), hydrogen radicals ($H^{\bullet}$) and hydrated electrons (e^-), followed by secondary ROS products, superoxide ($O_2^{\bullet -}$) and hydrogen peroxide (H_2O_2)—formed within 1 ps (10^{-12} s) after irradiation (Daly, 2009; Jung et al., 2017).

Microbial radiation resistance includes a combination of diverse defense mechanisms. One of them is the DNA repair system, which includes unique DNA repair signaling components, constitutively activated or expressed DNA repair machinery, or the presence of a polyploid chromosome set (Jung et al., 2017). Another mechanism is the enzymatic antioxidant system, which has a higher activity or expression of ROS-related proteins. Finally, the non-enzymatic antioxidant system comprises a high intracellular concentration of inorganic solutes, high Mn/Fe ratios, and pigments (Jung et al., 2017).

Microbial radiation sensitivity also depends on other factors (van Gerwen et al., 1999; Shuryak et al., 2017). One factor is the type of ionizing radiation, such as acute ionizing radiation (AIR) or chronic ionizing radiation (CIR) (Shuryak et al., 2017). Other factors are cell concentrations, physiological and genetic features, and the ability to apply defense mechanisms (Jung et al., 2017; Shuryak et al., 2017). It was also demonstrated that certain resistant microbial cells can protect radiosensitive cell types (Shuryak et al., 2017). In addition, the vegetative state of the microbial cell has an influence on microbial radiation sensitivity because spores have a radiation tolerance that is many times higher than that of vegetative cells (van Gerwen et al., 1999).

The radiation resistance of a microorganism is commonly measured by the decimal reduction dose (D10). This is defined as the radiation dose (kGy) required to reduce the number of that microorganism by one log (reducing 90% of the total number) (van Gerwen et al., 1999). The average D10 dose for most vegetative microorganisms was estimated to be 0.420 kGy, although it varies significantly between species and even strains (van Gerwen et al., 1999). Organisms with high radiation resistance were discovered within the three domains of life (Bacteria, Archaea, and Eucarya) (Jung et al., 2017). The most popular representative within the domain Bacteria is *Deinococcus radiodurans*, which was formerly named *Micrococcus radiodurans* and can survive high doses of gamma radiation (~17,000 Gy) (Daly, 2009). Studies on *D. radiodurans* revealed that in the non-enzymatic antioxidant defense system, the high cellular content of manganous ions play a major role (Daly, 2009; Sharma et al., 2017). Another example of a radiotolerant bacterium is *Kinecoccus radiotolerans*, which was isolated from a high-level radioactive waste cell at the Savannah River Site in Aiken, South Carolina. This indicated high levels of resistance to gamma radiation and desiccation (Philipps et al., 2002). The domain Archaea includes microorganisms from extreme hydrothermal or highly saline environments. For example, the extremophile *Thermococcus gammatolerans* was isolated from an enrichment of hydrothermal chimney samples collected at the Guaymas Basin that were submitted to gamma irradiation at a dose of 30 kGy (Jolivet et al., 2003). Halophilic archaea from the genus Halobacterium are highly resistant to desiccation, high vacuum, and Co-60 gamma irradiation (Kottemann et al., 2005). The *Halobacterium* sp. is able to repair extensive double-strand DNA breaks (DSBs) in its genomic DNA within hours of damage induction. The gamma resistance depends on the growth stage, with cultures in earlier stages exhibiting the highest resistance

(Kottemann et al., 2005). Furthermore, membrane pigments, specifically bacterioruberin, offered protection of *Halobacterium* sp. against cellular damages induced by high doses of gamma irradiation (5 kGy) (Kottemann et al., 2005).

Within the domain Eucarya, a radiation-resistant intraspecies of the filamentous fungus *Alternaria alternata* appears. Several strains originating from the highly radiation-polluted reactor of the Chornobyl (Ukraine) Nuclear Power Plant possess high radiation resistance. Genomic investigations showed that these strains are genetically adapted to this high-radiation habitat by means of selection, thus providing a natural source of genetically homogeneous fungal lineages (Mironenko et al., 2000). Melanized fungi, such as *Cryptococcus neoformans*, also belong to the radiation-resistant fungi. It was even postulated that melanin could employ γ-radiation as an energy source by converting electromagnetic energy into chemical energy and that this might increase the growth of melanized fungi (Dadachova and Casadevall, 2008).

Taken together, organisms with high radiation resistance were discovered within all three domains of life (Bacteria, Archaea, and Eucarya), and the extreme ionizing radiation resistance originates in most cases from a combination of DNA repair systems and enzymatic as well as non-enzymatic antioxidant processes (Jung et al., 2017). In addition, tolerance to radiation might be a common phenomenon among extremophile microorganisms (including thermophiles and halophiles), which must have evolved mechanisms to survive extreme environmental conditions such as desiccation. Furthermore, most of the organisms described above were detected in radioactively contaminated areas. Survival data from pure culture studies may not be fully applicable to the relatively nutrient-limited environment of a DGR, where different species of the community will be competing and where radiation is highly probably not the only selective stress (Černá and Bartak, 2019).

Gamma irradiation is also a common method used to sterilize rocks, soils, and sediments when it is necessary to distinguish between biotic and abiotic processes in laboratory experiments (Otte et al., 2018). Such studies give us additional information about how a natural microbial ecosystem reacts to the presence of radiation. The effects of ionizing radiation exposure on soil biota were studied by exposing soil microcosms to weekly bursts of Co-60 gamma radiation over 6 weeks (three levels of exposure: 0.1 kGy/h/wk [low], 1 kGy/h/wk [medium], and 3 kGy/h/wk [high]). The results showed that the bacterial diversity decreased. The diversity of fungi and algae, however, increased unexpectedly, and the functional gene diversity of algae, bacteria, fungi, and total biota increased as well. In addition, large overall changes in community composition were observed after radiation exposure, and several potential novel radiation-tolerant groups, such as Deinococcus-Thermus, phyla Chloroflexi (bacteria), Chytridiomycota (fungi) and Nanoarcheota (archaea), were identified (Ogwu et al., 2019).

Brown et al. (2015) studied the effect of ionizing radiation (8 weeks, 0.5 Gy h^{-1} or 30 Gy h^{-1}) on microbial communities in sediment systems. Results indicate that biogeochemical processes are likely not restricted by dose rates in such environments, and electron-accepting processes may even be stimulated by radiation. The effect of gamma radiation on the viability of a soil microbial community under conditions similar to those on the Mars surface was investigated by Cheptsov et al. (2018). Doses of gamma radiation of 100 kGy under −50°C and 1 Torr were applied. In this case, the irradiation did not result in the death of the microbial community. On the contrary, the number of living cells, metabolic activity, and functional diversity remained high. Most soil bacteria are eliminated by 20 kGy. A dose higher than 70 kGy, however, may be required to kill certain radio-resistant bacteria (McNamara et al., 2003). Furthermore, it was also mentioned that γ-irradiation might not be an appropriate method for all experiments as it can influence soil chemical properties, in particular, soil nitrate and ammonium levels (McNamara et al., 2003). To sum up, low doses of radiation influence biogeochemical processes, microbial diversity, and activity in natural rock, soil, or sediment environments, but these will not be completely restricted. However, a radiation dose higher than 70 kGy will effectively eliminate the bacterial presence in various soil materials. A high dose for a relatively short period represents only one aspect of radiation resistance. However, nuclear waste disposal in a deep geological repository is associated with chronic low-dose irradiation. Many microorganisms can grow under chronic gamma ionizing radiation dose rates of 13–126 Gy h^{-1}, but this does not mean that they can cope with acute ionizing radiation (Shuryak et al., 2017). Bacteria and fungi that exist in extremely radioactive waste and contaminated sites (e.g., Hanford, Chornobyl, Fukushima) must cope with chronic ionizing radiation. The diversity of bacterial communities exposed to radioactive contamination in Chornobyl soils was examined by a combination of culture-independent and culture-dependent approaches (Chapon et al., 2012). Both highly and weakly contaminated soils contained highly diverse bacterial communities, suggesting that long-term exposure to radionuclides does not lead to the extinction of bacterial diversity (Chapon et al., 2012). Subsequent analysis based on next-generation sequencing revealed profound changes in community composition at the phylum and operational taxonomic units (OTUs) levels and higher diversity in the trench soils than the outside and identified specific phylotypes affiliated to the phyla Crenarchaeota, Acidobacteria, Dormibacteraeota (formerly AD3), Chloroflexi, Proteobacteria, Verrucomicrobia, and Eremiobacterota (or WPS-2), which were unique for the trench soils (Theodorakopoulos et al., 2017).

In the multi-barrier concept, the buffer material at the interface with the container plays an important role regarding the radiation's effects on the mineralogy, its barrier performance, and the microbial communities. Bentonite is a suitable buffer material for clay and crystalline host rocks. Chemical and mineralogical analyses and physical testing of bentonite MX-80 after heating to 130°C with and without gamma radiation showed only insignificant alteration in the smectite content and physical properties (Pusch et al., 1992). The radiation sensitivity of naturally occurring microorganisms in bentonite and the sensitivity of *Bacillus subtilis* spores and *Acinetobacter radioresistense* in a buffer matrix were studied by Stroes-Gascoyne et al. (1995). The D10 values at a dose rate of 100 Gy min^{-1} were between 0.65 kGy and 1.68 kGy in these experiments.

Within the EU project Microbiology in Nuclear waste Disposal (MIND), the deliverables D1.2 and D1.3 reported the effects of radiation and microbial degradation of organic polymers and bitumen in low- and intermedium-level wastes. The effect of gamma radiation and pressure on the indigenous microbial

community in bentonite type BaM (Keramost, Czechia) enriched with granitic porewater VITA from the Josef Underground Research Center (Czechia), a natural source of anaerobic SRB, was studied. Microorganisms that adapted and survived under harsh conditions underwent further selection caused by gamma radiation. Notably, the application of a 19,656 Gy dose absorbed at a constant dose rate of 13 Gy h^{-1} did not completely eliminate bacteria in a bentonite suspension. A decline in the total microbial biomass but not species richness was observed. Minor changes in the microbial community structure were also noted (Černá et al., 2015). The results imply that some of the bacteria naturally present in bentonite are radiation resistant. However, the evolution of microbial communities under long-term low-level and high-level irradiation must still be investigated by long-term experiments under repository conditions, including the effect of irradiation and compaction of bentonite.

4.3 Inhibition of microbial activity and growth by bentonite

Natural and commercial uncompacted bentonites harbor a diverse microbial community, including SRB (Masurat et al., 2010; Lopez-Fernandez et al., 2015; Matschiavelli et al., 2019). The number of culturable cells (SRB and others) varies among different types of bentonites. For SRB, this number was correlated with the initial water content of the bentonite (Haynes et al., 2018; Vachon et al., 2021). Cultivation-based approaches are biased toward the species that can be cultivated and fail to detect viable but non-culturable species. Nevertheless, the indigenous bentonite microbial community is shown to be able to survive extreme conditions such as high pressures, high temperatures, and high levels of gamma irradiation (Masurat et al., 2010; Haynes et al., 2018). The number of culturable SRB depends on the treatment and the type of bentonite. Wyoming bentonite harbors the least amount of culturable SRB (Haynes et al., 2018).

The highly compacted bentonite buffer in a geological waste repository is expected to play an important role in precluding microbial activity due to its high swelling pressure and low water activity (Pedersen et al., 2000; Stroes-Gascoyne et al., 2010). Microbial activity may be limited when the water activity remains below 0.96 (Pedersen et al., 2000). Desiccation results in membrane disruption, denaturation of proteins and enzymes, and DNA damage. However, many bacteria have developed mechanisms to mitigate stress induced by desiccation by increasing the production of exopolysaccharides, changing the composition of the membrane, improving the stability of proteins, reducing oxidative stress, and repairing DNA damage (Esbelin et al., 2018; Greffe and Michiels, 2020). There seems to be a large overlap between responses to desiccation and radiation. For example, mechanisms that govern tolerance to desiccation are believed to be responsible for the high levels of radiation resistance in *D. radiodurans* (D_{10} = 16 kGy), the model organism for radiation resistance (Daly et al., 2007).

The high swelling pressure generated at high bentonite densities imposes space limitations, which interfere directly and indirectly with microbial growth and activity. Direct effects occur if the pore spaces are too small to enable the presence of microbial cells. Pore throats with a diameter >0.2 μm are essential to sustain microbial activity in subsurface environments (Fredrickson et al., 1997; Rebata-Landa and Santamarina, 2006). A decrease in pore space results in diffusion-limited nutrient transport. As microorganisms themselves become immobile in such conditions, access to nutrients is restricted, and microbial growth is inhibited (Kiczka et al., 2021). The decreasing rate of water inflow when the bentonite reaches its saturation state further limits transport. Full saturation of the bentonite, however, may take several years, and microbial growth was observed during the saturation phase. Nevertheless, no growth of SRB was observed during this phase, putatively due to the persistence of O_2 (perhaps as an adsorbed species) in the bentonite (Burzan et al., 2022).

Both water activity and swelling pressure depend on the dry density of the bentonite (Stroes-Gascoyne et al., 2007; Villar and Lloret, 2008). Water activity in bentonite decreases as the density increases in response to interactions with solutes and the adsorption of water to mineral surfaces (Stroes-Gascoyne et al., 2007). On the other hand, swelling pressure increases with increasing dry density (Kaufhold et al., 2015). As long as the bentonite buffer maintains a uniform dry density ≥1,600 kg m^{-3}, microbial activity is expected to be inhibited (Stroes-Gascoyne, 2010; Stroes-Gascoyne et al., 2011). However, the fundamental determinants of the threshold bentonite dry density at which microbial activity is inhibited remain unknown. It remains unclear why different boundaries are observed in different bentonites (Pedersen et al., 2000; Stroes-Gascoyne, 2010; Bengtsson and Pedersen, 2017). Furthermore, high density does not necessarily eliminate a viable microbial population in bentonite, and upon expansion of compacted bentonite into a void, the resulting reduction in dry density stimulated or restored microbial cultivability (Stroes-Gascoyne et al., 2011). Microbial viability at interfaces is comparatively much higher than that in bulk clay material as interfacial regions provide a more favorable environment with increased access to nutrients and water (Stroes-Gascoyne et al., 2002; Pedersen, 2010; Jalique et al., 2016). Long-term persistence of microorganisms has also been observed in laboratory and *in situ* experiments (Jalique et al., 2016; Bengtsson et al., 2017a; Bengtsson et al., 2017b; Burzan, 2021). Cultured species are often known as spore-forming bacteria, which could facilitate their long-term persistence (Jalique et al., 2016; Haynes et al., 2018; Vachon et al., 2021). Sporulation enables microorganisms to withstand unfavorable and potentially lethal environmental conditions by becoming metabolically inactive until conditions become more favorable for vegetative growth. The triggers that control endospore formation are still unclear (Hutchison et al., 2014).

Bentonite is considered a limited nutrient environment with very low amounts of available organic carbon, mainly composed of plant-derived waxes and highly aromatic carbon with low contributions from small molecules (Marshall et al., 2015). Based on the molecular-level analysis of the organic matter, it is believed to be recalcitrant for microbial reproduction. However, recent analysis showed the presence of alkanes, toluene, and other aromatic compounds, which are known as potential energy sources for microbial metabolism in bentonite. The amount of these more easily accessible electron donors, however, is not known (Pedersen, 2017; Matschiavelli et al., 2019). A recent study

showed that dissolved organic material from different types of bentonites is able to sustain a sulfate-reducing microbial community (Maanoja et al., 2020; Maanoja et al., 2021). Another possible mechanism to fuel sulfate reduction is autotrophic growth with H_2 as an electron donor and CO_2 as a carbon source (Muyzer and Stams, 2008). In turn, heterotrophic microorganisms can use the organic carbon generated by autotrophic hydrogen-oxidizing SRB. Hydrogen can originate from the radiolysis of water and the anoxic corrosion of steel but also from microbial metabolism, such as fermentation processes (Smart et al., 2001a; Smart et al., 2001b; Bagnoud et al., 2016). Hydrogen has been shown to fuel sulfate reduction in bentonite microcosm experiments (Matschiavelli et al., 2019). However, H_2 consumption within bentonite as a function of dry density remains inconclusive.

Based on this literature review, it is tempting to design experiments that capture repository conditions to assess the potential for microbially influenced corrosion of canisters. Such experiments would consider either pre-compacted bentonite or bentonite at a target dry density and physically, chemically, and biologically relevant conditions. However, such experiments preclude the real-time monitoring of processes and require appropriate controls that detangle the role of microorganisms. Furthermore, the timeline is an important parameter as transient processes are expected that could impact the overall conclusion. Bringing together all these conditions in a meaningful way is a considerable challenge.

5 Novel technological concepts for nuclear waste disposal canisters

Several different types of metallic and non-metallic materials have been, and continue to be, considered as candidate container materials. Each material has advantages and disadvantages, which are briefly reviewed here, along with a discussion of the prospects for continued development.

5.1 Ceramic materials and coatings

5.1.1 Ceramic containers

The minimization or complete avoidance of hydrogen generation due to metallic corrosion is one of the reasons for the evaluation of alternative solutions, such as that provided by bulk ceramic containers or ceramic coatings (Landolt et al., 2009).

The use of ceramics for nuclear waste disposal containers was first seriously considered in the 1970s (Mattson, 1980; Bienek et al., 1984) and has continued to be an option since the early 2000s (Adams et al., 2000; Wötting and Martin, 2007; Holdsworth, 2013; Kerber and Knorr, 2013; Baroux and Martin, 2016), albeit apparently without a high level of commitment. There seems to be insufficient motivation to invest in research, which would be necessary to overcome known difficulties when feasible metallic solutions have already been recognized (Holdsworth, 2013). The reluctance of ceramic component manufacturers to invest without external support is almost certainly due in part to insufficient customer demand for large ceramic pieces. Nevertheless, there have been significant developments relating to the consideration of ceramics as a candidate nuclear waste disposal canister material.

While ceramics are an attractive option in terms of their high corrosion resistance and lack of gas production, their low mechanical strength and fracture toughness are the principal issues to tackle for a disposal container application. Although the existing press and sintering furnace capacities around the world limit the size of the canister sections that can be manufactured, such limitations can be overcome with adequate investment. However, the main manufacturing challenges to be overcome through systematic development include i) efficient handling of very large lumps in both the green state immediately after shaping (before sintering) and during any retrieval operations that may be required and ii) achieving adequate density (porosity levels) and minimal flaws with section thicknesses ≥~40 mm. Moreover, achieving effective sealing of thick ceramics will never be possible without significant research and development. With no demand for large-diameter ceramic pressure vessels from any other industrial sector, funding for such R&D can only come from the nuclear waste disposal community. Recently, there have been significant changes related to the consideration of ceramics as a candidate material for containers for nuclear waste disposal (Holdsworth, 2013), and they have been comprehensively analyzed (Holdsworth et al., 2014). Potential ceramics candidates for nuclear waste disposal canister applications are alumina (Al_2O_3), pure or in combination with silicon oxide (SiO_2) (Baroux and Martin, 2016) (Mattson1980), silicon carbide (SiC) (Wötting and Martin, 2007; Kerber and Knorr. 2013), silicon nitride (Si_3N_4), partially stabilized zirconia (PSZ), and titania (TiO_2) because of their chemical stability, reasonable mechanical properties, and ready availability (Wilfinger, 1994). At present, the main attention is paid to the alumina (Al_2O_3) and the SiC solutions.

5.1.2 Alumina

The development of alumina or alumina-silica canister ceramics has been the subject of several studies.

5.1.2.1 SKB (Sweden)

A patent by Larker (1980) presents a concept of a ceramic-metal capsule. In this concept, the waste (in the form of spent fuel or vitrified waste) is placed in the alumina capsule, consisting of an open container and a cover fitting the open end of the container. These two parts are produced from ceramic powder material (alumina), which is then compacted by hot isostatic pressing (1,300°C–1,400°C, 0.5 kbar–2 kbar). The capsule is then enclosed in a gas-tight metal casing and joined by means of hot isostatic pressing (at the same pressure and temperature conditions as described for the compaction of the container and the cover fitting) to obtain a homogeneous monolithic body. The developed capsule allows waste to be stored in a single cavity or multiple separate ones. A thermal insulating material can be placed between the waste and the body of the ceramic container to limit the temperature in the vicinity of the waste during the closure phase of the capsule. A ceramic insert is placed in the lid of the container to mechanically reinforce the sealing area.

5.1.2.2 Lawrence Livermore National Laboratory (USA)

In the early 1990s, the Lawrence Livermore National Laboratory was commissioned to study alternative solutions to metal containers for the geological disposal of radioactive waste at Yucca Mountain (Wilfinger, 1994). Two exploratory paths were chosen:

- bulk ceramic containers
- composite containers: a metal structure for mechanical strength and a ceramic coating/liner for chemical durability

The specifications state that these cylindrical containers (5.50 m high and 1.80 m in diameter) have no transport function and will be placed "nose to nose" in horizontal tunnels dug into the rock. They must allow for the storage of spent fuel assemblies or vitrified waste, be identifiable and retrievable for 50 years, and be leakproof for 300 to 1,000 years. The closure system of these containers must be feasible remotely in a radiation hot cell without thermal damage to the waste package. Different selection criteria were identified for the materials and associated manufacturing processes on the basis of these specifications:

- Good tensile strength and impact resistance of the material.
- High toughness.
- Dense material with no open pores or cracks.
- Joint or weld areas must have the same properties as the body material.
- Good chemical resistance of the material in the storage environment.
- Sufficient thermal conductivity to remove heat from the waste.
- Use of conventional processes requiring only minor adaptations.

For the last two criteria, the difficulty of manufacturing large ceramic parts was highlighted. Cost was not the primary criterion but must be taken into account. The authors point out that these developments of large objects will require development time.

5.1.2.3 BNL/Nucon (USA)

In the late 1990s, the Nucon company developed containers for the transport and storage of nuclear waste in the USA (Rockhvarger and Khizh, 1998; Rockhvarger and Khizh, 1999; Rockhvarger and Khizh, 2000). These containers, based on the Russian doll system, were composed of a multilayer system ensuring radiological, mechanical, and corrosive protection of the encapsulated waste both during transport and for geological disposal of the waste. The different liners used were:

- a first ceramic container that encloses the waste. This first structure acts as a thermal, chemical, and radiological protection,
- a second ceramic liner acts as a mechanical and corrosion barrier, and
- the space between these two ceramic bodies is filled with graphite or metal powder, which acts as a radiation shield.

Two concepts were proposed depending on the size of the waste to be encapsulated (Rockhvarger and Khizh, 2000).

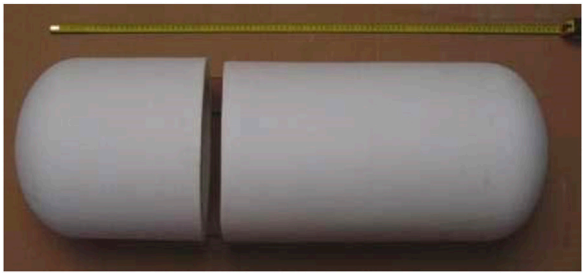

FIGURE 8
Half-scale model of Al_2O_3/SiO_2 VHLW canister. The tape measure is unrolled to 1 m for scale (Baroux and Martin, 2016).

The watertight sealing of ceramic containers made of $MgAl_2O_4$ is based on a microwave process. The sealing is carried out using a ceramic paste of the same composition as the parts to be joined. This paste is doped to promote the absorption of microwaves by the material (hydrogenation of the powder).

The switch to compounds doped with ceramic fibers is envisaged. In addition to the mechanical reinforcement of the container, the addition of ceramic fibers can favor the thermal treatment of the material (e.g., SiC, which has a high permittivity value and is preferentially heated during microwave heat treatment) or increase the radiological properties of the container (addition of boron nitride).

5.1.2.4 Andra (France)

The first part of the work (2007–2009) focused on the development and characterization of alumino-silicate ceramics with leaching resistance and mechanical properties superior to conventional silicate ceramics (Baroux and Martin, 2016):

- the development of a ceramic with an alumina-rich composition that meets the required physical and chemical properties. After chemical characterization using pure water Soxhlet tests at 100°C and column tests in Callovian-Oxfordian deep groundwater at temperatures between 50°C and 90°C, it was concluded that the chemical durability of the ceramic was suitable, with an effective thickness reduction of ~3–4 mm over a period of 1,000 years.
- the design (shape and thickness) of a container for high-activity nuclear wastes adapted to the ceramic material.
- the development of casting, drying, and sintering processes adapted to these thick ceramic parts.

These developments have made it possible to demonstrate the feasibility of the body and lid of a ½ scale, 4-cm-thick container (Figure 8). This constitutes a real advance compared to the current state of the art in the industry.

The technological roadblock for these new silico-alumina containers remains the closure of such a system. Current studies focus on the development of a sealing technology adapted to the application, with constraints associated with the vitrified waste and the watertightness of the waste disposal container (Kalfayan, 2019). In order to preserve the containment properties of the glass matrix of the waste, the sealing process must meet two major constraints:

- a maximum temperature of 450°C for the vitrified waste
- a heating technology localized to the closure area.

One of the ways identified to assemble ceramic parts is to use the interaction of a dedicated sealing material (ceramic or glass) and microwaves to locally heat the joining area until the sealing material melts, in order to achieve a tight weld. Much work is currently being performed on the sintering of ceramic materials, in particular for alumina (Clark and Sutton, 1996; Zhang and Datta, 2003; Zymelka, 2013). These works resulted in a better understanding of these microwave/material interactions. This process can now be considered for the welding of ceramic specimens with an alumino-silicate composition. The work carried out since 2014 made it possible:

- to improve the quality of the ceramic/glass sealing interface via a two-stage enameling process: first firing in a conventional furnace, then sealing the enameled parts by microwave heat treatment. The process can then be industrialized with this pre-firing, which can be carried out by the manufacturer supplying the ceramic container,
- to confirm that the selected and tested sealing materials have processing temperatures compatible with the constraints imposed by the presence of the primary package,
- to confirm the feasibility of sealing by microwave heating (no influence of the microwave frequency on the process, and the sizing of a furnace will not be limited by the wave–material interaction),
- to make a clear improvement in the quality of the joints for heating under minimal load, and
- to verify the viability of the process, a study was carried out with an industrial manufacturer of microwave ovens. An industrial prototype was designed, taking into account the size of the full-scale container and the localized heating constraint.

With a view to going further and designing and testing a first prototype to reinforce the proof of concept, the following avenues are being considered:

- to produce a prototype furnace for testing the annular shapes of test bodies and the localized heating of these parts,
- to understand the resistance of the ceramic to the thermal gradients resulting from localized heating, and
- to optimize the compositions of sealing materials to reinforce their mechanical and leaching resistance (example: glass-ceramics).

5.1.3 Silicon carbide

It has previously been shown that SiC is a viable option for container fabrication (Knorr et al., 2008; Holdsworth, 2013). Until recently, it was only feasible to manufacture large pieces out of silicon-impregnated silicon carbide(SiSiC) and recrystallized silicon carbide (RSiC). However, there is now the possibility of making larger pieces from conventional sintered silicon carbide (SSiC) (Kerber and Knorr, 2013) and even high-strength grades of SSiC (Wötting and Martin, 2007).

The study of SiC behavior (as material for SF/HLW containers) under aggressive conditions is highly relevant. Nowadays, the world's leading R&D centers make corrosion resistance tests of SiC and SiC with various alloying additions under conditions simulating the various environmental conditions.

In 2018, two companies, General Atomics and Westinghouse Electric, conducted corrosion tests of modern fuel pipes made of SiC/SiC composites under conditions of normal operation of water-cooled reactors (Deck et al., 2018). The composition of the liquid in the autoclave during the tests corresponded to different types of coolants, and the tests were carried out for 3 months. The results obtained indicate that SiC has a high corrosion resistance; the authors calculated the dissolution rate of 1 μm per year, which is approximately 1% of the total thickness of the fuel cladding.

The positive effect of Cr on the corrosion resistance of SiC ceramics (Lobach et al., 2020) was experimentally shown under conditions simulating the inner environment of a VVER-1000 reactor. It was shown that doping of SiC with Cr decreases the dissolution rate of SiC(Cr) compared to SiC without additives due to the formation of corrosion-resistant products (Cr_2O_3) that significantly affect the ability of SiO_2 films to passivate the surface of the samples. Also, it should be noted that Lobach et al. (2018) showed the effect of Cr additives on the mechanical properties of SiC and found that doping of SiC with 0.5 wt.% Cr leads to an increase in fracture toughness (K1c) by 25%–50% (from 4.2 MPa $m^{1/2}$ to 6.2 MPa $m^{1/2}$), while maintaining a high level of hardness with a value of 28.0 GPa.

The results of scientific research indicate that SiC-based ceramics have high corrosion resistance in hydrothermal conditions and are promising for use as a material for fuel claddings. Despite the fact that the leaching tests of SiC were carried out under severe conditions (350°C, 16.8 MPa), there is a need to study the mechanisms of corrosion processes in the system (SiC–compound–SiC) under the conditions simulating geological disposal (t = 90°C) because the interconnection of SiC segments is an important issue. There are two most promising approaches:

- The laser joining method (Knorr et al., 2008) is based on a combination of pure oxidic braze filler (trademark: CERALINK®) and a laser beam. The filler inside the joining zone is melted locally by using a laser beam. CERALINK® shows an ideal wetting of the ceramic surface and high oxidization resistance. The ceramic joint surface does not need pre-treatments (no metallization). This article indicates that the joints obtained are gas-tight, have high mechanical strength, and have no cracks. Joining surfaces does not require preliminary treatment, and
- Soldering based on various materials (for example, glass-ceramic). Wang et al. (2020) joined SiC/SiC composites using the material Y_2O_3-Al_2O_3-SiO_2 (YAS). Shear strength tests showed an increase in the strength of the joining with increasing soldering temperature; maximum strength reached 51.7 MPa at a soldering temperature of 1,400°C.

5.2 Ceramic coatings

The main requirement of a ceramic coating applied to a carbon steel (or cast iron) nuclear waste disposal canister is the prevention, over a period from a few hundred to several tenths of thousands of years, of access of pore waters to the substrate via cracking or leaching (Holdsworth et al., 2018). Ceramic coatings for SF/HLW disposal canisters appear to be less mature than metallic coatings. The main issues to be addressed are related to the inherent brittleness of ceramics, the mismatch of thermal expansion coefficient with the underlying steel, the requirement for very low porosity, the adherence to the substrate, and the abrasion resistance. Nevertheless, yttria-stabilized zirconia or graded multilayer coatings of alumina and titania appear to be promising options that would require additional development before their feasibility can be better assessed. Irrespective of the selected ceramic coating material, methods for covering the lid-to-canister weld and for coating repair would also need to be developed.

Physical vapor deposited (PVD) coatings usually provide good corrosion protection compared to coatings that are deposited by traditional spraying. Despite the smaller thickness of the PVD coatings, they have much lower through porosity than the coatings deposited by spraying. Also, a serious advantage of the PVD methods over the methods of electrochemical deposition is the environmental friendliness of the process.

5.2.1 Titanium oxide-based coatings

The most studied class of high-hardness coatings formed by the PVD methods (magnetron sputtering and cathodic arc evaporation) are titanium nitrides and carbides. Problems in the synthesis of various metal oxides by the vacuum arc method were discussed in a review (Tay et al., 2006). Previously, the Kharkiv Institute of Physics and Technology (KIPT) developed vacuum-arc nanostructured TiO_2-based coatings (structure–anatase) with controlled bactericidal activity for orthopedic implants (Belous et al., 2013). The influence of the negative bias potential of the substrate was investigated by the authors (Belous et al., 2018). It is shown that titanium coatings deposited in an oxygen medium under pressure of 0.03 Pa produce a dispersed system of oxides, the composition of which depends on the magnitude of the bias potential on the substrate. The results of electrochemical measurements show that the current density characterizing the dissolution of steel coated with titanium nitrides and oxynitrides thickness of ~6 μm is one-half to one order of magnitude lower than for uncoated steel. With an increase in the coating thickness to 12 μm, the samples corroded more slowly, which correlates to a decrease of the coating porosity, with the corrosion current density decreasing by 2–3 orders of magnitude. The highest corrosion resistance was observed in the samples with a coating thickness of ~12 μm deposited from the oxygen and nitrogen mixture at an oxygen pressure $P_{O2} = 3 \times 10^{-2}$ Pa. These coatings provide high corrosion resistance of steel close to that of a pure titanium nitride coating in a 3% aqueous solution of NaCl (Belous et al., 2018). The anodized and thermally oxidized Ti samples with TiO_2 coatings showed relatively high corrosion resistance in 4M HCl and 4M H_2SO_4 solutions at 100°C ± 5°C, and the passive current density of the thermally oxidized samples was five orders of magnitude lower under the electrochemical testing condition than that of the anodized titanium sample (Minhas et al., 2021). The protection against corrosion provided by the conversion layer combined with TiO_2 coating on stainless steel in pure water and saline solution was quite good (Bamoulid et al., 2008). The corrosion test results showed that TiO_2 films deposited on $MgCa_2ZnGd_3$ effectively protect this alloy from corrosion in Ringer's solution at 37°C (Kania et al., 2021). While it is difficult to relate these qualitative electrochemical corrosion data to long-term repository performance, it can be assumed that titanium oxide coatings deposited by PVD methods are promising for the corrosion protection of carbon steel containers. Additional studies are needed on the mechanisms of long-term corrosion processes in the TiO_2 coating-steel substrate system under conditions simulating geological disposal.

5.2.2 Chromium nitride coatings

Chromium nitride (CrN) has proven to be one of the most successfully and extensively used PVD coatings in the industry due to its high hardness, excellent wear resistance, and remarkable stability against corrosion (Milošev et al., 1997). The CrN coating deposited on AISI 304 stainless steel possesses high corrosion resistance in 0.5 M H_2SO_4 solution and 0.5 M NaCI solution (Milošev and Navinšek, 1993). The demand for high-quality coatings in recent years has led to intensive research into the further evolution of chromium-based coatings (Cedeno-Vente et al., 2021). Daub et al. (2015) provided a comparative analysis of corrosion resistance of 2–4 μm-thick CrN-, TiAlN-, and AlCrN-coated Zry-4 alloy. It was shown that CrN demonstrates better overall performance in both aqueous and steam environments. CrN coatings on Stellite™ (cobalt-based alloy) samples showed excellent wear and corrosion resistance in high-temperature and high-pressure water when exposed to γ-irradiation at a dose rate of 100 Gy/h using a ^{60}Co source (Kawana et al., 1996). The Co elution rate from Stellite decreased drastically with film thickness, up to about four orders of magnitude for a CrN coating thickness of 7 μm. This is the only publication known to us where the effect of γ-radiation on the corrosion resistance of coatings has been studied. Chromium nitride coatings are promising for corrosion protection of carbon steel, but additional studies are needed on the long-term corrosion processes in simulated geological disposal conditions.

5.3 Metallic materials and coatings

5.3.1 Metallic containers

The concepts for deep geological disposal in Finland, Sweden, Canada, Korea, and Switzerland propose copper as an outer barrier material for containers. Several other metallic materials have been investigated as candidates for containers, such as carbon steel, stainless steel, nickel, and titanium alloys. Several extensive review reports and articles have been made comparing the metallic candidate materials (King et al., 2016; Padovani et al., 2017). In these reports, the key properties and engineering aspects of candidate materials are extensively presented together with their interactions with certain geological environments. This chapter aims to summarize the main aspects of scientific interest in these material candidates and give background for the motivation

behind studies on the corrosion of new materials and material grades.

Commonly considered corrosion phenomena impacting metallic containers are general corrosion, pitting corrosion, hydrogen-induced cracking (HIC), and stress corrosion cracking (SCC). The materials planned for use in the final disposal may be subjected to these corrosion phenomena, and it is recognized that their susceptibility varies between materials and environments. The corrosion phenomena listed above do not necessarily occur simultaneously but merely become relevant during the different phases of the final disposal.

Regarding mechanical aspects, tensile strength, ductility, compressive strength, creep resistance, and thermal resistance are properties that are required during the disposal phase. Sufficient tensile strength and ductility are required against external stresses that may be applied to the waste canister. Sufficient compressive strength is required against external isostatic pressure yielding, such as from hydrostatic loads. During the initial oxic phase, metallic materials may be exposed to creep due to the elevated temperature and load from the swelling bentonite, isostatic pressure of the groundwater, or residual stresses (e.g., in welds).

Properties that are required prior to the disposal phase include resistance to mechanical impact, grain size, weldability, and machinability. The waste canister should withstand a mechanical impact without fracturing if the canister is accidentally dropped during handling. The material should have a certain grain size to enable non-destructive testing by ultrasonic inspection (Raiko and Salo, 1999). Weldability and machinability are required for proper sealing of the canister and to produce the desired surface finish, respectively.

5.3.1.1 Low alloyed steels

Along with copper, steel is among the most studied canister material options. Conventional carbon steels have several benefits as they are widely available at a reasonable price and are easy to machine (Landolt et al., 2009). This enables construction with relatively thick walls that result in good mechanical strength and radiation shielding. Compared to copper, the corrosion resistance of carbon steel is low, although during the anaerobic phase, the corrosion rate of steel is low, and the prevalent corrosion mechanism (uniform corrosion) is relatively easily modeled. The SCC risk for low alloyed steels exists in carbonate–bicarbonate environments that may arise as the container cools. However, SCC could occur not only at neutral pH but also in highly alkaline environments. A carbon steel canister is considered for example, in the French, Swiss, and Belgian concepts (Patel et al., 2012; Crusset et al., 2017; Padovani et al., 2017).

5.3.1.2 Lead

Lead is studied to some extent as a candidate material for canisters in waste programs in Argentina, Brazil, and Russia, although the technical feasibility is still unclear (Xiong et al., 2021). The superior radiation shielding ability and low cost of lead is an asset. However, uncertainties lie in the corrosion behavior, mechanical strength, and especially environmental aspects of using lead. Therefore, it is not considered a potential candidate, at least in the near future.

5.3.1.3 Stainless steels

Stainless steels are passive materials for which the corrosion resistance is based on the thin passive film formed on the surface of the metal (Landolt et al., 2009). They exhibit very low, uniform corrosion rates, with the major concern being localized corrosion. It is known that stainless steel is susceptible to localized corrosion in chloride-containing solutions. Additionally, the self-healing properties of the protective passive film on stainless steel are only effective in oxic conditions.

5.3.1.4 Titanium

Titanium alloys are also passive alloys that are extremely corrosion resistant in waste disposal environments (Braithwaite et al., 1980). The uniform corrosion rate is practically negligible due to the inertness of the titanium oxide passive layer. The alloys are immune to pitting in most aqueous environments (Landolt et al., 2009). The corrosion-related challenge of titanium alloys is the crevice corrosion risk during the oxic phase and was considered as a critical failure mechanism in early studies, and the need for further research in this area is recognized (Padovani et al., 2017). However, it is also stated that the risk of crevice corrosion of titanium alloys can be avoided by using alloys with Pd or Ru (Schutz, 1996; Landolt et al., 2009). HIC has also been considered as a potential risk for titanium alloys under anoxic conditions. The absorption of hydrogen is shown to be linked to corrosion at residual impurities in grain boundaries.

5.3.1.5 Nickel alloys

There are six major groups of Ni alloys, each characterized by the principal alloying elements: Ni-Cu, Ni-Mo, Ni-Cr, Ni-Cr-Mo, Ni-Fe-Cr, and Ni-Fe-Cr-Mo. All of the alloys selected in the various international HLW/SF programs belong to either the Ni-Cr-Mo group (i.e., Alloys 625 and 22, Hastelloy C-4, and C-276) or the Ni-Fe-Cr-Mo group (Alloy 825), primarily because of their resistance to corrosion under both oxidizing (due to the presence of Cr) and reducing (due to the presence of Mo) conditions. Furthermore, Mo (and W in Alloys 22 and Hastelloy C-276) provides improved resistance to localized corrosion. Silicon can improve the corrosion performance under high-temperature oxidizing conditions through the formation of protective Si-O films. Manganese is added as a deoxidant, but it can increase the susceptibility to localized corrosion because of the tendency for film breakdown to occur at MnS inclusions (King, 2014a).

5.3.1.6 Copper

There is a wide range of copper alloys with an equally wide range of corrosion properties. Up until this point, oxygen-free copper has been primarily considered as a container material, typically with a purity of ≥99.3 wt.% (Hall et al., 2021). Almost all research to date has focused on the custom OFP copper, which is oxygen-free copper with the addition of phosphorus and is further described later in this chapter.

The copper material selected for the KBS-3 concept is specified so that it fulfills standard EN 1976:1988 (UNS C10100) for the grades Cu-OFE or Cu-OF1 with additional requirements for the concentrations for critical elements/impurities (Andersson et al., 2004). The requirements for

TABLE 2 Properties of proposed novel copper alloys (Aurubis, 2022).

	Cu-OFP	Cu-XLP	Cu-DLP	Cu-HCP
Code		UNS 103000 CW020A	UNS C12000 EN CW023A	UNS C10300 EN CW021A
Description	Very pure, oxygen-free copper	Low phosphorus content	Deoxidized, oxygen-free copper, low residual P content	Deoxidized, oxygen-free copper, low residual P content
Composition	Cu (min. 99.99 wt.%) Bi (max. 0.0005 wt.%) Pb (max. 0.005 wt.%) O (max. 0.001 wt.%)	Cu (min. 99.95 wt.%) P (0.001–0.005 wt.%)	Cu (min. 99.90 wt.%), P (0.005–0.013 wt.%), Bi (max. 0.0005 wt.%) Pb (max. 0.005 wt.%)	Cu (min. 99.95 wt.%) P (0.002–0.007 wt.%)
Typical use	Current canister material in national concept	Telecommunication cables, terminals, cladding products, busbars, electrical conductors	Architecture, roofing, components of electrical engineering, cladding band, wire, heat exchangers, transistors, air conditioners, hydraulic, and oil pipes	Telecommunication cables, terminals, clad products, busbars, base plates for power modules, electrical conductors, pressure vessels

critical elements are as follows: O < 5 ppm, P 30–70 ppm, H < 0.6 ppm, and S < 8 ppm (Andersson et al., 2004). The EN standard has a lower limit for the phosphorous content, and therefore, the name "OFE + P" has been used for the selected alloy. Table 2 lists several commercial phosphorus-containing copper alloys that could be suitable alternatives to OFP copper.

The benefits of copper are its superior corrosion resistance and good mechanical properties. The downside, especially for highly pure copper grades, is the high cost.

5.3.2 Coatings

Titanium, chromium, and copper are well-known materials for corrosion protection (Ahmad, 2006). The use of copper as a corrosion barrier has been considered for many years by many WMOs, including SKB and Posiva, and by Canada's Nuclear Waste Management Organization (NWMO) (Keech et al., 2014). In the Canadian program, the copper coating methods are still under development, and the exact composition and property requirements of the copper are not yet established.

Candidate titanium coating solutions for application to carbon steel nuclear waste disposal canisters are immune to microbially induced corrosion. Open questions for the use of titanium, chromium, and copper as protective coatings on steel substrates include the required thickness to exclude through porosity, the effect of through defects, and the effect of irradiation on corrosion resistance.

Nickel alloys are widely used in industry as corrosion barriers, and specific alloys, such as the C22 that is proposed as the waste package material for Yucca Mountain, can provide extremely low corrosion rates. Also, coating with Ni-based alloys is well developed, and numerous options exist. However, even though nickel alloys tend to be resistant to microbially induced corrosion, they are not immune, and MIC can increase the rate of general corrosion (King, 2020). Consequently, inherent uncertainties associated with MIC rates and mechanisms would be eliminated completely by adopting a different material that is known to be immune to MIC.

Titanium alloys are known to be immune to MIC (King, 2020). They also exhibit extremely low general corrosion rates and high resistance to corrosion under irradiation, and certain alloys are also immune to localized forms of corrosion (Hua et al., 2005). Titanium coatings deposited by PVD were studied mainly using electrochemistry methods (Zhou, 2012). Titanium coatings possess better corrosion resistance in both corrosive media (0.5 N NaCI and 0.5 N Na_2SO_4 + 0.1 N H_2SO_4) than uncoated steel (Zhujing et al., 1991). Hydrogen absorption as a result of anaerobic general corrosion under disposal conditions will occur. However, such processes are generally predictable, and long canister lifetimes can be expected with confidence. No study of the corrosion resistance of titanium, copper, and chromium PVD coatings on carbon steel under specific nuclear waste repository environment conditions has been published to date.

The concept of manufacturing a dual-shell container with a copper coating for corrosion protection directly on the steel structure was raised to avoid the drawbacks related to classical manufacturing approaches, including machining/forging (Lee et al., 2011; Keech et al., 2014; Legoux, 2014). There is also the possibility of creep and stress corrosion cracking of the copper shell in the case of a gap between the outer copper corrosion barrier and the steel insert with the conventional dual-shell container design (King, 2017). The benefits of a copper-coated design are as follows: no issues with tolerance of fabrication of copper part; the copper layer is produced directly on the steel part without any gap between layers; a welding joint could be covered by copper after welding the steel vessel. Several deposition processes are available.

The method reviewed here is cold spray coating (CSC), which satisfies the requirements of the dual-shell container concept: able to produce thick layers of copper on steel surfaces, guarantee a low level of copper oxidation during treatment, nd deposit copper coating on a localized surface, and can be applied in a radioactive environment. The principles of cold spray are described in the following references: Alkhimov et al. (2012a), Alkhimov et al. (2012b), Sova et al. (2013a), Sova et al. (2013b), and Sova et al. (2013c).

While the corrosion behavior of bulk copper in waste repository conditions is well known and guarantees a very long-lived containment (King, 2017; King, 2020), some further development work is required on copper cold spray coating materials both on the process itself and the materials obtained.

From a general point of view, the quality of coatings (density, absence of porosity) contributes to an increase in both the

mechanical and resistance to corrosion properties. This quality is strongly dependent on the CSC process parameters.

One of the first parameters of CSC is the nozzle displacement, in particular, the influence of nozzle traverse speed and distance between deposited tracks. It has been shown that cold spraying copper–silicon carbide powder at low nozzle traverse speed leads to the formation of thick tracks with quasi-triangular cross-sections (Matts et al., 2019). Consequently, the particle impact angle on the sides of the spraying track increases. Thus, the particle deformation at impact on the track periphery becomes insufficient, and local porosity arises. An increase in nozzle traverse speed allows for increasing coating density and mechanical properties due to the amelioration of particle deformation conditions. Compressive tests revealed significant anisotropy of the mechanical properties of copper–silicon carbide cold spray deposits. In particular, the compressive strength measured in the vertical direction (perpendicular to the substrate) was significantly higher than the compressive strength measured in the horizontal plane (parallel to the substrate). This anisotropy can be explained by the orientation of the particle deformation pattern during impact.

The carrier gas velocity and nature also have a significant effect on copper cold spray coating quality (Jakupi et al., 2015). The grain size and number of coincident site lattice grain boundaries increased, and plastic strain decreased with carrier gas velocity. Post-annealing treatment (4 h at 400°C) improved the quality of the coatings by increasing texture and coincidence site lattices but also increased the number of physical voids, especially when a low-temperature cold spray carrier gas was used. Tensile testing showed a better adherent coating to the steel substrate when He carrier gas is used instead of N_2 gas.

The mechanical performance of bonded thick copper coatings on steel has been assessed by Boyle and Meguid (2015). They showed that the mechanical performance of the annealed cold spray coatings was comparable to or exceeded that of the reference wrought copper and was suitable for the container design with adhesion strengths exceeding 45 MPa. In general, cold spray is used for the production of metal deposits. However, the possibility of deposition of metal–ceramic composite coatings by spraying different mixtures of metal and ceramic powders has also been studied (Sudharshan Phani et al., 2007; Ogawa et al., 2008; Koivuluoto and Vuoristo, 2010; Lee et al., 2017; Yin et al., 2017; Fernandez and Jodoin, 2018). In this case, the adhesion of the metal to the substrate, as well as primary matrix formation, is ensured by the plastic deformation of metal particles, whereas the ceramic particles stick to the surface by a mechanical anchoring mechanism and form hard inclusions in the softer metal binder (Koivuluoto and Vuoristo, 2010; Wang et al., 2014; Triantou et al., 2015). Previous studies showed that the addition of ceramic powder to the metal increases the coating adhesion and density and ameliorates its mechanical properties and corrosion resistance compared to the cold spray deposits of the pure metal without ceramic inclusions (Sudharshan Phani et al., 2007; Ogawa et al., 2008; Koivuluoto and Vuoristo, 2010; Wang et al., 2014; Triantou et al., 2015; Lee et al., 2017; Yin et al., 2017; Fernandez and Jodoin, 2018). Several studies also revealed increased performance in wear resistance behavior. For example, Triantou et al. (2015) compared pure copper and copper–alumina cold spray deposits and found that the wear resistance of composite deposits is higher due to the presence of alumina in the copper matrix. In addition, the hardness, density, and corrosion resistance were also improved.

No corrosion resistance study of CSC under specific nuclear waste repository environment conditions has been published to date. The environments selected for corrosion studies are NaCl solutions under anoxic or oxygenated conditions to simulate the long- and short-term redox conditions (Keech et al., 2014; Lee et al., 2011) and more or less acidic environments to quickly screen the corrosion resistance between wrought copper and cold spray copper coating (Lee et al., 2011). The corrosion behavior of Cu cold spray coatings and wrought Cu in 3 mol/L NaCl under both sets of conditions are similar (Keech et al., 2014). No evidence was observed to suggest the particle boundaries in the cold-sprayed coating were preferential corrosion sites. In more concentrated NaCl solution and acidic 10% HCl solution, the corrosion rate was slightly higher in the CSC coppers than in the commercial wrought coppers. The authors indicated, however, that more experiments, such as a field test for the CSC copper, would be beneficial to further clarify these findings.

6 Prediction tools for assessment of long-time barrier integrity

6.1 Process and performance assessment models

In radioactive waste disposal, the main aims of modeling corrosion processes of SF/HLW disposal canisters are to:

- predict the durability of the disposal canister (and the uncertainties associated with durability estimates) to provide key input into performance assessments (PAs) and
- consolidate and demonstrate a scientific understanding of the processes involved in the evolution of the disposal container and, more broadly, engineered barrier system (EBS) to underpin the treatment of container durability PAs, which are typically very simple, even if the results of the models are not used directly in PAs in any calculations of risk. A diverse range of approaches has been taken to modeling corrosion processes, mechanisms, and underpinning experimental results. These process models have been reviewed by King (2014b) in the context of spent fuel/HLW disposal containers. Reviews focusing on corrosion and the associated gas-generation processes of materials relevant to the disposal of intermediate-level waste, including metallic materials present in some wastes, are also available (Hoch et al., 2010; Smart and Hoch, 2010).

6.2 Process models

6.2.1 Copper containers

Among the process models developed for predicting the uniform copper corrosion of spent nuclear fuel canisters located in deep geological repositories, the copper corrosion model (CCM) (King et al., 2008) has been the most complete approach to the

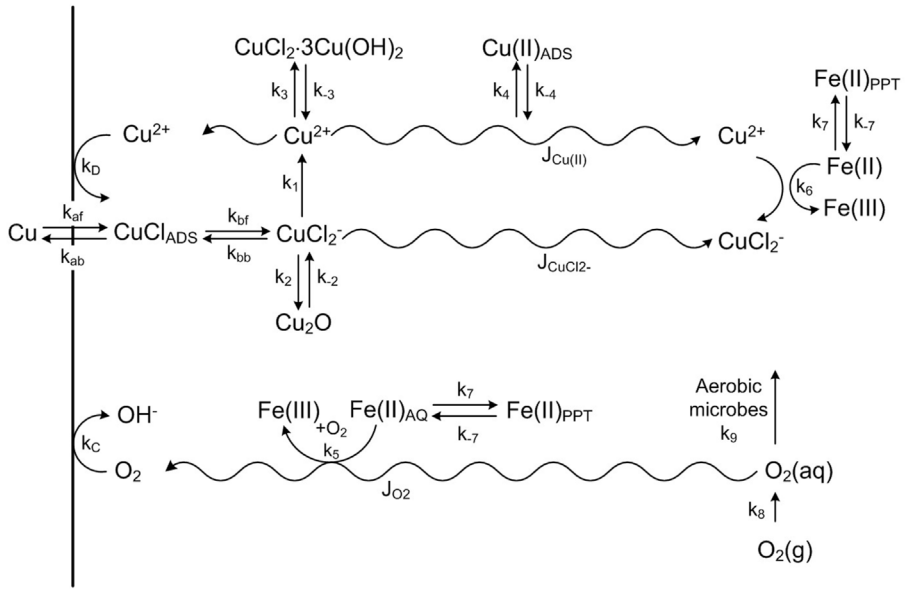

FIGURE 9
Schematic representation of the copper corrosion model (CCM). The letters j and k refer to diffusive fluxes and rate constants for various processes, respectively (King et al., 2008).

phenomenon. The model accounts for electrochemical processes at the container surface together with reactive transport and heat transfer in the near-field and provides a continuous description of the corroding environment. The equations are solved in a 1D domain using finite difference methods. The first version included the 10 most relevant species when focusing on chloride and oxygen transport-controlled corrosion (Figure 9). The model has been progressively updated (King et al., 2010) and extended to include long-term anoxic corrosion due to sulfide with the copper sulfide model (CSM) (King, 2008b; King and Kolář, 2019).

Next, several relevant issues for a proper estimation of the corrosion of copper containers are presented. Some of them have already been widely addressed by the CCM and CSM models, such as microbial sulfide production or the interaction of sulfide with Fe-bearing mineral phases, but some others need to be further analyzed and modeled. In this sense, alternative transport models in compacted bentonite have been reviewed, along with the impact of two-phase flow on sulfide fluxes in the near-field at the early transient stage during groundwater intrusion into the repository. Finally, the last sub-section is fully devoted to irradiation-induced corrosion, which might be relevant in the short term for dose rates over 100 Gy h^{-1}, according to King et al. (2010).

6.2.1.1 Reactive-transport models in compacted bentonite

The diffusion coefficient of dissolved species in compacted bentonite is known to strongly influence corrosion due to the limited mass-transport rate of corroding agents from the near-field to the metal surface. According to Wersin et al. (1994), values of pore diffusivity have an uncertainty of a factor of 10 (Brandberg and Skagius, 1991). In the CCM (King et al., 2008), Fickian diffusion is considered with an effective diffusivity that is directly proportional to empirical values of tortuosity and effective porosity of the medium (King and Kolář, 2019). In the case of sulfide, diffusivity has been estimated experimentally (King et al., 2010).

The definition of effective porosity and the assumptions regarding different types of porosity have led to several mechanistic and empirical approaches for describing the diffusion of ions through compacted bentonite. Idiart and Coene (2019) tested these models by quantifying the diffusion of the radionuclide $^{36}Cl^-$ across the bentonite backfill in the SFL repository (Sweden). The multi-porosity model (Appelo, 2013) considered three porosity types: free, electrical double layer (EDL), and interlayer, which was assumed to be inaccessible to anions due to its structural negative charge. The size of the EDL porosity was coupled with the porewater ionic strength, which made this model more computationally demanding than the alternatives. In this sense, Wersin et al. (2014) simplified the formulation by deriving an empirical expression for the effective diffusion coefficient as a function of bentonite dry density and ionic strength and considering that the interlayer porosity was also devoid of anions.

Van Loon et al. (2007) proposed an empirical approach that related the available porosity to the ionic strength of the external solution for the range between 0.01 mM and 1 mM before applying Archie's law for the effective diffusion coefficient. On the other hand, Ochs and Talerico (2004) proposed a table of values of available porosity, effective diffusivity, and distribution coefficient for 38 different elements and oxidation states.

Finally, the Donnan equilibrium model (Birgersson and Karnland, 2009) assumed a single interlayer porosity with a net positive charge to compensate for the structural negative charge of the smectite sheets. Consequently, a concentration jump appears at the clay–water interface, thus leading to limited transport of anions through the bentonite (anion exclusion), as observed in the results obtained by Idiart and Coene (2019). This hypothesis posed a new

uncertainty for the calculation of chloride and sulfide fluxes in the oxic and anoxic corrosion of copper canisters, respectively. In this sense, the CSM model was recently extended with a dual-porosity transport model accounting for Donnan equilibrium (King and Kolář, 2019), leading to higher corrosion rates. Idiart et al. (2019) and Pękala et al. (2019) also applied dual continuum approaches to assess copper corrosion in the canister of a KBS-3V repository due to the presence of sulfide. While the former implemented a model in the reactive-transport modeling framework iCP (Nardi et al., 2014), an interface coupling COMSOL Multiphysics (COMSOL, 2020) and PhreeqC (Parkhurst and Appelo, 2013), the latter adapted PFLOTRAN to include dual porosity according to the approach proposed by Gimmi and Alt-Epping (2018) (see below). It was found that it had a relatively small effect on the results as compared to the traditional modeling approach: only a slightly reduced mackinawite precipitation and increased sulfide fluxes reaching the canister were observed. However, this model did not account for the barriers outside the bentonite buffer, where significant sulfide generation is expected to take place. In both cases, it was concluded that further research was needed for a proper understanding of the impact of considering the Donnan equilibrium on the transport of sulfide through compacted bentonite.

In terms of numerical tools for a complete electrochemical description of corrosion, Gimmi and Alt-Epping (2018) derived a Nernst–Planck equation accounting for immobile charge and the Donnan equilibrium, which allowed a coupled transport simulation of all components while preserving the different diffusivities depending on their charges and the concentrations in the electrolyte. Note, however, that in that work, there is no analysis of corrosion processes, and the scope is restricted to bentonite.

6.2.1.2 Modeling of sulfide fluxes in the early transient stage

Sulfide is considered the main corroding agent for copper canisters during the long anoxic phase in a nuclear waste repository. The flux of sulfide depends on different sources distributed in the host rock, the backfill, and the buffer. Sulfate-bearing waters, gypsum in the bentonite, and SRB are the main factors in sulfide generation, whereas the formation of iron sulfide phases (mainly mackinawite) though the dissolution of Fe-bearing minerals is expected to be the main sink.

According to the models developed as part of the work by Wersin et al. (2014) with FASTREACT (FrAmework for Stochastic REACtive Transport, Trinchero et al., 2014) and PFLOTRAN (Hammond et al., 2014), the concentration levels foreseen in a repository are too low for significant corrosion to occur. Severe damage to the copper coating was only predicted in a few extreme cases that applied multiple conservative assumptions. Similar outcomes were obtained by Cloet et al. (2017), Wersin et al. (2017), Pękala et al. (2019), Pękala et al. (2020), and the CSM (King et al., 2011). However, these models did not consider a hypothetical early transient stage during which higher sulfide concentrations may reach the container surface. This scenario, although restricted by the low microbial activity in the buffer materials due to its low porosity, would be possible in the case of relevant sulfide sources together with limited iron availability.

Wersin et al. (2014) analyzed the maximum sulfide fluxes that could reach the buffer and the canister, assuming that the reduction of sulfates takes place at the backfill/rock interface and no precipitation of iron sulfides occurs, although the early transient phase was not specifically considered in this study. First, the evolution of the gypsum inventory in the backfill and the corresponding sulfate fluxes were calculated with a 1D diffusion-reaction model implemented in PhreeqC (Parkhurst and Appelo, 2013) for both saline and brackish groundwaters in Olkiluoto (Finland). Then, the maximum sulfide flux was derived analytically as a balance between diffusion to the buffer and flow transport to the host rock. It was found that 5%–11% of the generated sulfide reached the canister surface, which would be enough to induce corrosion failure. However, it was also stated that the transport of all of the sulfide to the container surface was totally unrealistic as ferrous minerals would capture a significant part of the sulfate inventory.

In addition to geochemistry, the thermal and hydrological conditions in the repository must also be assessed, which can significantly affect both diffusive and advective transport of sulfide. For example, Briggs et al. (2017) developed a 3D model with COMSOL Multiphysics of sulfide diffusion within the Canadian repository concept (NWMO) and concluded that the isothermal assumption was not realistic as changes in the saturation profile around the canister during the initial thermal transient might have a strong influence on the transport of sulfides until the system reaches the cool and anoxic state. In this sense, the effect of two-phase flow during the early water intrusion in the repository should be analyzed. Significant vapor and liquid fluxes are expected due to the high temperatures at the container surface and the heat dissipation in the near-field. This, together with the motion of trapped gas bubbles, might lead to less regular sulfide fluxes in the short term than those predicted by Wersin et al. (2014) or by the CSM model (King and Kolář, 2019), which only consider transport under the stable saturated conditions expected during the long-term anoxic period. A key concern that arises for this is the potential for gaseous H_2S to be transported during the unsaturated period. H_2S is corrosive to copper in dry atmospheres, even at comparatively low concentrations (>3 ppb), and becomes increasingly corrosive at higher temperatures and higher relative humidity. H_2S is also corrosive to carbon steel and, under certain conditions, can lead to localized corrosion and environmentally assisted cracking.

6.2.1.3 Modeling of microbial sulfide production

In the early non-saturated phase of the repository, oxygen consumption by aerobic microbes, which is expected to limit corrosion, was already implemented in the first version of the CCM model with a rate constant derived from *in situ* tests (King et al., 2008). This protective effect of microbes is removed when the system turns anoxic and microbial reduction of sulfate becomes dominant. In this sense, this model was updated by King et al. (2010) with 15 processes, including microbial sulfide production and a mass balance for each organic agent (CCM-MIC), so the microbial population could be tracked in space and time. According to King and Kolář (2006), who used the model to predict the microbial population in a Canadian repository, the presence of microbes in the near-field was minimal, and the sulfide concentrations reaching the canister were predicted to be small due to mackinawite precipitation in the buffer and backfill. Moreover, the elevated temperatures and lack of water foreseen

for the initial thermal–hydraulic transient were expected to suppress most of the microbial activity.

The definition of the kinetic rate constant for microbial sulfate reduction was addressed by the joint SKB-Posiva Integrated Sulfide Project. Bengtsson et al. (2017a) quantified this parameter (6.1×10^{-11} s^{-1}) after monitoring radioactively labeled sulfate in an experimental setup consisting of copper test plates buried in compacted bentonite with groundwater containing SRB (Pedersen, 2010). Results showed no SRB activity for bentonite wet densities of 1,900 kg/m^3 and above, whereas iron sulfide precipitates were observed on the plate surface at a wet bentonite density of 1,750 kg/m^3. The maximum sulfate reduction rate determined in MX-80 bentonite was 8.2×10^{-7} mol s^{-1} m^{-3} in bentonite porewater. The experimentally measured kinetic rate constant was used to feed a transport model using finite differences as a next step toward the quantification of the amount of sulfide reaching the surface of the test plates.

The CSM model has been recently extended by King et al. (2021) with two different pathways for microbial sulfate reduction: organotrophic (dissolved organic carbon as an electron donor) and chemotrophic (H_2 as an electron donor). It has also been applied to the KBS-3 concept for the disposal of spent nuclear fuel, leading to the precipitation as mackinawite of 98.5% of the microbially generated sulfide due to the dominance of siderite over organic matter in the buffer and the backfill. As a result, only 3 μm of copper would be corroded after one million years. However, this outcome might be less beneficial in repositories with higher amounts of organic material and gypsum and lower reactive Fe(II) contents because a smaller fraction of the microbially produced sulfide would precipitate before reaching the canister.

The most recent 3D reactive-transport sulfide model developed for the KBS-3 repository in Olkiluoto, Finland (Posiva, 2021b) also considers organic carbon and H_2 as pathways for microbial sulfate reduction, which is represented with a kinetic Monod model. The selected maximum SRB activity rate constants were defined as 5×10^{-5} mol sulfide/L and 10^{-4} mol sulfide/L of porewater, respectively, based on experimental and field studies from the literature. The simulations showed corrosion depths below 1 mm averaged over the whole copper canister surface after one million years. The maximum cell-resolved depths, however, were higher, in the range of one to a few millimeters.

6.2.1.4 Modeling the interaction of sulfide with Fe-bearing mineral phases

In the SR-Site safety assessment, it was assumed that pyrite dissolution could lead to the corrosion of the canister (SKB, 2010c). The extent of corrosion was estimated according to mass balance and mass transport, leading to a maximum depth of canister corrosion of 0.1 mm and 0.9 mm for MX-80 and Ibeco-RWC bentonites, respectively. However, when the limited solubility of pyrite and the low diffusivity of sulfide were considered, it was found that only the pyrite within 2 cm of the canister surface contributed to corrosion after one million years, resulting in 1 μm of corrosion for the reference values of solubility and diffusivity (SKB, 2010c). Simulations using the CSM (King et al., 2011) predicted long-term corrosion rates of the order of <1 nm/year, of the same order of magnitude as those predicted for the SR-Site safety assessment (SKB, 2010c), with the contribution of pyrite dissolution being less than 5% of the total extent.

Similarly, Marty et al. (2010) used the reactive-transport code KIRMAT to predict the alteration of bentonite for the French nuclear waste program. In this case, as well as in the model developed with CRUNCH by Bildstein et al. (2006), the rate constant for the anaerobic dissolution of pyrite was taken to be that of the oxidative dissolution. In a later extension of the CSM (King and Kolář, 2019), the rate constant for the anaerobic dissolution of pyrite was excluded from the model after a review of its properties by King (2013b) due to its extremely low solubility. Instead, the CSM provided a wider description of the interaction between sulfide and ferrous minerals, especially the precipitation of FeS leading to reduced sulfide fluxes. In this sense, four Fe(II) solid phases were included in the reaction scheme: biotite ($K(Mg_{0.6-1.8}Fe(II)_{2.4-1.2})(Si_3Al)O_{10}(OH,F)_2$), which is initially present in the backfill and rock layers, and which undergoes temperature-dependent dissolution releasing Fe(II), pyrite (FeS_2), which is expected to be fully oxidized during the aerobic phase, iron carbonate ($FeCO_3$), which is initially present in both the buffer and backfill materials and which precipitates reversibly in the presence of excess Fe(II), and, finally, mackinawite (FeS), which precipitates if the dissolved Fe(II) and HS^- concentrations exceed the value of the solubility product. With all these considerations, and assuming the expected conditions in a KBS-3 repository, the long-term corrosion extent was predicted to be less than 10 μm after one million years.

An alternative hydrogeochemical model using PhreeqC (Parkhurst and Appelo, 2013) was presented by Wersin et al. (2014). A similar outcome was obtained, including copper corrosion limited to 1%–1.7% of the total inventory and sulfide fluxes controlled by mackinawite precipitation.

In the 3D reactive-transport model used for the recent safety case of the spent fuel repository in Olkiluoto, Finland (Posiva, 2021b), the main sources of iron reacting with sulfide are ferric (oxyhydr)oxides present in the buffer and backfill as accessory minerals. The reaction of sulfide with Fe(III) follows a complex redox reaction scheme, leading to oxidized sulfur species (elemental sulfur, polysulfides) and Fe(II). The latter reaction products further react with sulfide to form iron sulfide (mackinawite).

6.2.1.5 Modeling irradiation-induced corrosion

The radiation from a spent fuel canister could affect the chemical conditions in the near-field. The ionizing radiation will produce both molecular and radical oxidants and reductants through radiolysis. The concentrations of the different species formed during radiolysis depend on the type of radiation, the dose rate, the composition of the aqueous solution, and the material of fabrication and wall thickness of the canister (King, 2020). In the gamma-irradiated system, the reducing electron and hydrogen radicals (e– and H•), formed with yields higher than oxidizing species, rapidly react with both H_2O_2 and O_2, decreasing the concentrations of the corroding species (Soroka et al., 2021).

In addition to extensive experimental work, a number of numerical simulations have been performed of the effect of water radiolysis on iron and copper corrosion (Wada et al., 2016; Soroka et al., 2021). Soroka et al. (2021) performed numerical simulations using MAKSIMA-CHEMIST and considered the full set of chemical reactions describing the radiation chemistry of water together with a

reaction of Cu oxidized by O_2. The simulations showed that the amount of molecular oxygen produced directly via γ-radiolysis of water and via catalytic decomposition of radiolytically produced H_2O_2 on the oxide surface could account for the amount of corrosion observed in the experiment. Wada et al. (2016) performed radiolysis calculations with the radiolysis code SIMFONY and determined the temporal evolution of the generated O_2, H_2, and H_2O_2 by gamma radiation (no comparison with experimental data was included). Recently, the complete set of kinetic reactions dealing with the recombination of water radiolysis species has been modeled in COMSOL Multiphysics in the context of spent fuel corrosion (Riba et al., 2020).

6.2.2 Steel containers

6.2.2.1 Modeling of steel canister corrosion

Modeling studies on iron canister corrosion in contact with different geotechnical barriers (i.e., bentonite, cement) or pure clay minerals (i.e., montmorillonite) performed in the last 15 years (Savage, 2012) have been mainly simulated by mechanistic reactive-transport models in porous media, including more or fewer simplifications (Montes-H et al., 2005; Bildstein et al., 2006; Wilson et al., 2006a; Wilson et al., 2006b; Hunter et al., 2007; Peña et al., 2008; Samper et al., 2008; Wersin et al., 2008a; Marty et al., 2010; Savage et al., 2010; Lu et al., 2011; Bildstein et al., 2012; Samper et al., 2016; Mon et al., 2017; Chaparro et al., 2021). Most of the works mentioned are related to long-term simulations (>10,000 years) and predict that magnetite is the principal steel corrosion product in contact with bentonite, along with significant alteration of the clay minerals to a mixture of non-swelling silicates, such as chlorite, berthierine or cronstedtite, and zeolites (Ngo et al., 2014; Wilson et al., 2015). Although some authors have focused on the principal reaction products (i.e., magnetite) considering the sorption of Fe on clay surfaces (Hunter et al., 2007; Samper et al., 2008; Lu et al., 2011), others have tried to model the growth of iron-bearing aluminosilicates (Wersin et al., 2008b; Savage et al., 2010; Marty et al., 2010). On the other hand, Peña et al. (2008) modeled the attenuation of the corrosion of carbon steel canisters due to the influence of diffusive transport through the corrosion product and compared it with data from Smart et al. (2006a), who studied the corrosion rate of steel in bentonite under a wide range of conditions. However, all of these models are inherently geochemical models designed to predict the consequences of steel container corrosion on the buffer material and host rock. These are not corrosion models in the true sense of the term, and indeed, the corrosion rate is an input to these models rather than an output.

Bataillon et al. (2010) were the first to develop a true corrosion model for steel containers aimed at predicting the corrosion rate. They developed the Diffusion Poisson Coupled Model (DPCM) as a tool to investigate the corrosion processes at the surface of carbon steel canisters. The numerical scheme was implemented in the simulation code CALIPSO. This code was recently coupled with a geochemistry-transport code, KIRMAT (Gerard et al., 1998). This makes it possible to give a realistic representation of both the corrosion behavior of iron and the alteration of clay base material.

More recently, another model (Marion, 2014; Mohamed-Said, 2017) has been developed to predict the evolution of the corrosion rate of carbon steel under a protective deposit. This model was proposed to describe the oxidation of iron in anaerobic neutral or slightly alkaline conditions. These chemical conditions correspond to those expected in the French HLW disposal concept. The model allows the assessment of the evolution of the carbon steel corrosion rate (reduction by oxide layer formation), the chemical species released, and the characteristic time of these processes. The model assumes that the solution is in contact with a dense, disordered spinel-like oxide layer that covers the iron. Two interfaces bound the oxide layer: 1) the inner interface, which corresponds to the metal/oxide layer, and 2) the outer interface, which corresponds to the oxide layer/solution interface. The metal (an electronic conductor) could be charged either by accumulation or depletion of electrons. The solution (ionic conductor) could be charged either by accumulation of cations or anions. The oxide layer is a mixed electronic and ionic conductor. The outer and the inner interfaces could move with time. The model considers the electrostatic and kinetic effects and accounts for moving boundaries. The electrostatic module gives the potential profile in the solution–oxide layer–metal system. The kinetics module gives the concentration profiles, one per charge carrier. The moving boundaries module gives the locations of the two interfaces that bound the oxide layer. These three modules are coupled because each module involves the solution of the others. Bataillon et al. (2010) tested the DPCM in a simplified situation where the locations of the outer and the inner interfaces are fixed and, after that, with moving boundaries. These data could be used to estimate the lifetime of the carbon steel overpack and the pressure rise resulting from hydrogen release. The convergence of the scheme was studied by Chainais-Hillairet et al. (2015) for the two-species model on a fixed domain. Chainais-Hillairet and Gallouët (2016) presented an updated version of the model of Bataillon et al. (2012) by studying the pseudo-stationary state for a corrosion model. The approach implemented in the CALIPSO code has the potential to be coupled with multicomponent reactive-transport models to study the interactions at the steel–iron–bentonite interface and the effects of corrosion products on bentonite.

King et al. (2014) have developed a mixed-potential model for the anaerobic corrosion of carbon steel containers in contact with a bentonite buffer. Using a similar approach to that used for copper containers and the CCM, the steel corrosion model (SCM) couples interfacial electrochemical expressions for the dissolution of Fe (as Fe(II)) and for the cathodic reduction of H_2O and/or HCO_3^- to the transport of reactants and products toward and away from the corroding interface through various mass-transport layers representing the buffer and backfill materials and surrounding host rock. The model also incorporates the impact of the precipitation of corrosion products (as $Fe(OH)_2$, Fe_3O_4, or $FeCO_3$), both on the buffer material (via precipitation in the buffer pores or adsorption of Fe(II) by the bentonite) and, more importantly, on the interfacial electrochemical reactions. The effect of gas production (in the form of H_2) and transport through the buffer is also predicted, as is the periodic release of H_2 as the build-up of pressure exceeds the gas breakthrough pressure for the engineered barriers.

6.2.2.2 Modeling gas generation due to corrosion

One of the main concerns about the anaerobic corrosion of ferrous materials in a repository is the production of hydrogen due

to its potential implications for damage to the structure of the EBS and the possible transport of gaseous radionuclides to the biosphere. A model known as the Simple Model for Gas Generation (SMOGG) has been developed with the aim of predicting the amount of gas that may arise due to both corrosion and radiolysis under various conditions. Literature reviews and assessments of the corrosion rate data for steel and Zircaloy (Smart and Hoch, 2010) and reactive metals (Magnox, uranium, and aluminum, Hoch et al., 2010) have been prepared to identify corrosion data that should be applied in the SMOGG model to predict the amount of gas produced by anaerobic corrosion.

A similar model, referred to as the Gas Generation Tool (Poller et al., 2016), has been developed for the calculation of generated gas in the Swiss deep geological repository. The model covers both the corrosion of steel SF/HLW disposal canisters and the generation of gases in the low- and intermediate-level waste (L/ILW) due to the corrosion and degradation of organics. The output of the model is used as input to two-phase flow modeling for the demonstration of the fate of repository-generated gas and the performance of the disposal system (Diomidis et al., 2016).

6.3 Performance assessment models

6.3.1 PA models for copper containers

6.3.1.1 Introduction

Oxygen-free copper has been considered as a canister material in several European and international waste management programs. Key countries of interest include Sweden (SKB, 2010a), Finland (Posiva 2007), Switzerland (Johnson and King, 2003), the United Kingdom (RWM, 2016), and Canada (NWMO, 2016). The furthest developed disposal concept in Europe is the KBS-3 concept, which utilizes a ~50-mm-thick barrier layer of phosphorus-doped, oxygen-free copper (SKB, 2010a). It is worth noting that performance assessments typically indicate expected depths of corrosion substantially less than the container wall thickness. However, the assumed wall thickness is currently conceived to both sustain the canister under its own weight (including during manufacture) and to ensure sufficient resistance to the risk of creep rupture. An alternative copper canister design comprises a copper coating, a few mm thick, applied to a carbon steel substrate, which is considered in the Canadian (NWMO, 2016) and Swiss concepts (Johnson and King, 2003). The corrosion allowance is considerably less for the coated designs than for the thicker copper canister designs; consequently, a greater certainty regarding the prevailing corrosion mechanisms is required for coated containers. Currently, electrodeposition and cold spray are being considered as possible coating methodologies.

Copper canisters used to dispose of spent nuclear fuel (SNF) and HLW are designed to be emplaced within a bentonite buffer. Unless specific environmental conditions are present in the groundwater (e.g., high carbonate and/or sulfate content and low chloride content), copper would not be expected to passivate in a repository environment, and much of its lifetime can be predicted based on general corrosion occurring with moderate uniformity. For a particular corrosion process (e.g., oxic corrosion, anoxic sulfide-driven corrosion, microbiologically influenced corrosion, pitting), the loss of material is either bounded by a maximum loss of material that is distributed over an area or is ascribed a rate of loss of thickness that is applicable over a particular phase in the repository lifetime. (e.g., early aerobic post-closure conditions, long-term anaerobic conditions) (Scully and Edwards, 2013; RWM, 2016).

Early in the repository lifetime and for a comparatively short-lived period [previously estimated at decades (Johnson and King, 2003) but more recently estimated as shorter based on the results of full-scale field testing experiments (Huertas et al., 2005)], the corrosion of copper is governed by the concentration of oxidants within proximity to the canister, including trapped O_2, radiolysis products and Cu(II) species produced by the oxidation of Cu(I) corrosion products. Over time, these species are consumed and not replaced (or not replaced at the same rate), leading to a reduction in the oxidizing power of the environment and a change in the dominant corrosion mechanisms that are predicted to prevail over the long term. In this phase, the corrosion of copper is expected to be governed by the flux of sulfide to the copper surface from outside the near-field. This process is expected to be kinetically limited by the low solubility and slow diffusion of sulfide through compacted bentonite (Scully and Edwards, 2013). In the absence of other degradation processes, which are not expected to occur, provided the swelling pressure of the buffer is maintained, copper canisters are predicted to last more than 10^5 years (Johnson and King, 2003; RWM, 2016) and potentially more than 10^6 years (Keech et al., 2020).

The main types of corrosion affecting copper-based canisters that must be considered in any performance assessment are as follows:

- Corrosion under unsaturated conditions.
- General corrosion.
- Localized corrosion.
- Microbiologically influenced corrosion.
- Radiation-assisted corrosion.
- Environmentally assisted cracking.

6.3.1.2 Corrosion in unsaturated conditions

Corrosion of the copper overpack during the unsaturated phase (including any corrosion before emplacement in the buffer and within the buffer before groundwater resaturation occurs) has been evaluated for a KBS-3 repository environment. Based on empirical evidence from the literature, corrosion rates are expected to be negligible (SKB, 2010a; Posiva, 2013). In these conditions, it is assumed that the elevated surface temperature of 50°C will ensure that the relative humidity close to the canister surface is lower than the critical relative humidity required to cause corrosion, generally considered to be approximately 50%–70% RH (SKB, 2010a). In dry air, the corrosion rate of copper increases with temperature and is predicted to be of the order of 10s of nm/a at temperatures between 50°C–150°C (Pinnel et al., 1979; Roy and Sircar, 1981; SKB, 2010b). These values are consistent with measurements made at the underground Äspö Hard Rock Laboratory in Sweden, which indicated corrosion rates <0.1 μm a^{-1} at 75°C (Taxén, 2003). Consequently, the atmospheric corrosion of copper canisters awaiting disposal is pessimistically bounded by assuming the corrosion will not exceed 1 μm and will produce a copper oxide surface film (SKB, 2010a).

6.3.1.3 General corrosion

For copper canisters emplaced within clay buffer materials, oxygen is assumed to be present within the void space in both the buffer and backfill materials after closure of the repository. A pessimistic assumption is that all the oxygen present in the buffer material reaches the canister surface and is consumed uniformly by corrosion (SKB, 2010b; Keech et al., 2020). A more realistic assumption, applied to the Swedish KBS-3 repository design, is that oxygen will also diffuse toward the oxygen-free rock and away from the canister; hence, only approximately 50% may reach the canister surface, which equates to an expected corrosion loss of approximately 17 μm that is bounded at 36 μm. The backfill is estimated to contain a greater amount of trapped oxygen than the buffer owing to its greater total volume; however, it is assumed that a smaller fraction of the oxygen trapped in the backfill would reach the canister. This fraction has been estimated for the KBS-3 design by considering the ratio of the canister diameter in relation to the diameter of the deposition hole, with the assumption that the oxygen is consumed as it diffuses downward by reaction with only the canister lid and the top 10% of the canister height. Under these assumptions, a further corrosion loss of approximately 106 μm is anticipated, which gives a total expected loss of 123 μm (SKB, 2010b). In the Swiss program, the amount of copper corrosion arising from trapped O_2, assuming all the trapped O_2 reacts with the canister to form Cu(I), was estimated at approximately 70 μm (Johnson and King, 2003). No credit was taken for the consumption of oxygen by reaction with steel rock supports, microbial activity, or oxidation of Fe(II), making the approach conservative.

Once the oxygen has been consumed, sulfide will be the primary oxidant remaining in the repository (or, more precisely, copper will corrode with the evolution of hydrogen in the presence of sulfide). An initial inventory of sulfide present as minerals (e.g., pyrite) within the buffer and backfill may dissolve and diffuse toward the canister surface during hydration of the borehole. The corrosion of copper by sulfide will lead to the formation of copper sulfide (Eqs 13, 14), although other reactions are also possible). Sulfide is also produced by microbial activity, as previously discussed.

$$2Cu(s) + HS^- + OH^- \rightarrow Cu_2S(s) + H_2O + 2e^- \text{ anodic process} \quad (13)$$

$$2H_2O + 2e^- \rightarrow H_2 + 2OH^- \text{ cathodic process} \quad (14)$$

The contribution of the sulfide present as pyrite in the buffer can be pessimistically bounded by a mass balance estimate for the residual oxygen. The contribution of the dissolution of pyrite and the diffusional transport of sulfide from the pyrite to the canister surface has been considered a source of corrosion in the KBS-3 repository design (SKB, 2010b); however, an allowance is not currently made for it owing to the low solubility of sulfide in the buffer.

In PA models, the corrosion rate due to the diffusion of corrosive species toward the canister surface is typically treated using the assumption that they react immediately upon contact with the canister surface and that any future reaction rate is unhindered by the formation of corrosion products. In the case of the copper/bentonite system, this assumption is justified by the slow rate of transport of sulfide in compacted bentonite in relation to the inherent reaction rate of copper with sulfide. Under these conditions, the corrosion reaction is treated as being transport-limited, and the rate of corrosion is proportional to the flux of species reaching the surface (SKB, 2010b). It has been demonstrated that for copper corroding due to reaction with HS^-, the shift from kinetic limitation to transport limitation occurs at HS^- fluxes lower than 2×10^{-12} mol cm^{-2} s^{-1}, which is considerably greater than the anticipated long-term sulfide fluxes through an intact bentonite buffer (~10^{-14} mol cm^{-2} s^{-1}) (King et al., 2017b). The lack of impact of corrosion product formation on the subsequent corrosion rate is supported by experimental observations that copper sulfide corrosion product layers are porous and non-protective at the pH and sulfide concentration anticipated within a bentonite buffer (King et al., 2017b; Keech et al., 2020). The mass-transport approach can also be applied to any oxygen that is trapped in the buffer and backfill materials, although in conventional disposal scenarios (effectively sealed DGR tunnels), the treatment based on mass balance is considered both cautious and sufficient. On the other hand, while this approach is still conservative (as the consumption of oxygen by other sources is also not considered), this approach could be used to treat the corrosion of disposal canisters in relevant scenarios, including tunnels that were either deliberately or inadvertently unsealed during the DGR operational period (i.e., while operations in other tunnels are still taking place) or access of glacial melt water (see below) (King et al., 2011).

Corrosion of copper by sulfide transport in groundwater is evaluated by mass-transport limitation. The equilibrium concentration of sulfide in the groundwater is determined by the source (i.e., sulfate reduction by microbial activity) and sink (i.e., oxidation and precipitation with metals) terms (SKB, 2010b). Mass-transport modeling has been used to evaluate the effect of buffer erosion on the sulfide transport from flowing groundwater supplied from a rock fracture to the canister surface for a KBS-3 repository (SKB, 2010b). For an intact buffer and a sulfide concentration of the order of 0.01 mM, corrosion rates lower than 0.001 μm year^{-1} have been predicted for all conditions modeled, with vastly lower corrosion rates predicted for most cases. Predicted corrosion rates are much higher for a partially eroded buffer, and under the most pessimistic combinations of flow rate and sulfide combination (≥0.161 m/s and 0.12 mM), failure of a canister (taken as 47 mm of corrosion or greater) could occur within 10^5 years (SKB, 2010b). However, for a more realistic sulfide concentration (0.01 mM), failure is only predicted to occur after approximately 850,000 years, even at a high flow rate of 0.251 m/s (SKB, 2010b). Likewise, similar hydrogeology models are used to evaluate oxygen transport from glacial meltwater. This can be done by assuming an upper limit of oxygen concentration (1.5 mM) in the groundwater that is supplied to the canister surface from a rock fracture intersecting a deposition hole over a fixed exposure period of 1,000 years, resulting in a corrosion loss of less than 6 mm (SKB, 2010b). In the Swiss disposal system, the corrosion loss based on the diffusion of HS^- to the container surface has been estimated as 80 μm over 10^6 years. This is based on reactive-transport modeling of sulfide in bentonite (Cloet et al., 2017).

6.3.1.4 Localized corrosion

Pitting of copper canisters is only considered viable during the aerobic early post-closure phase, while conditions are oxidizing, but

water chemistry is still quite dilute as the groundwater will have not yet reached the disposal container (or buffering by the initial porewater still occurs) (RWM, 2016). Based on short-term laboratory testing in simulated DGR conditions and *in situ* corrosion testing in disposal programs, copper has been shown to exhibit non-uniform general corrosion rather than the formation of discrete "classical" pits that are characterized by a small, fixed anode spatially separated from a supporting cathode. Consequently, the relative non-uniformity in the extent of corrosion across the surface is anticipated to decrease over time (RWM, 2016). Therefore, predictions of pit depths based on the assumption of a fixed anode that corrodes at a greater rate than the mean corrosion rate are unrealistically pessimistic (e.g., empirical pitting factor and extreme-value statistical analysis).

Another form of localized corrosion that has been evaluated in some disposal programs, for example, the Canadian disposal concept, is under-deposit corrosion (Scully and Edwards, 2013). The specific mechanism of concern is a form of crevice corrosion that proceeds underneath a precipitated surface film. The film would act as a selective ion exchange membrane and enable the development of a locally aggressive solution chemistry, forming a permanent anodic region. Such a mechanism would preclude the use of a surface roughening factor to account for local attacks in favor of the more conservative pitting factor (Scully and Edwards, 2013). Localized corrosion, including under-deposit corrosion, has been considered by ascribing a 0.1 mm corrosion allowance to this mechanism on the assumption that anodic and cathodic sites will not remain permanently fixed but will change with time within the overall anodic region (under the deposit) (Scully and Edwards, 2013; Keech et al., 2020). The assumption is underpinned by measurements of the surface profiles produced from the corrosion of copper underneath precipitated films in simulated Canadian repository conditions. The results showed a depth of attack of approximately 50 μm following 18 months of exposure under conditions that were conservative, with respect to oxygen concentration, in comparison to those anticipated during the aerobic phase in the DGR (King et al., 1992; Scully and Edwards, 2013).

6.3.1.4.1 Empirical pitting factor. Pitting factors for buried copper and copper alloys have been found to vary between 0 and 25 but exhibit a tendency to decrease with time. The longest exposure durations used to determine pitting factors are those of bronze-age artifacts (~3,000 years) reported by (Bresle and Arrhenius, 1983) and gave pitting factors between 2 and 5. These values are broadly consistent with measurements made of buried lightning conductor plates, which exhibited pitting factors of between 0 and 5 following exposures between 50 years and 80 years (Hallberg et al., 1984). Hence, for buried copper canisters, a pessimistic pitting factor of 5 may be assumed (SKB, 2010a). A pitting factor of 5 was applied to give a conservative estimation of the maximum depth of penetration of a copper canister in a Swiss repository due to sulfide flux (Johnson and King, 2003). However, the use of a pitting factor for copper is, in general, considered to be overly conservative when applied to DGR performance assessment. This is due to a shift to less oxidizing conditions (i.e., decreasing concentrations of O_2 and Cu(II)) and the progression of general corrosion into the surface, both of which act against the separation of anodes and cathodes (SKB, 2010a). Consequently, it is anticipated that a measured pitting factor would decrease with increasing time of exposure, consistent with archaeological observations.

6.3.1.4.2 Empirical extent of surface roughening. Roughening of ±50 μm has been applied for copper corrosion due to initially entrapped oxygen (SKB, 2010a; SKB, 2010b), based on observations by Brennenstuhl et al. (2002) and Litke et al. (1992). Similarly, in the Canadian system, a corrosion allowance of 100 μm has been assigned to address surface roughening during conditions where the oxygen level is still relatively high (Scully and Edwards, 2013; Keech et al., 2020) and is based on arguments supporting the switching of anodic and cathodic regions (Kwong, 2011).

6.3.1.4.3 Extreme-value statistical analysis. Pitting data generated by (Bresle and Arrhenius, 1983; Hallberg et al., 1984; Romanoff, 1989) were analyzed by King and Kolář (2000) and King and LeNeveu (1992) and fitted to an extreme-value distribution (Eq. 15). Application of these data to a copper canister in the KBS-3 type repository environment led to the prediction of a 10^{-6} chance of a pit exceeding 7.5 mm after 10^6 years and a 10^{-6} chance of a pit exceeding 5 mm after only 10 years (SKB, 2010a).

$$F(x) = exp[-exp(-ax + b)] \tag{15}$$

An underpinning observation that indicates that long-term prediction of pit depths making use of extreme-value statistical analysis (and empirical pitting factors) may not be particularly meaningful is that copper will not passivate under anticipated repository conditions, as passivation is required to cause pitting (King and Lilja, 2014). In the early oxic period, where pitting is more feasible, the presence of Cl^- ions tends to promote general active corrosion at near-neutral pH, with passivation occurring more readily in more alkaline solutions with a lower salinity (Qin et al., 2017; Briggs et al., 2020). In the long term, corrosion proceeds via the formation of copper sulfide, which has been shown to form porous non-protective films under anticipated repository conditions in Canada, Sweden, and Finland (King et al., 2017b).

6.3.1.4.4 Comparison of corrosion potential to critical potential for localized corrosion. For copper in neutral conditions, when the oxygen concentration is sufficiently low that hydrogen evolution is the dominant cathodic reaction, the anodic overpotential required to cause pitting is estimated as being approximately 600 mV based on the potential at which copper oxide formation occurs. Pitting of a copper oxide film is expected to occur more readily with increasing chloride concentration and less favorably with increasing HCO_3^- concentration due to their destabilizing and stabilizing influence on passivity, respectively (Drogowska et al., 1992). When sulfide is present, the pitting potential of the protective sulfide film was shown to shift in the negative direction with increasing HS^- concentration (de Chialvo et al., 1985). For copper in the presence of 0.01 M HS^-, an anodic overpotential of approximately 200 mV is assumed necessary to induce pitting corrosion based on corrosion potentials reported by Escobar et al. (1999). While pitting of copper oxides and

sulfides has been shown to be possible under certain conditions, the potentials at which such pitting occurs are hundreds of mV more positive than anticipated in repository environments (King et al., 2010).

6.3.1.5 Radiation-assisted corrosion

Radiation-assisted corrosion is considered separately for the saturated and unsaturated environment, as the prevalent corrosion mechanisms in each case are quite different. In unsaturated conditions, the major corrosion mechanism considered in safety case assessment is that caused by radiolytically produced nitric acid that arises from irradiation of the humid air trapped within the buffer. Once saturation is complete, radiolysis of the anoxic porewater leads to the production of oxidants, primarily H_2O_2, which, in high enough concentrations, can influence the corrosion rate and shift the corrosion potential in the positive direction (King and Behazin, 2021).

6.3.1.5.1 Mass balance of radiolytically produced oxidants. In the unsaturated phase, the influence of radiolytically generated oxidants on the corrosion of copper canisters within a bentonite buffer has been estimated by calculating the radiolytic yield within a given volume around the canister (liquid or gas phase) and assuming the oxidants produced will react with the canister surface to give a bounding value (SKB, 2010b).

This approach is adopted to take into account the formation of nitric acid from gamma irradiation of the humid air present in the canister–buffer gap during the buffer saturation phase. The total amount of nitric acid generated is calculated from the G-value for NHO_3 generation, the total absorbed gamma dose, and the irradiated volume (e.g., a 1 cm gap around the canister) (SKB, 2010b).

Radiolysis of water is considered to form hydrogen and oxidants that will react with the canister material, causing corrosion. It is assumed that there exists a volume around the canister in which all radiolytically generated oxidants will reach the canister surface (e.g., a 5 mm gap around the canister) and that there is a fixed stoichiometric ratio between the moles of oxidant produced and the moles of metal that are corroded uniformly from the surface of the canister (SKB, 2010b). Overall, the effect of radiolysis on copper in the Swedish system (KBS-3 type repository), after taking into account the aforementioned contributions, is approximately 7 nm of corrosion (SKB, 2010a).

A similar approach has been adopted to bound the extent of corrosion that may be experienced by copper due to radiolysis of water in the KBS-3 concept. If it is assumed that all the radiolytically produced oxidants within 5 mm of the canister can reach the surface, and it is also assumed that Cu is oxidized as efficiently as dissolved Fe(II), then approximately 14 μm of corrosion would be expected.

6.3.1.5.2 Reasoned argument for exclusion. Intact canisters provide shielding against alpha and beta radiation, with only gamma and neutrons penetrating through the walls to cause radiolysis of the porewater and groundwater. Due to the shielding afforded by the canister, the surface radiation dose is greatly attenuated. For the thinner-walled Canadian design, the surface dose rate is approximately 1 Gy h^{-1} (Keech et al., 2020), whereas the average surface dose is approximately 0.055 Gy h^{-1} for the thicker KBS-3 containers. At these dose rates, it is anticipated that there will be no enhancement of the corrosion rate (Pusch et al., 1992; Posiva, 2013). This perspective is supported by King and Behazin (2021), who compared the general corrosion enhancement by gamma radiation at dose rates from 0–20 Gy h^{-1} and total absorbed doses from 1,000 Gy to 50,000 Gy. At dose rates relevant to repository conditions (<10 Gy h^{-1}), there was either no effect or an inhibiting effect of radiation. There is no consensus within the literature about dose rates >10 Gy h^{-1}, with some studies showing an increase in corrosion and others showing an inhibition of corrosion compared to uninhibited rates. These studies also showed that for all dose rates considered, there was no consistent effect of increasing cumulative radiation dose.

Of the articles considered by King and Behazin (2021), the only studies that demonstrated an increase in corrosion rate due to gamma radiation were conducted at dose rates considerably greater than those anticipated at a copper canister surface during emplacement within a DGR. Moreover, King and Behazin (2021) draw attention to the mechanistic impacts of radiation dose rate on corrosion potential, which supports the suggestion that radiation dose rate is a critical factor in determining the influence of gamma radiation on the corrosion rate of emplaced canisters. Consequently, laboratory studies at dose rates far in excess of 10s Gy h^{-1} are not expected to accurately simulate the corrosive conditions encountered within a DGR.

6.3.1.6 Microbiologically influenced corrosion

6.3.1.6.1 Reasoned argument for exclusion. It has been shown that microbial activity is suppressed in highly compacted bentonite above a certain density due to the low water activity (≤0.96) (Scully and Edwards, 2013), the high swelling pressure, and the lack of physical space. In the Swedish SR-Site safety case, microbial activity leading to sulfide production via sulfate reduction was not considered within the intact bentonite buffer whose dry density exceeds 1,800 kg/m^3 (SKB, 2010a). In the Finnish safety case for the disposal of spent fuel at Olkiluoto, a bentonite dry density greater than ~1,650 kg/m^3 was considered the upper threshold for microbial activity (Posiva, 2013). Consequently, microbial corrosion is generally not considered feasible within the bentonite buffer, provided it remains compact and retains its density. Microbial activity is instead considered away from the near-field (e.g., in the backfill) (Johnson and King, 2003; SKB, 2010a; Posiva, 2013; Scully and Edwards, 2013).

6.3.1.6.2 Mass transport. Corrosion of copper by microbiologically generated sulfide outside of the near-field in a KBS-3 repository environment is pessimistically bounded by the supply of nutrients for microbes (SKB, 2010a). The amounts of nutrients available have been estimated in several ways. The backfill contains an abundance of organic matter, but it would be unrealistic to assume the whole inventory is available for dissolution and could be used to produce sulfide that could reach the canister surface within the lifetime of the repository. Bounding calculations based on 1D diffusion of sulfide formed at the same location as the organic matter predict that only a fraction of the sulfide that could be produced would reach the canister surface within 10^6 years. A bounding corrosion loss from sulfide in the backfill is obtained

by 1D diffusion modeling using pessimistic values for diffusivity and sulfide concentration (10^{-4} M) and applying the assumption that sulfur transported from the backfill is consumed by corrosion of the top 10% of the canister uniformly and gives a depth of penetration of 2 mm (SKB, 2010b). In the Canadian system, a corrosion allowance for microbial activity of 1 mm is considered sufficient, provided the buffer remains intact (Wolfaardt and Korber, 2012; Scully and Edwards, 2013).

The contribution of H_2, generated via anaerobic corrosion of rock bolts and other iron components, to the formation of sulfide via acetogenesis and sulfate reduction has also been considered and bounded for specific repository conditions based on the amounts of steel present (SKB, 2011). If a conservative mass balance approach is adopted that assumes that all of the sulfide produced by acetogenesis reacts with the canister, then an upper bound corrosion loss of 300 μm is obtained (SKB, 2010b).

6.3.1.6.3 Empirical rates of sulfide formation. Another method of estimating bounding rates of sulfide production has been based on experimental studies performed in conditions that are more favorable for microbial activity than expected in a repository environment. The rates of copper sulfide production were measured in different densities of bentonite that were supplemented with lactate to act as a source of organic carbon and nutrients (Masurat et al., 2010). The experimentally determined rates of sulfide production were converted into equivalent corrosion rates, and the wall thickness loss after 10^6 years was extrapolated linearly to give a pessimistic estimation of thickness loss of about 3 mm (SKB, 2010b).

6.3.1.7 Environmental-assisted cracking

6.3.1.7.1 Reasoned argument for nonsusceptibility. A combination of stress, aggressive ions, and oxidizing conditions are required for SCC of copper to occur. Even in the early oxic period, where temperatures are elevated, it is unlikely that sufficient concentrations of aggressive ions would be available within the KBS-3 type repository. No known mechanistic arguments can justify the assumption that copper cracking could be sustained over the long term in the anaerobic phase of the repository environment (King et al., 2010; SKB, 2010b; Posiva, 2013).

This argument has been further underpinned by experimentally validated mixed-potential modeling of the anticipated E_{corr} of copper, evaluated over a repository lifetime based on the interfacial chemistry as predicted by reactive-transport modeling. Modeling of E_{corr} and the surface pH demonstrated that a CuO_2/CuO surface film is not thermodynamically stable, which is a requirement for the SCC of copper (Maak and King, 2006) beyond the initial aerobic period (Posiva, 2013).

In the Canadian concept, SCC is not considered to be likely during the steady-state conditions encountered during deep geological disposal. Specifically, the interfacial pH and corrosion potential are expected to be far from the range in which SCC is a feasible corrosion mechanism, given the lack of aggressive species. Certain species, such as ammonia, nitrate ions, acetate, and sulfides, are known to promote the SCC of copper; however, the concentrations in groundwater are below the threshold levels for which they have been shown to promote SCC. It has been acknowledged that activities such as mining could lead to an increase in such species; however, the increase in SCC susceptibility is somewhat offset by the presence of Cl^-, which reduces the risk of SCC by promoting general corrosion (Kwong, 2011).

The risk of gradual embrittlement of copper by long-term anoxic exposure to HS^- at concentrations of approximately 10^{-4} mol/L has been highlighted as a risk to copper canisters (Scully and Edwards, 2013). However, it has also been argued that HS^- transport in bentonite is sufficiently slow that corrosion by sulfide could be transport-limited, resulting in surface or crack tip concentrations approaching zero, assuming that Cu(I) will sequester sulfide by precipitation of CuS_2 (Jacobs and Edwards, 2000). It was similarly concluded that for the KBS-3 concept, the possibility of SCC of copper, even at high sulfide fluxes, is not anticipated, and even if copper were susceptible to SCC in the presence of sulfide, the sulfide fluxes in the repository environment are not at a level that could induce SCC (SKB, 2019).

6.3.1.8 Mechanical degradation and combined corrosion–mechanical effects

Several modes of mechanical degradation could potentially affect the integrity of waste containers, specifically fracture, plastic deformation, and creep. Detrimental interactions between mechanical factors and corrosion processes are also possible (Figure 10). These issues have been discussed in detail by King et al. (2016). Fracture processes can be subdivided into brittle fracture, characterized by cleavage or intergranular failure, and ductile fracture, resulting in the typical "cup and cone" dimpled fracture surface. Brittle fracture is normally caused by some form of embrittlement process, such as radiation embrittlement, solute segregation within the metal, or hydrogen embrittlement. Plastic deformation can occur when a metal is overloaded past its yield strength, eventually leading to ductile failure if the load is sufficiently high. This form of failure is avoided in container design by choosing wall thicknesses that are appropriate to the expected loads. If the load tolerance is exceeded, deformation of the container may occur.

Creep involves the slow deformation of a material under the influence of an applied static load below the yield stress. In the case of copper, this problem is ameliorated by the use of oxygen-free, phosphorus-doped copper, which has a higher creep ductility.

It is possible that some forms of corrosion may have an effect on the mechanical performance of the container and *vice versa*. This includes environmentally assisted cracking, which is considered in the previous section, where the mechanical factors affect the corrosion susceptibility, and conversely, corrosion processes such as general corrosion will cause wall thinning, leading to a loss of wall strength and load-bearing capacity, and hence an increased risk of wall deformation or buckling. These interactions have been examined in detail by King et al. (2016) and are summarized in Figure 10. Other corrosion phenomena of note in this context are hydrogen-induced degradation of mechanical properties because hydrogen may be generated by the anaerobic corrosion of iron or may be present in the geological environment and expansive corrosion due to the formation of a corrosion product with a larger volume than the original metal. The latter effect has been examined experimentally by Smart et al. (2003a) and by comparison to analogs, such as archaeological artifacts (Smart et al., 2003a; Smart et al., 2006b).

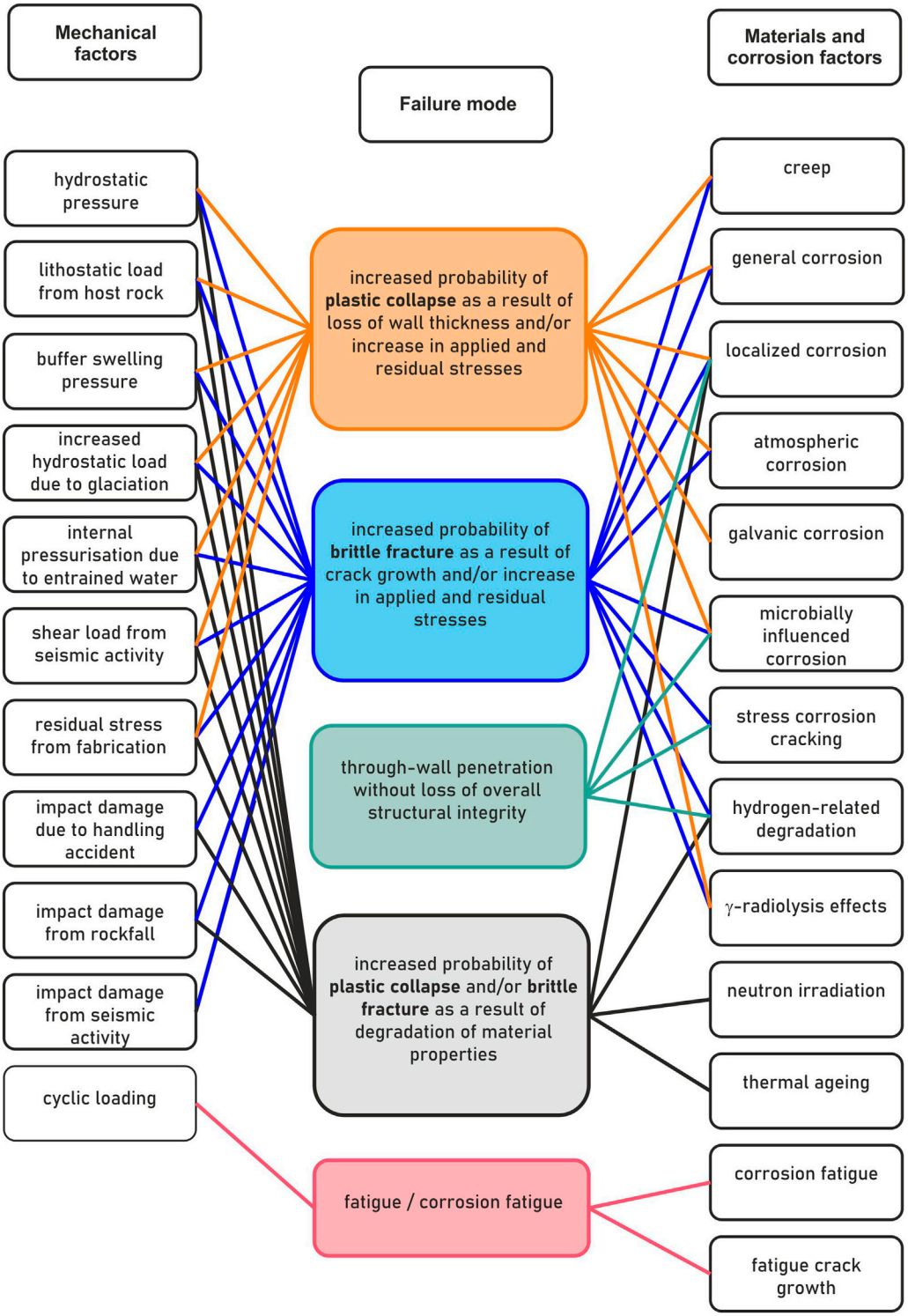

FIGURE 10
Schematic illustration of the mechanical and material-related factors that could lead to container failure and their relationship to various failure modes (King et al., 2016).

6.3.1.9 Prediction of canister lifetimes and implications for PA

At present, the most comprehensive predictions of canister lifetime have been performed for the KBS-3 concept, and estimates have been made for the maximum corrosion loss that may be caused by each mechanism over a period of 10^6 years. In the absence of buffer erosion, no single process gives an estimated corrosion loss of greater than a few mm, with the greatest loss

TABLE 3 Comparison of approaches currently taken to account for different types of corrosion in performance assessments for copper canisters by international waste management organizations (blank cells reflect an absence of information within the public domain).

Mode of corrosion	Canada	Finland	Sweden	Switzerland	United Kingdom
Oxidic general corrosion	Mass balance within corrosion allowance				
Radiolysis-induced corrosion	Excluded or mass balance within corrosion allowance				
Sulfide-induced anaerobic corrosion	Mass-transport controlled—key factor driving corrosion allowance				
MIC before buffer saturation		Exclude by reasoned argument			
SCC	Exclude by reasoned argument				
Pitting	Fixed corrosion allowance to account for surface roughening		Fixed corrosion allowance to account for surface roughening		

estimated to arise from sulfide flux caused by microbiological reduction of sulfate in a buffer on the assumption that all the organic material in the backfill is available to support this process. If the estimated contributions from each process are added together, the total loss estimated over 10^6 years is less than 5 mm (SKB, 2010b).

For scenarios involving erosion of the buffer by groundwater flow, the maximum predicted corrosion rates are greater than for any other mechanism considered. However, extremely high rates of corrosion are only estimated when the least favorable conditions are assumed (i.e., maximum flow rate and maximum sulfide concentration). When a statistical analysis is performed that considers the range of possible flow rates and the range of possible sulfide concentrations, the likelihood of a canister failing within 10^6 years can be estimated based on the number of canisters being stored. Application of this methodology estimates that between 0 and 2 canisters would fail within 10^6 once uncertainties are taken into account (SKB, 2010b).

For the Canadian system, a corrosion allowance of 1.27 mm over 10^6 years was described by Kwong (2011) and was based on several assumptions that have since been shown to be highly conservative (Keech et al., 2020). In particular, the corrosion allowance is dominated by sulfide corrosion due to an assumed sulfide concentration of 3 ppm (Kwong, 2011), which has subsequently been shown to be considerably higher than what is expected in Canadian deep subsurface water (Keech et al., 2020).

Table 3 summarizes the approaches taken for dealing with the corrosion of copper in performance assessments by various WMOs, according to the various possible corrosion mechanisms for copper.

Confidence in the predictions of the longevity of containers can be increased by reference to results from i) *in situ* corrosion experiments, where the environmental conditions are close to those expected in the real repository, with the exception of the external radiation dose rates, and the temperature, and ii) comparison with natural and archaeological analogs (IAEA, 1989; IAEA, 2005). Natural analogs include geological deposits, for example, native copper deposits (Milodowski et al., 2000; Milodowski et al., 2002), which have been found to exist for millions of years, and archaeological artifacts, such as a bronze cannon (King, 1995) and an iron–copper helmet (Smart et al., 2003b).

6.3.2 PA models for steel containers

6.3.2.1 Introduction

Carbon steel has been proposed as a canister material for SNF and HLW in several national disposal concepts, including the United Kingdom (RWM, 2016), Belgium (Kursten et al., 2017), France (Andra, 2005), Japan (JNC, 2000) and Switzerland (Patel et al., 2012). Different WMOs specify different alloys for the canister material but in general, low-strength, low-carbon alloys are favored. Carbon steel is a desirable canister material as its corrosion mechanisms are well characterized and predictable, based on decades of research, which enables canisters to be designed with suitable corrosion allowances (RWM, 2016). Moreover, due to the extensive use of carbon steel as an engineering material, it can be readily sourced and fabricated, and it is considerably cheaper than many alternative canister materials such as copper, nickel alloys, and titanium.

Carbon steel has been considered for use with both bentonite and cementitious buffers, as well as crushed rock (RWM, 2016). The high pH environment afforded by a cementitious buffer material supports the formation of a stable passivating magnetite film, which reduces the corrosion rate. However, under repository conditions, anaerobic corrosion of steel (even when passivated) leads to the formation of hydrogen gas, which has the potential to destabilize the surrounding buffer material. There is also concern that the interaction of ferrous ions released by corrosion could adversely alter the characteristics of the surrounding bentonite buffer.

In Switzerland, steel canisters for the disposal of SNF and HLW emplaced within a bentonite buffer have a regulatory lifetime requirement of 1,000 years, with the expectation that 10,000-year lifetimes may be readily achieved (Nagra, 2002), and this is the design lifetime. Similarly, complete containment provided by the Belgian Supercontainer concept is expected to endure for at least 5,000 years (for conditions defined within the design reference scenario), although considerably longer lifetimes are anticipated if long-term corrosion behavior is governed by the uniform anaerobic corrosion rate (Weetjens et al., 2012). In the Czech concept, the double-walled steel canister comprising an inner stainless steel layer surrounded by an outer carbon steel layer is designed to last for a minimum of 10,000 years (Pospiskova et al., 2017), whereas the Japanese concept, which has an inner stainless steel HLW cask surrounded by an outer carbon steel layer focuses on a 1,000 years

lifetime specification but is expected to last considerably longer (NUMO, 2021).

6.3.2.2 Atmospheric corrosion

The atmospheric corrosion behavior of steel canisters in air is dependent on the relative humidity; below ~60% RH, the corrosion rate is considered to be extremely low (Nagra, 2002). The presence of hygroscopic salt deposits (e.g., NaCl and $CaCl_2$) on the canister surface can influence the relative humidity at which corrosion can occur, depending on the chemical composition of the contaminating salt (Schindleholtz et al., 2014). However, due to the elevated temperature within the buffer close to the container surface, the canister is expected to remain dry even when the outer layers of bentonite begin to saturate (Nagra, 2002). Consequently, in the initial dry period, which is estimated to persist for a few decades, the extent of corrosion is expected to be less than 100 μm (Nagra, 2002) and has been accounted for in an Opalinus clay repository by applying a corrosion allowance of <1 mm (Johnson and King, 2008). This value is in broad agreement with atmospheric corrosion rates reported in RWM (2016), which shows that the atmospheric corrosion of embedded iron in subterranean environments is on the order of a few μm a^{-1}. It is anticipated that the atmospheric corrosion of iron will generally form iron (hydr)oxides, and this is not expected to directly undermine the integrity of the containers significantly in environments of limited corrosivity. However, there is uncertainty regarding the impact that the formation of a layer of rust could have on the corrosion performance of a steel container during the long-term post-closure phase (RWM, 2016).

6.3.2.3 General corrosion

Following the depletion of oxygen within the repository and a shift to more reducing conditions, the long-term corrosion of emplaced steel canisters is expected to occur as uniform general corrosion under anoxic conditions. In this environment, a corrosion rate of ~1 μm a^{-1} is anticipated for corrosion occurring in a bentonite buffer (Smart et al., 2011), but there are indications that the rates are even lower if sufficiently long experiments are performed (Diomidis et al., 2023). These rates are within the range reported for natural analogs, which exhibit corrosion rates as low as 0.1 μm a^{-1} for conditions that are not aerated (Miller et al., 1994). For the Czech concept, uniform anoxic corrosion of the outer carbon steel canister when emplaced in Czech bentonite is assumed to occur at a rate of 5 μm a^{-1}, based on average corrosion rates determined by mass loss over a 4-month period. However, the use of these rates to make lifetime predictions is known to be conservative, as in the same study, a comparison of the total corrosion loss of specimens after 2- and 4-month exposures implied that the instantaneous corrosion rate after 2 months had reduced to less than 1 μm a^{-1} (Pospiskova et al., 2017).

For concepts involving a cementitious buffer, such as the Belgian Supercontainer concept, the high pH (>13) cement porewater that is anticipated to form upon hydration of the buffer ensures that the steel will passivate by forming a stable magnetite surface film. The passive corrosion rate under these conditions can fall below 0.1 μm a^{-1} (Weetjens et al., 2012).

In the Japanese disposal concept, the corrosion rate of carbon steel in a bentonite buffer is considered in a range of rock types and groundwater chemistries of varying chloride and carbonate concentrations. Based on laboratory testing, it was found that corrosion rates dropped after 1 year of exposure and remained linear for several years at rates less than 2 μm a^{-1}. Based on these observations, an anaerobic general corrosion rate of 2 mm over the 1,000-year design life can be assumed. However, due to the possibility of uneven corrosion, a 6 mm corrosion allowance is applied based on an assumed pitting factor of 3 (NUMO, 2021).

6.3.2.4 Localized corrosion

Classical pitting corrosion of emplaced steel canisters is only considered to be feasible in the early oxic period. The extent of inhomogeneity in the corrosion of carbon steel was evaluated from the results of long-term field burial tests (JNC, 2000). From these tests, it has been highlighted (Johnson and King, 2003) that the pitting was initially characterized by high empirical pitting factors of ~100; however, once general corrosion had reached a depth of ~0.3 mm, pitting factors reduced to ~10. Consequently, a corrosion allowance of 10 mm has been estimated for pitting in the oxic phase of the Swiss disposal concept (Johnson and King, 2003).

The presence of a passivating magnetite film introduces the risk of localized corrosion if a breakdown of the film occurs, particularly in a high pH environment, such as a hydrated cementitious buffer. The propensity for pitting was examined using electrochemical measurements for conditions relevant to the Belgian disposal concept (Kursten et al., 2017) and demonstrated that the pitting potential had a strong dependence on chloride concentration (between 0.01 M and 1 M), with the pitting potential shifted in the active direction at higher chloride concentrations. A similar effect was observed at elevated temperatures, where increasing the temperature from 25°C to 85°C caused a shift in the pitting potential in the active direction. In the most aggressive conditions considered (1 M chloride, 85°C), and taking account of statistical variations in the pitting potential, the lowest potential at which pitting was observed was ~+200 mV vs. the corrosion potential.

In the Japanese concept, pitting corrosion during the long-term anoxic phase is excluded due to the combination of near-neutral bentonite pore water pH, a carbonate concentration of less than 0.5 mol/L, and the absence of strong oxidizing species. However, the non-uniformity of general corrosion is treated with a pitting factor of 3, which considerably increases the level of conservatism in the design. Moreover, treatment of the expected pitting corrosion during the oxic phase by use of a combined mass balance and extreme-value statistical analysis approach is also conservative, leading to an allowance of up to 12 mm (NUMO, 2021).

6.3.2.5 Radiation-assisted corrosion

As with the corrosion of copper, radiolysis can lead to the formation of oxidants such as nitric acid during the unsaturated phase and H_2O_2 during the saturated phase, which can lead to an acceleration of the corrosion rate during the period in which the waste form is still sufficiently radioactive. However, because the corrosion rate of carbon steel is greater than that of copper in repository conditions due to the spontaneous corrosion of steel in

10.3389/fnuen.2024.1404739

TABLE 4 Comparison of approaches currently taken to account for various types of corrosion in performance assessments for iron-based canisters by international waste management organizations (blank cells reflect an absence of information within the public domain).

Mode of corrosion	France	Belgium	Switzerland	Japan	United Kingdom	Czechia
Anaerobic general corrosion	Empirical corrosion rate		Empirical corrosion rate and pitting factor		Empirical corrosion rate	
Radiolysis-induced corrosion	Limit dose rate to 10 Gy h^{-1}	No effect for dose rate of 25 Gy h^{-1}	Design requirement (<1 Gy h^{-1})	Limit dose rate to 3 Gy h^{-1}		
Localized corrosion		Reasoned argument based on passivity of surface film	Depth-dependent pitting factor	Mass balance and extreme-value statistical analysis		
SCC	Specify resistant material	Exclude by reasoned argument				
MIC			Corrosion allowance based on mass transport	Excluded by reasoned argument—negligible rate		

anoxic porewater, the additional oxidation of steel by radiolysis products is small in comparison to the general corrosion loss by water oxidation.

In a series of year-long corrosion tests, Andra investigated the influence of gamma irradiation on the corrosion rate of carbon steel in humid air to simulate conditions arising in the unsaturated phase of a repository. Compared to unirradiated conditions, a gamma dose rate of 80 Gy h^{-1} was found to increase the corrosion rate, whereas no effect was observed for dose rates of 20 Gy h^{-1}; hence, no influence of radiation is expected at the overpack surface, as the design limits the external surface dose rate to less than 10 Gy h^{-1} (Crusset et al., 2017).

Gutierrez et al. (2018) consider the influence of radiolysis on corrosion of steel canisters for HLW and SNF to be negligible in the saturated phase, owing to the thickness of the canister walls (14 cm), which provides sufficient radiation shielding to attenuate the initial surface gamma dose to ~0.2 Gy h^{-1}, which is significantly below the critical value expected to increase corrosion (Marsh and Taylor, 1988). Corrosion testing in support of the Czech concept considers surface dose rates approximately ten times greater, at approximately 0.3 Gy h^{-1} (Pospiskova et al., 2017), but these are still assumed to be too low to significantly accelerate the corrosion process. Similarly, acceleration of corrosion by gamma radiation is eliminated in the Japanese concept by the use of an 80 mm shielding allowance, which is expected to attenuate the surface dose rate to significantly below the threshold of ~3 Gy h^{-1}, which is considered to influence corrosion under relevant conditions (NUMO, 2021). Under conditions relevant to the Belgian Supercontainer concept (i.e., young cement water containing thiosulfate, sulfide, and chloride at 25°C and 80°C), dose rates of up to 25 Gy h^{-1} had no significant effect on the anaerobic corrosion rate of carbon steel, with rates as low as 0.03 μm a^{-1} measured by hydrogen gas evolution (Kursten et al., 2017).

6.3.2.6 Microbiologically influenced corrosion

As with copper–bentonite systems, the high bentonite density is expected to reduce microbial activity to the extent where sulfate reduction is negligible. Equally, the high pH of the porewater within a cementitious buffer is also expected to restrict microbiological activity to negligibly low levels such that sulfate reduction is only considered in the far-field (Nagra, 2002; Kursten et al., 2017; NUMO, 2021). Consequently, for an intact buffer, the influence of MIC is only attributable to sulfate reduction in the far-field, leading to a sulfate flux through the buffer to the canister surface. This process is the same as that for a copper-based system because the flux is determined largely by the microbial activity and the properties of the buffer material (e.g., pH, thickness, etc.).

Because the anaerobic corrosion rate of carbon steel is greater than that of copper in repository conditions, steel corrosion losses due to a sulfide flux tend to be less significant than general anaerobic corrosion arising from water reduction. As an example, in an Opalinus clay environment, Nagra (2002) considers the extent of corrosion that could occur due to a sulfide flux to the container surface due to microbiological sulfate reduction from outside the buffer to lead to ~0.02 mm of corrosion loss over a period of 10^3 years, whereas, the

estimated anaerobic corrosion rate due to water reduction over this period is 1 mm (Johnson and King, 2003).

6.3.2.7 Environmental-assisted cracking

SCC at a weld has been evaluated and deemed unlikely based on a range of reported studies (JNC, 2000). Nagra (2002) also considers SCC of welded steel containers to be unlikely owing to the anticipated pH of the bentonite porewater (~7.3), which is outside the range at which SCC of steel in HCO_3^-/CO_3^{2-} occurs (i.e., approximately pH 10–11 or approximately pH 6) (Johnson and King, 2003). Furthermore, if a crack were able to initiate, its growth is expected to be stifled in a repository environment, owing to the absence of cyclic loading (Nagra, 2002).

Cracking of carbon steel by SCC and hydrogen embrittlement is excluded by reasoned argument in the Japanese concept. This is achieved by considering the chemical environment, the material properties (e.g., strength of steel), and the expected stress levels. In particular, the use of heat treatments, both on the bulk material and for welds, is expected to largely eliminate tensile residual stresses or reduce them to levels where they are insignificant from an environmental-assisted cracking perspective (NUMO, 2021).

The susceptibility of both plain and welded carbon steel to SCC in high pH (13.6) porewater was investigated for conditions relevant to the Belgian Supercontainer concept. Slow strain rate testing was performed at 140°C in the presence of sulfide concentrations up to 15.6 mM. During testing, the fracture properties of plain carbon steel in the test solution were comparable to that in argon, indicating no susceptibility to SCC. In comparison, welded specimens exhibited a slight reduction in ductility but not to the extent that would constitute a susceptibility to SCC, and this was supported by fractographic analysis of the fracture surfaces, which exhibited ductile fracture features. Hence, it was concluded that carbon steel is immune to SCC in the conditions tested (Kursten et al., 2017).

The risk of hydrogen embrittlement of carbon steel containers was reviewed in the context of the Swiss concept by Turnbull (2009). This assessment concluded that the risk of hydrogen embrittlement and cracking of the carbon steel canisters was minimal.

6.3.2.8 Weld corrosion

In the Japanese concept, the risk of weld corrosion is accounted for by allowing an additional 3 mm corrosion allowance for welded regions to account for the possibility of undetected welding defects of up to 3 mm in depth. Preferential weld corrosion is also considered and is mitigated by the use of Ni doping of the weld material.

6.3.2.9 Prediction of canister lifetimes and implications for PA

Steel canisters are designed with conservative lifetimes of 1,000 to 10,000 years, which is considerably shorter than that of copper canisters owing to continuous corrosion during anoxic conditions of the order of <0.1 μm a^{-1} for cementitious alkaline conditions or 1–2 μm a^{-1} for carbon steel in bentonite (Nagra, 2002; Kursten et al., 2017; NUMO, 2021). However, due to the level of conservativism adopted, it is expected that actual canister lifetimes will far exceed the design life. For example, in the Japanese concept, the overpack is expected to last in excess of 17,000 years, which is far beyond the design life.

Table 4 summarizes the approaches taken for dealing with the corrosion of iron-based canisters in PAs by various WMOs, according to the various possible corrosion mechanisms for steel.

7 Summary and conclusion

ConCorD (Container Corrosion under disposal Conditions) is one of the work packages of the European Joint Programme on Radioactive Waste Management (EURAD). Its main aims are:

- to assess the corrosion mechanisms of traditional container materials (i.e., carbon steel and copper) in complex disposal scenarios where the corroding environment is under the influence of irradiation, temporal changes of the near-field environment, or microbial activity,
- to assess the potential of novel materials for optimization of the container performance, and
- to integrate experimental evidence on container degradation into the prediction of container corrosion and lifetime assessment.

The state of the art on these research targets has been summarized as a basis for the development of the ConCorD research activities.

External γ-radiation fields for HLW/SF containers are modest, with a maximum of a few Gy/h or lower, although the total accumulated dose over the lifetime of the container can be several MGy. Past work on the effects of radiation-induced corrosion indicates that the maximum additional wall loss due to radiation is of the order of a few tens of μm, although it is unclear whether predictions of the corrosion allowance should be based on the dose rate or the total dose. Furthermore, relatively few studies of the effects of radiation in representative systems, including the presence of compacted buffer material and of unsaturated (atmospheric) conditions, have been conducted.

For the first few thousand years following emplacement, the container will be exposed to an evolving near-field environment. In addition to the time-dependent decay of the external radiation field, the container will also be subject to a thermal transient, the evolution of redox conditions as the initially trapped atmospheric O_2 is consumed, and a saturation transient that affects both the availability of H_2O to support corrosion as well as the external load applied to the container. In turn, the buffer porewater composition and the extent of microbial activity will also change over time. Although the effects of some of these time-dependent environmental conditions have been studied, the work in ConCorD seeks to examine the combined effects of the early transient behavior.

Near-field microbial activity can produce metabolic by-products, such as sulfide, that can lead to corrosion of the container. Although it has been known for some time that microbial activity is suppressed in compacted bentonite buffer material, the underlying physiological cause is uncertain. The activity of anaerobes, such as SRB, may also be suppressed by the presence of residual oxygen "trapped" in the bentonite. Irradiation may affect the viability and survivability of various microbial species.

Of the various candidate container materials, most attention has been paid to the performance of copper and steel. However, there is a

wide range of other materials, both metallic and non-metallic, that exhibit certain advantages and disadvantages as container materials. Ceramics have been considered in several international programs, and work within ConCorD will seek to resolve the long-standing issue of how to join such materials at sufficiently low temperatures that the waste inside the container is not thermally damaged. Coatings, both ceramic and metallic, may offer a cost-effective solution as a corrosion barrier. With the exception of copper coatings, however, the development of coated container solutions is relatively immature. The optimization of existing container designs is also an area of ongoing study, such as the investigation of commercial grades of phosphorus-containing copper as an alternative to the custom grade currently specified for the KBS-3 container.

The outcomes of research in the different areas discussed above and in other areas are ultimately incorporated into the safety case and, specifically, used to support container lifetime predictions. Such information may be used directly in the development and validation of predictive models, either process models focused on specific corrosion processes or performance assessment models aimed at predicting container performance under repository conditions. A range of process and performance assessment models have been developed for both copper and carbon steel containers. Alternatively, the research outcomes may be used more generally as part of the safety case documentation to demonstrate a sound mechanistic understanding of the corrosion processes to which the container will and will not be subject. An important component of the ConCorD project is the implementation of the results of the different experimental activities to improve the overall modeling and lifetime prediction of HLW/SF containers.

Author contributions

AM: writing–original draft, writing–review and editing. AA: writing–original draft. UA: writing–original draft. AF: writing–original draft. RB-L: writing–original draft. AC: writing–original draft. RG: writing–original draft. JH: writing–original draft. NS: writing–original draft. CP: writing–original draft. KM: writing–original draft. VM: writing–original draft. AI: writing–original draft. AP: writing–original draft. OR: writing–original draft. NF: writing–original draft. AS: writing–original draft. FK: writing–original draft. ND: writing–original draft, writing–review and editing.

Funding

The author(s) declare that no financial support was received for the research, authorship, and/or publication of this article.

Acknowledgments

eurad
European Joint Programme on Radioactive Waste Management

Conflict of interest

Authors JH, NS, and CP are employed by Jacobs. AI, AP, and OR are employed by Amphos 21. FK is employed by Integrity Corrosion Consulting Ltd.

The remaining authors declare that the research was conducted in the absence of any commercial or financial relationships that could be construed as a potential conflict of interest.

The handling editor BG declared a shared affiliation with the author AA at the time of review.

The author(s) declared that they were an editorial board member of Frontiers, at the time of submission. This had no impact on the peer review process and the final decision.

Publisher's note

References

Adams, J., Cowgill, M., Moskowitz, P., and Rokhvarger, A.E. (2000). *Effect of radiation on spinel ceramics for permanent containers for nuclear waste transportation and storage*. Upton NY: Brookhaven National Laboratory. BNL Report BNL-67518.

Ahmad, Z. (2006). *Principles of Corrosion Engineering and Corrosion Control*. Butterworth-Heinemann, 672.

Ahn, T.M., and Soo, P. (1995). Corrosion of low-carbon cast steel in concentrated synthetic groundwater at 80 to 150°C. *Waste Management* 15, 471–76. doi:10.1016/0956-053x(96)00001-3

Alkhimov, A.P., Kosarev, V.F., Klinkov, S.V., and Sova, A.A. (2012a). Effect of a conical separation region on cold gas-dynamic spraying. *Journal of Applied Mechanics and Technical Physics* 53, 948–953. doi:10.1134/s0021894412060193

Alkhimov, A.P., Kosarev, V.F., Klinkov, S.V., Sova, A.A., Trubacheev, G.V., and Zaikovsky, V. N. (2012b). Conical separation zone formation at impingement of supersonic jet on obstacle under cold spraying. *Thermophysics and Aeromechanics* 19, 225–232. doi:10.1134/s0869864312020060

Amendola, R, and Acharjee, A (2022 Apr 4). Microbiologically Influenced Corrosion of Copper and Its Alloys in Anaerobic Aqueous Environments: A Review. *Front Microbiol* 13, 806688. doi:10.3389/fmicb.2022.806688

Andersson, C.-G., et al. (2004). *SKB TR-04-23 - Status report, canister fabrication*. SKB, 96.

Andra (2005). *Dossier 2005 Argile - Phenomenological evolution of a geological repository*.

Appelo, C. A. J. (2013). *A review of porosity and diffusion in bentonite*. Finland: Posiva Oy. Working Report 2013-29.

Arcos, D., Hernán, P., de la Cruz, B., Herbert, H.-J., Savage, D., Smart, N.R., Villar, M.V., and Van Loon, L.R. (2005). NF-PRO: Understanding and physical and numerical modelling of the key processes in the nearfield and their coupling for different host rocks and repository strategies, EDZ development and evolution. *RTDC-2 Synthesis report, EC integrated project NF-PRO Deliverable D-No:2.6.4*.

Arcos, D., Cuevas, J., Fernández, A.M., Herbert, H.-J., Hernan, P., Van Loon, L., Martin, P.L., Savage, D., Smart, N., and Villar, M.V. (2008). "Key Processes affecting the Chemical

Evolution of the Engineered Barrier System," in *Conference proceedings Euradwaste'08. 7th European Commission conference on the management and disposal of radioactive waste*.

Aurubis (2022). *Finland Oy - Download Center, datasheets 2022*. available/link: Download Center - Aurubis Finland Oy).

Bagnoud, A., de Bruijn, I., Andersson, A. F., Diomidis, N., Leupin, O. X., Schwyn, B., et al. (2016). A minimalistic microbial food web in an excavated deep subsurface clay rock. *FEMS microbiology ecology* 92, fiv138. doi:10.1093/femsec/fiv138

Bamoulid, L., Maurette, M. T., De Caro, D., Guenbour, A., Ben Bachir, A., Aries, L., et al. (2008). An efficient protection of stainless steel against corrosion: Combination of a conversion layer and titanium dioxide deposit. *Surf. Coat. Technol.* 202, 5020–5026. doi:10.1016/j.surfcoat.2008.05.011

Baroux, C., and Martin, C. (2016). Summary Report of the preliminary feasibility study for ceramic HLW overpacks. *Andra Report CG.RP.ASCM.13.0023*.

Bataillon, C., Bouchon, F., Chainais-Hillairet, C., Desgranges, C., Hoarau, E., Martin, F., Tupin, M., Talandier, J., et al. (2010). Corrosion modelling of iron based alloy in nuclear waste repository. *Electrochimica Acta* 55 (15), 4451–4467. doi:10.1016/j.electacta.2010.02.087

Bataillon, C., Bouchon, F., Chainais-Hillairet, C., Fuhrmann, J., Hoarau, E., and Touzani, R. (2012). Numerical methods for the simulation of a corrosion model with moving oxide layer. *Journal of Computational Physics* 231 (18), 6213–6231. doi:10.1016/j.jcp.2012.06.005

Beese-Vasbender, P.F., Nayak, S., Erbe, A., Stratmann, M., and Mayrhofer, K.J.J. (2015). Electrochemical characterization of direct electron uptake in electrical microbially influenced corrosion of iron by the lithoautotrophic SRB Desulfopila corrodens strain IS4. *Electrochim. Acta* 167, 321–329. doi:10.1016/j.electacta.2015.03.184

Belous, V.A., et al. (2013). Development of Ion-Plasma Technology of Deposition of the Nanostructure Bactericidal Coatings on Orthopaedic Implantats and Fixative Devices. Production of Pilot Samples for Verification of their Use in Clinic. *Science and Innovation* 9, 46–60. ISSN 1815-2066. doi:10.15407/scin9.06.046

Belous, V.A., Lunyov, V.M., Kuprin, A.S., and Bortnitskaya, M.A. (2018). Structure and properties of TiOx and TiNxOy coatings formed in vacuum arc plasma fluxes. *Probl. At. Sci. Technol.* 118, 297–299.

Ben Lagha, S., Crusset, D., Mabille, I., Tran, M., Bernard, M.C., and Sutter, E. (2007). Corrosion of iron: A study for radioactive waste canisters. *J. Nucl. Mater.* 362, 485–492. doi:10.1016/j.jnucmat.2007.01.257

Bengtsson, A., and Pedersen, K. (2017). Microbial sulphide-producing activity in water saturated Wyoming MX-80, Asha and Calcigel bentonites at wet densities from 1500 to 2000 kgm^{-3}. *Appl. Clay Sci.* 137, 203–212. doi:10.1016/j.clay.2016.12.024

Bengtsson, A., Blom, A., Hallbeck, B., Heed, C., Johansson, L., Stalén, J., and Pedersen, K. (2017a). *Microbial sulphide-producing activity in water saturated MX-80, Asha and Calcigel bentonite at wet densities from 1 500 to 2000 kg m−3*. Sweden: SKB TR-16-09, SKB.

Bengtsson, A., Blom, A., Taborowski, T., Schippers, A., Edlund, J., Kalinowski, B., and Pedersen, K. (2017b). *FEBEX-DP: Microbiological Report. NAB 16-015*. Switzerland: Nagra.

Bessho, Oki, Y., Akimune, N., Matsumura, H., Masumoto, K., Sekimoto, S., et al. (2015). Corrosion of copper in water and colloid formation under intense radiation field. *J. Radioanal. Nucl. Chem.* 303, 1117–1121. doi:10.1007/s10967-014-3464-8

Bienek, H., Finkbeiner, R., and Wick, W. (1984). Container closure means for storage of radioactive material. *US Patent* 4, 437–578.

Bildstein, O., Trotignon, L., Perronnet, M., and Jullien, M. (2006). Modelling iron–clay interactions in deep geological disposal conditions. *Phys. Chem. Earth* 31, 618–625. doi:10.1016/j.pce.2006.04.014

Bildstein, O., Lartigue, J., Pointeau, I., Cochepin, B., Munier, I., and Michau, N. (2012). "Chemical evolution in the near field of HLW cells: interactions between glass, steel and clay-stone in deep geological conditions," in *5th ANDRA International Meeting, 22–25 Oct 2012*.

Birgersson, M., and Karnland, O. (2009). Ion equilibrium between montmorillonite interlayer space and an external solution – Consequences for diffusional transport. *Geochim. Cosmochim. Acta* 73, 1908–1923. doi:10.1016/j.gca.2008.11.027

Björkbacka, Å., Hosseinpour, S., Leygraf, C., and Jonsson, M. (2012). Radiation Induced Corrosion of Copper in Anoxic Aqueous Solution. *Electrochem. Solid-State Lett.* 15, C5–C6. doi:10.1149/2.022205esl

Björkbacka, A., Hosseinpour, S., Johnson, M., Leygraf, C., and Jonsson, M. (2013). Radiation induced corrosion of copper for spent nuclear fuel storage. *Radiat. Phys. Chem.* 92, 80–86. doi:10.1016/j.radphyschem.2013.06.033

Björkbacka, A., Yang, M., Gasparrini, C., Leygraf, C., and Jonsson, M. (2015). Kinetics and mechanisms of reactions between H_2O_2 and copper and copper oxides. *Dalton Trans.* 44, 16045–16051. doi:10.1039/c5dt02024g

Bjorkbacka, Å., Johnson, C.M., Leygraf, C., and Jonsson, M. (2016). Role of the oxide layer in radiation-induced corrosion of copper in anoxic water. *J. Phys. Chem. C* 120, 11450–11455. doi:10.1021/acs.jpcc.6b00269

Bjorkbacka, A., Johnson, C.M., Leygraf, C., and Jonsson, M. (2017). Radiation induced corrosion of copper in humid air and argon atmospheres. *J. Electrochem. Soc.* 164, C201–C206. doi:10.1149/2.1331704jes

Boyle, C.H., and Meguid, S.A. (2015). Mechanical performance of integrally bonded copper coatings for the long-term disposal of used nuclear fuel. *Nucl. Eng. Des.* 293, 403–412. doi:10.1016/j.nucengdes.2015.08.011

Bradbury, M.H., and Baeyens, B. (2002). Porewater chemistry in compacted re-saturated MX-80 bentonite: physico-chemical characterisation and geochemical modelling. *PSI Bericht*, 02–10.

Braithwaite, J.W., Magnani, N.J., and Munford, J.W. (1980). *Titanium alloy corrosion in nuclear waste environments*. NACE CONF-800305, p. SAND-79-2023C.

Brandberg, F., and Skagius, K. (1991). *Porosity, sorption, and diffusivity data compiled for the SKB 91 study. TR 91-16*. Sweden: SKB.

Brehm, W.F. (1990). *Corrosion of Ferrous Materials in a Basaltic Environment, in Workshop on corrosion of nuclear fuel waste containers*, 227–233. AECL-10121.

Brennenstuhl, A.M., McBride, A., Ramamurthy, S., and Davidson, R. (2002). The effects of microstructural and environmental factors on underdeposit corrosion of oxygen-free phosphorous-doped copper. Report 06819-REP-01200-10079-R00, Ontario Power Generation. *Nuclear Waste Management*.

Bresle, S.Å., and Arrhenius, B. (1983). *Studies in pitting corrosion on archaeological bronzes*. Svensk Kärnbränslehantering AB. Copper. SKB TR 83-05.

Briggs, S., McKelvie, J., Keech, P., Sleep, B., and Krol, M. (2017). Transient modelling of sulphide diffusion under conditions typical of a deep geological repository. *Corros. Eng. Sci. Technol.* 52, 200–203. doi:10.1080/1478422x.2017.1288336

Briggs, S., Lilja, C., and King, F. (2020). Probabilistic model for pitting of copper canisters. *Mater. Corros.* 72, 308–316. doi:10.1002/maco.202011784

Brown, A.R., Boothman, C., Pimblott, S.M., and Lloyd, J.R. (2015). The Impact of Gamma Radiation on Sediment Microbial Processes. *Appl. Environ. Microbiol.* 81, 4014–4025. doi:10.1128/aem.00590-15

Burzan, N. (2021). *Growth and viability of microorganisms in bentonite and their potential activity in deep geological repository environments*. Lausanne: École Polytechnique Fédérale de Lausanne EPFL. PhD Thesis.

Burzan, N., Lima, R.M., Frutschi, M., Janowczyk, A., Reddy, B., Rance, A., Diomidis, N., and Bernier-Latmani, R. (2022). Growth and persistence of an aerobic microbial community in Wyoming bentonite MX-80 despite anoxic *in situ* conditions. *Frontiers in Microbiology* 13, 858324. doi:10.3389/fmicb.2022.858324

Carlson, L., Karnland, O., Olsson, S., Rance, A., and Smart, N. (2006). Experimental studies on the interactions between anaerobically corroding iron and bentonite. *Posiva Working Report 2006-06. Posiva*.

Carlsson, T., and Muurinen, A. (2008). *A Practical and Theoretical Basis for Performing Redox-measurements in compacted Bentonite _ A Literature Survey*. Posiva Working Report 2008-51. Posiva, Eurajoki, Finland.

Cedeno-Vente, M.L., Manríquez, J., Mondragón-Rodríguez, G., Camacho, N., Gómez-Ovalle, A., Gonzalez-Carmona, J., et al. (2021). Application of a transmission line model to evaluate the influence of structural defects on the corrosion behavior of arc-PVD CrN coatings. *Ceram. Int.* 47, 20885–20899. doi:10.1016/j.ceramint.2021.04.087

Černá, K., and Bartak, D.S. (2019). *State of art – attachment I to the Work report 2019, Project Limiting Factors for survivability and proliferation of microorganisms significant for corrosion of deep geological repository barrier systems (BioBen) Project number: TAČR TK02010169*.

Černá, K., Černoušek, T., Polívka, P., Ševců, A., and Steinová, J. (2015). *MIND Deliverable 2.15: Survival of microorganisms in bentonite subjected to different levels of irradiation and pressure*. Available at: https://www.mind15.eu/deliverables/.

Červinka, R., and Vašíček, R. (2018). *Kompletní charakterizace bentonitu*. BCV 2017, SÚRAO TZ 419/2019.

Chainais-Hillairet, C., Colin, P.-L., and Lacroix-Violet, I. (2015). Convergence of a finite volume scheme for a corrosion model. *Int. J. Finite* 12, 1–27.

Chainais-Hillairet, C., and Gallouët, T.O. (2016). Study of a pseudo-stationary state for a corrosion model: existence and numerical approximation. *Nonlinear Analysis: Real World Applications* 31, 38–56. doi:10.1016/j.nonrwa.2016.01.010

Chaparro, C., Finck, Metz V., and Geckeis, H (2021). Reactive Transport Modelling of the Long-Term Interaction between Carbon Steel and MX-80 Bentonite at 25 °C. *Minerals* 11, 1272. doi:10.3390/min11111272

Chapon, V., Piette, L., Vesvres, M.-H., Coppin, F., Marrec, C.L., Christen, R., Theodorakopoulos, N., Février, L., Levchuk, S., Martin-Garin, A., Berthomieu, C., and Sergeant, C. (2012). Microbial diversity in contaminated soils along the T22 trench of the Chernobyl experimental platform. *Appl. Geochem.* 27, 1375–1383. doi:10.1016/j.apgeochem.2011.08.011

Chatterjee, M., Fan, Y., Cao, F., Jones, A. A., Pilloni, G., and Zhang, X. (2021). Proteomic study of Desulfovibrio ferrophilus IS5 reveals overexpressed extracellular multi-heme cytochrome associated with severe microbiologically influenced corrosion. *Sci. Rep.* 11, 15458. doi:10.1038/s41598-021-95060-0

Cheptsov, V.S., Vorobyova, E.A., Gorlenko, M.V., Manucharova, N.A., Pavlov, A.K., and Lomasov, V.N. (2018). Effect of gamma radiation on viability of a soil microbial community under conditions of Mars. *Paleontol. J.* 52, 1217–1223. doi:10.1134/s0031030118100088

Christensen, Th.H., Bjerg, P.L., Banwart, S.A., Jakobsen, R., Heron, G., and Albrechtsen, H.-J. (2000). Characterization of redox conditions in groundwater contaminant plumes. *Journal of Contaminant Hydrology* 45 (Iss. 3–4), 165–241. doi:10.1016/s0169-7722(00)00109-1

Clark, D.E., and Sutton, W.H. (1996). Microwave Processing of Materials. *Ann. Rev. Mater. Sci.* 26, 299–331. doi:10.1146/annurev.matsci.26.1.299

Cloet, V., Pekala, M., Smith, P., Wersin, P., and Diomidis, N. (2017). *An evaluation of sulphide fluxes in the nearfield of a HLW repository*. Switzerland: Nagra. Technical Report 17-04.

COMSOL (2020). *COMSOL Multiphysics® v. 5.6*. Sweden: COMSOL AB.

Costello, J.A. (1974). Cathodic depolarization by sulfate-reducing bacteria. *S. Afr. J. Sci.* 70, 202–204.

Couture, R.A. (1985). Steam rapidly reduces the swelling capacity of bentonite. *Nature* 318, 50–52. doi:10.1038/318050a0

Crusset, D., Deydier, V., Necib, S., Gras, J.-M., Combrade, P., Féron, D., and Burger, E. (2017). Corrosion of Carbon Steel Components in the French High-Level Waste Programme: Evolution of Disposal Concept and Selection of Materials. *Corros. Eng. Sci. Technol.* 52, 17–24. doi:10.1080/1478422X.2017.1344416

Čuba, V., Silber, R., Múčka, V., Pospíšil, M., Neufuss, S., Bárta, J., and Vokál, A. (2011). Radiolytic Formation of Ferrous and Ferric Ions in Carbon Steel – Deaerated Water System. *Radiat. Phys. Chem.* 80, 440–45. doi:10.1016/j.radphyschem.2010.09.012

Cuevas, J., Villar, M., Fernández, A., Gomez, P., and Martín, P. (1997). Pore waters extracted from compacted bentonite subjected to simultaneous heating and hydration. *Appl. Geochem.* 12, 473–481. doi:10.1016/s0883-2927(97)00024-3

Curti, E. (2011). "Comparison of bentonite pore water calculations carried out with conventional and novel models," in *PSI Internal Report AN-44-11-18* (Villigen, Switzerland: Paul Scherrer Institute).

Dadachova, E., and Casadevall, A. (2008). Ionizing radiation: how fungi cope, adapt, and exploit with the help of melanin. *Curr. Opin. Microbiol.* 11, 525–531. doi:10.1016/j.mib.2008.09.013

Daly, M.J. (2009). A new perspective on radiation resistance based on *Deinococcus radiodurans*. *Nat. Rev. Microbiol.* 7, 237–245. doi:10.1038/nrmicro2073

Daly, M.J., Gaidamakova, E. K., Matrosova, V. Y., Vasilenko, A., Zhai, M., Leapman, R. D., et al. (2007). Protein Oxidation Implicated as the Primary Determinant of Bacterial Radioresistance. *PLOS Biology* 5, e92. doi:10.1371/journal.pbio.0050092

Dante, J.F., and Kelly, R.G. (1993). The Evolution of the Adsorbed Solution Layer during Atmospheric Corrosion and Its Effects on the Corrosion Rate of Copper. *J. Electrochem. Soc.* 140, 1890–1897. doi:10.1149/1.2220734

Daub, K., Van Nieuwenhove, R., and Nordin, H. (2015). Investigation of the impact of coatings on corrosion and hydrogen uptake of Zircaloy-4. *J. Nucl. Mater.* 467, 260–270. doi:10.1016/j.jnucmat.2015.09.041

Daub, K., Zhang, X., Noël, J.J., and Wren, J.C. (2011). Gamma-radiation-induced corrosion of carbon steel in neutral and mildly basic water at 150 °C. *Corros. Sci.* 53, 11–16. doi:10.1016/j.corsci.2010.09.048

Daub, K., Zhang, X., Noël, J.J., and Wren, J.C. (2010). Effects of γ-Radiation versus H_2O_2 on Carbon Steel Corrosion. *Electrochim. Acta* 55, 2767–2776. doi:10.1016/j.electacta.2009.12.028

Daub, K., Zhang, X., Noël, J.J., and Wren, J.C. (2019). Gamma Radiation-Induced Carbon Steel Corrosion. *ECS Trans* 33, 15–24. doi:10.1149/1.3557748

de Chialvo, M.R., Salvarezza, R.C., Vasquez, M.D., and Arvia, A.J. (1985). Kinetics of passivation and pitting corrosion of polycrystalline copper in borate buffer solutions containing sodium chloride. *Electrochim. Acta* 30, 1501–1511. doi:10.1016/0013-4686(85)80012-8

De Combarieu, G., Barboux, P., and Minet, Y. (2007). Iron corrosion in Callovo-Oxfordian argilite: From experiments to thermodynamic/kinetic modelling. *Physics and Chemistry of the Earth* 32, 346–358. doi:10.1016/j.pce.2006.04.019

De Windt, L., Miron, G.D., Fabian, M., Goethals, J., and Wittebroodt, C. (2020). "First results on the thermodynamic databases and reactive transport models for steel-cement interfaces at high temperature," in *Final version of deliverable D2.8 of the HORIZON 2020 project EURAD* (EC Grant agreement).

Debruyn, W. (1988). Corrosion of Container Materials under Clay Repository Conditions. *Proceedings of a workshop on corrosion of nuclear fuel waste containers* 148, 148–162.

Deck, C.P., Khalifa, H.E., and Shapovalov, K.S. (2018). SiC-SiC Composite Cladding Development for Accident Tolerant Fuel. *Trans. Am. Nucl. Soc.* 118, 1305–1308.

Deissmann, G., Ait Mouheb, N., Martin, C., Turrero, M.J., Torres, E., Kursten, B., Weetjens, E., Jacques, D., Cuevas, J., Samper, J., Montenegro, L., Leivo, M., Somervuori, M., and Carpen, L. (2021). *Experiments and numerical model studies on interfaces. Final version as of 12.05.2021 of deliverable D2.5 of the HORIZON 2020 project EURAD*. EC Grant agreement no: 847593.

Delage, P. (2010). A microstructure approach to the sensitivity and compressibility of some Eastern Canada sensitive clays. *Géotechnique* 60 (5), 353–68. doi:10.1680/geot.2010.60.5.353

Diler, E., Leblanc, V., Gueuné, H., Larché, N., Deydier, V., Linard, Y., et al. (2021). Potential influence of microorganisms on the corrosion of carbon steel in the French high- and intermediate-level long-lived radioactive waste disposal context. *Mater. Corros.* 72, 218–234. doi:10.1002/maco.202011779

Diomidis, N., and Johnson, L.H. (2014). Materials options and corrosion-related considerations in the design of spent fuel and high-level waste disposal canisters for a deep geological repository in Opalinus clay. *JOM* 66, 461–470. doi:10.1007/s11837-014-0876-4

Diomidis, N., Cloet, V., Leupin, O., Marschall, P., Poller, A., and Stein, M. (2016). "Production, consumption and transport of gases in deep geological repositories according to the Swiss disposal concept," in *Nagra Technical Report NTB 16-03* (Wettingen, Switzerland: Nagra).

Diomidis, N., Guillemot, T., and King, F. (2023). "Definition of reference corrosion rates for performance and safety assessments," in *Nagra Working Report NAB 23-22* (Wettingen, Switzerland: Nagra).

Drogowska, M., Brossard, L., and Ménard, H. (1992). Copper dissolution in $NaHCO_3$ and $NaHCO_3$ + NaCl aqueous solutions at pH 8. *J. Electrochem. Soc.* 139, 39–47. doi:10.1149/1.2069196

Duro, L., Bruno, J., Grivé, M., Montoya, V., Kienzler, B., Altmaier, M., and Buckau, G. (2014). Redox processes in the safety case of deep geological repositories of radioactive wastes. Contribution of the European RECOSY Collaborative Project. *Appl. Geochem.* 49, 206–217. doi:10.1016/j.apgeochem.2014.04.013

Ekeroth, E., Roth, O., and Jonsson, M. (2006). The relative impact of radiolysis products in radiation induced oxidative dissolution of UO_2. *J. Nucl. Mater.* 355, 38–46. doi:10.1016/j.jnucmat.2006.04.001

El Hajj, H., Abdelouas, A., El Mendili, Y., Karakurt, G., Grambow, B., and Martin, C. (2013). Corrosion of carbon steel under sequential aerobic-anaerobic environmental conditions. *Corros. Sci.* 76, 432–440. doi:10.1016/j.corsci.2013.07.017

El Mendili, Y., Abdelouas, A., Karakurt, G., Ait Chaou, A., Essehli, R., Bardeau, J.-F., and Grenèche, J.-M. (2015). The effect of temperature on carbon steel corrosion under geological conditions. *Appl. Geochem.* 52, 76–85. doi:10.1016/j.apgeochem.2014.11.008

Enning, D., Venzlaff, H., Garrelfs, J., Dinh, H. T., Meyer, V., Mayrhofer, K., et al. (2012). Marine sulfate-reducing bacteria cause serious corrosion of iron under electroconductive biogenic mineral crust. *Environ. Microbiol.* 14, 1772–1787. doi:10.1111/j.1462-2920.2012.02778.x

Enning, D., and Garrelfs, J. (2014). Corrosion of Iron by Sulfate-Reducing Bacteria: New Views of an Old Problem. *Appl. Environ. Microbiol.* 80, 1226–1236. doi:10.1128/aem.02848-13

Esbelin, J., Santos, T., and Hébraud, M. (2018). Desiccation: An environmental and food industry stress that bacteria commonly face. *Food Microbiol* 69, 82–88. doi:10.1016/j.fm.2017.07.017

Escobar, I S, Silva, E, Silva, C, and Ubal, A (1999). "Study of the effect of sulphide ions on the corrosion resistance of copper for use in containers for high-level waste," in *Proceedings of 4th International Conference Copper 99 – Cobre 99* (Warrendale, PA: Metals, and Materials Society), 371–386.

Fernández, A.M. (2019a). *Gas and water sampling from the FEBEX* in situ *test. Nagra Working Reports. NAB 16-13, 155*. NAGRA Technical Report.

Fernández, A.M., and Villar, M.V. (2010). Geochemical behaviour of a bentonite barrier: results up to 8 years of thermo-hydraulic treatment in the laboratory. *Appl. Geochem.* 25, 809–824. doi:10.1016/j.apgeochem.2010.03.001

Fernández, A.M, Baeyens, B., Bradbury, M., and Rivas, P. (2004). Analysis of the porewater chemical composition of a Spanish compacted bentonite used in an engineered barrier. *Phys. Chem. Earth* 29, 105–118. doi:10.1016/j.pce.2003.12.001

Fernández, A.M., Sánchez-Ledesma, D.M., Melón, A., Robredo, L.M., Rey, J.J., Labajo, M., Clavero, M.A., Fernández, S., and González, A.E. (2018). "Thermo-hydro-chemical (THC) behaviour of a Spanish Bentonite after dismantling Heater#1 and Heater#2 of the FEBEX *in situ* test at the Grimsel Test Site," in *Nagra Working Reports. NAB 16-25* (NAGRA), 583.

Fernández, A.M., Marco, J.F., Nieto, P., León, F.J., Robredo, L.M., Clavero, M.A., Cardona, A., Fernández, S., Svensson, D., and Sellin, P. (2022). Characterization of Bentonites from the *in situ* ABM5 Heater Experiment at Äspö Hard Rock Laboratory, Sweden. *Minerals* 12, 471. doi:10.3390/min12040471

Fernandez, R., and Jodoin, B. (2018). Cold Spray Aluminum–Alumina Cermet Coatings: Effect of Alumina Content. *J. Therm. Spray Technol.* 27, 603–623. doi:10.1007/s11666-018-0702-6

Féron, D., and Crusset, D. (2014). Microbial induced corrosion in French concept of nuclear waste underground disposal. *Corros. Eng. Sci. Technol.* 49, 540–547. doi:10.1179/1743278214y.0000000193

Finsterle, S., Muller, R.A., Baltzer, R., Payer, P., and Rector, J.W. (2019). Thermal Evolution near Heat-Generating Nuclear Waste Canisters Disposed in Horizontal Drillholes. *Energies* 12, 596. doi:10.3390/en12040596

Fredrickson, J.K., McKinley, J. P., Bjornstad, B. N., Long, P. E., Ringelberg, D. B., White, D. C., et al. (1997). Pore-size constraints on the activity and survival of subsurface bacteria in a late cretaceous shale-sandstone sequence, northwestern New Mexico. *Geomicrobiol. J.* 14, 183–202. doi:10.1080/01490459709378043

Gens, A., Sánchez, M., Guimarães, L., Alonso, A.A., Loret, A., Olivella, S., Villar, M.V., and Huertas, F.A. (2009). A full-scale *in situ* heating test for high-level nuclear waste disposal: observations, analysis and interpretation. *Géotechnique* 59, 377–399. doi:10.1680/geot.2009.59.4.377

Gérard, F., Clement, A., and Fritz, B. (1998). Numerical validation of a Eulerian hydrochemical code using a 1D multisolute mass transport system involving heterogeneous kinetically controlled reactions. *Journal of Contaminant Hydrology* 30 (3-4), 201–216. doi:10.1016/s0169-7722(97)00047-8

Gimmi, T., and Alt-Epping, P. (2018). Simulating Donnan equilibria based on the Nernst-Planck equation. *Geochim. Cosmochim. Acta* 232, 1–13. doi:10.1016/j.gca.2018.04.003

Giroud, N. (2014). *FEBEX - Assessment of Redox Conditions in Phase 2 before Dismantling*. Switzerland: Nagra. Technical Report NAB 14-55.

Giroud, N., Tomonaga, Y., Wersin, P., Briggs, S., King, F., Vogt, T., and Diomidis, N. (2018). On the fate of oxygen in a spent fuel emplacement drift in Opalinus Clay. *Applied Geochemistry* 97, 270–278. doi:10.1016/j.apgeochem.2018.08.011

Grandia, F., Domènech, C., Arcos, D., and Duro, L. (2006). Assessment of the oxygen consumption in the backfill. *Geochemical modelling in a saturated backfill. SKB Report, R-06-106 SKB Stockholm*.

Gray, W. J. (1987). Effects of Radiation on the Oxidation Potential of Salt Brine. *MRS Proceedings* 112, 405. doi:10.1557/PROC-112-405

Greffe, V.R.G., and Michiels, J. (2020). Desiccation-induced cell damage in bacteria and the relevance for inoculant production. *Appl. Microbiol. Biot.* 104, 3757–3770. doi:10.1007/s00253-020-10501-6

Grousset, S., Urios, L., Mostefaoui, S., Dauzeres, A., Crusset, D., Deydier, V., et al. (2020). Biocorrosion detection by sulphur isotopic fractionation measurements. *Corros. Sci.* 165, 108386. doi:10.1016/j.corsci.2019.108386

Guinan, M.W. (2001). *Radiation effects in spent nuclear fuel canisters*. SKB-TR-01-32.

Gutierrez, M.M., Caruso, S., and Diomidis, N. (2018). Effects of materials and design on the criticality and shielding assessment of canister concepts for the disposal of spent nuclear fuel. *App. Radiat. Isot.* 139, 201–208. doi:10.1016/j.apradiso.2018.05.016

Hadi, J., Wersin, P., Serneels, V., and Greneche, J.M. (2019). Eighteen years of steel-bentonite interaction in the FEBEX "*in situ*" test at the Grimsel Test Site in Switzerland. *Clays Clay Miner.* 67, 111–131. doi:10.1007/s42860-019-00012-5

Hall, D.S., Behazin, M., Jeffrey Binns, W., and Keech, P. G. (2021). An evaluation of corrosion processes affecting copper-coated nuclear waste containers in a deep geological repository. *Prog. Mater. Sci.* 118, 100766. doi:10.1016/j.pmatsci.2020.100766

Hallberg, R.O., Engvall, A.G., and Wadston, T. (1984). Corrosion of copper lightning conductor plates. *Br. Corros. J.* 19, 85–88. doi:10.1179/000705984798273335

Hammond, G., Lichtner, P., and Mills, R. (2014). Evaluating the performance of parallel subsurface simulators: An illustrative example with PFLOTRAN. *Water Resour. Res.* 50, 208–228. doi:10.1002/2012wr013483

Hasal, M., Michalec, Z., and Blaheta, R. (2019). *Provedení předběžného výpočtu tlaku na UOS*. Final report. – MS SÚRAO, TZ 388/2019, Praha (CZ).

Havlova, V., Kiczka, M., Mendoza Miranda, A., Klajmon, M., Wersin, P., Pekala, M., Jenni, A., Hadi, J., Samper, J., Montenegro, L., Mon, A., Fabian, M, Osan, J., Dauzeres, A., and Jacques, D. (2020). "Modelling of the steel-clay interface – approaches, first results and model refinements," in *Final version as of 28 08 2020 of deliverable D2.6 of the HORIZON 2020 project EURAD*. EC Grant agreement no: 847593.

Haynes, H.M., Pearce, C.I., Boothman, C., and Lloyd, J.R. (2018). Response of bentonite microbial communities to stresses relevant to geodisposal of radioactive waste. *Chem. Geol.* 501, 58–67. doi:10.1016/j.chemgeo.2018.10.004

Hoch, A.R., Smart, N.R., Wilson, J.D., and Reddy, B. (2010). "A," in *Survey of Reactive Metal Corrosion Data for Use in the SMOGG Gas Generation Model*. Serco Report SA/ENV-0895, issue 2.

Holdsworth, S.R. (2013). *Ceramic Material Solutions for Nuclear Waste Disposal Canisters*. NAGRA working report NAB12-45.

Holdsworth, S.R., Graule, T., and Mazza, R. (2014). *Feasibility evaluation study of candidate canister solutions for the disposal of spent nuclear fuel and high-level waste-A status review*. NAGRA working report NAB14-90.

Holdsworth, S.R., King, F., and Diomidis, N. (2018). *Alternative coating Materials as Corrosion Barriers for SF and HLW Disposal Canisters*. NAGRA report NAB18-19.

Hua, F., Mon, K., Pasupathi, P., Gordon, G., and Shoesmith, D. (2005). A Review of Corrosion of Titanium Grade 7 and Other Titanium Alloys in Nuclear Waste Repository Environments. *CORROSION* 61 (10), 987–1003. doi:10.5006/1.3280899

Huertas, F., et al. (2005). *Full-Scale Engineered Barriers Experiment for a Deep Geological Repository for High-Level Waste in Crystalline Host Rock – Phase II*, 21922. Euratom EUR.

Hunter, F., Bate, F., Heath, T., and Hoch, A. (2007). Geochemical Investigation of Iron Transport into Bentonite as Steel Corrodes. *SKB Report TR-07-09*.

Hutchison, E.A., Miller, D.A., Angert, E.R., Eichenberger, P., and Driks, A. (2014). Sporulation in Bacteria: Beyond the Standard Model. *Microbiol. Spectr.* 2. doi:10.1128/microbiolspec.TBS-0013-2012

IAEA (1989). *Natural Analogues in Performance Assessments for the Disposal of Long Lived Radioactive Wastes*. IAEA Technical Reports Series No. 304.

IAEA (2005). *Anthropogenic analogues for geological disposal of high level and long lived waste, Final report of a coordinated research project 1999–2004*. IAEA report IAEA-TECDOC-1481.

Ibrahim, B., Zagidulin, D., Behazin, M., Ramamurthy, S., Wren, J.C., and Shoesmith, D.W. (2018). The corrosion of copper in irradiated and unirradiated humid air. *Corros. Sci.* 141, 53–62. doi:10.1016/j.corsci.2018.05.024

Idiart, A., and Coene, E. (2019). *Modelling diffusion through compacted bentonite in the BHA vault. R-19-10*. Sweden: SKB.

Idiart, A., Coene, E., Bagaria, F., Román-Ross, G., and Birgersson, M. (2019). "Reactive transport modelling considering transport in interlayer water," in *New model, sensitivity analyses and results from the Integrated Sulphide Project inter-model comparison exercise* (Sweden: SKB). TR-18-07.

Itälä, A. (2009). *Chemical Evolution of Bentonite Buffer in a Final Repository of Spent Nuclear Fuel During the Thermal Phase*. VTT Publications 721, 78.

Jacobs, S., and Edwards, O. (2000). Sulfide scale catalysis of copper corrosion. *Water Res* 34, 2798–2808. doi:10.1016/s0043-1354(00)00025-7

Jakupi, P., Keech, P., Barker, I., Ramamurthy, S., Jacklin, R., Shoesmith, D., et al. (2015). Characterization of commercially cold sprayed copper coatings and determination of the effects of impacting copper powder velocities. *J. Nucl. Mater.* 466, 1–11. doi:10.1016/j.jnucmat.2015.07.001

Jalique, D.R., Stroes-Gascoyne, S., Hamon, C. J., Priyanto, D. G., Kohle, C., Evenden, W. G., et al. (2016). Culturability and diversity of microorganisms recovered from an eight-year old highly-compacted, saturated MX-80 Wyoming bentonite plug. *Appl. Clay Sci.* 126, 245–250. doi:10.1016/j.clay.2016.03.022

Jenni, A., Wersin, P., Thoene, T., Baeyens, Ferrari, A., Gimmi, T., Mäder, U., and Marschall, P. (2019). *Bentonite backfill performance in a high-level waste repository: A geochemical perspective*. Nagra Technical Report 19-03.

Jia, R., Unsal, T., Xu, D.K., Lekbach, Y., and Gu, T.Y. (2019). Microbiologically influenced corrosion and current mitigation strategies: A state of the art review. *Int. Biodeterior. Biodegrad.* 137, 42–58. doi:10.1016/j.ibiod.2018.11.007

JNC (2000). "H12: Project to establish the scientific and technical basis for HLW disposal in Japan, Supporting report 2 - Repository Design and Engineering Technology," in *Technical report JNC TN1410 2000-003. Japan Nuclear Cycle Development Institute*.

Johnson, L.H., and King, F. (2003). *Canister Options for the Disposal of Spent Fuel*. Wettingen, Switzerland: National Cooperative for the Disposal of Radioactive Waste. Technical report 02-11.

Johnson, L.H., and King, F. (2008). The effect of the evolution of environmental conditions on the corrosion evolutionary path in a repository for spent fuel and high-level waste in Opalinus Clay. *J. Nucl. Mater.* 379, 9–15. doi:10.1016/j.jnucmat.2008.06.003

Johnson, L.H., LeNeveu, D.M., King, F., Shoesmith, D.W., Kolar, M., Oscarson, D.W., Sunder, S., Onofrei, C., and Crosthwaite, J.L. (1996). *The disposal of Canada's nuclear fuel waste: a study of postclosure safety of in-room emplacement of used CANDU fuel in copper containers in permeable plutonic rock. Volume 2: vault model*. Atomic Energy of Canada. Report AECL-11494-2, COG-96-552-2.

Jolivet, E., L'Haridon, S., Corre, E., Forterre, P., and Prieur, D. (2003). Thermococcus gammatolerans sp. nov., a hyperthermophilic archaeon from a deep-sea hydrothermal vent that resists ionizing radiation. *Int. J. Syst. Evol. Microbiol.* 53, 847–851. doi:10.1099/ijs.0.02503-0

Jonsson, M., Emilsson, G., and Emilsson, L. (2018). *Mechanical Design Analysis for the Canister: Posiva SKB Report 04*.

Jung, K.-W., Lim, S., and Bahn, Y.-S. (2017). Microbial radiation-resistance mechanisms. *J. Microbiol.* 55, 499–507. doi:10.1007/s12275-017-7242-5

Kalfayan, G (2019). PhD-Thesis. Procédé d"assemblage par chauffage micro-ondes à température modérée d"un matériau céramique alumino-silicaté pour conteneur de déchets radioactifs. *École nationale supérieure des Mines de Saint-Etienne*.

Kania, A., Szindler, M.M., and Szindler, M. (2021). Structure and corrosion behavior of TiO2 thin films deposited by ALD on a biomedical magnesium alloy. *Coatings* 11, 70–84. doi:10.3390/coatings11010070

Karnland, O., Olsson, S., Dueck, A., Birgersson, M., Nilsson, U., Hernan-Håkansson, T., Pedersen, K., Nilsson, S., Eriksen, T., and Rosborg, B. (2009). *Long term test of buffer material at the Äspö Hard Rock Laboratory, LOT project. Final report on the A2 test parcel*. Svensk Kärnbränslehantering AB. SKB Technical Report TR-09-29.

Kaufhold, S., Baille, W., Schanz, T., and Dohrmann, R. (2015). About differences of swelling pressure — dry density relations of compacted bentonites. *Appl. Clay Sci.* 107, 52–61. doi:10.1016/j.clay.2015.02.002

Kawana, A., Ichimura, H., Iwata, Y., and Ono, S. (1996). Development of PVD ceramic coatings for valve seats. *Surf. Coat. Technol.* 86-87, 212–217. doi:10.1016/s0257-8972(96)02983-0

Keech, P.G., Vo, P., Ramamurthy, S., Chen, J., Jacklin, R., and Shoesmith, D. W. (2014). Design and development of copper coatings for long term storage of used nuclear fuel. *Corros. Eng. Sci. Technol.* 49, 425–430. doi:10.1179/1743278214y.0000000206

Keech, P.G., Behazin, M., Binns, J.W., and Briggs, S. (2020). An update on the copper corrosion program for the long-term management of used nuclear fuel in Canada. *Mater. Corros.* 72, 25–31. doi:10.1002/maco.202011763

Kerber, A., and Knorr, J. (2013). SiC encapsulation of high-level waste for long-term immobilization. *atw* 58, 8–13.

Kiczka, M., Pekala, M., Maanoja, S., Muuri, E., and Wersin, P. (2021). Modelling of solute transport and microbial activity in diffusion cells simulating a bentonite barrier of a spent nuclear fuel repository. *Appl. Clay Sci.* 211, 106193. doi:10.1016/j.clay.2021.106193

King, F. (1995). A natural analogue for the long-term corrosion of copper nuclear waste containers – reanalysis of a study of a bronze cannon. *Appl. Geochem.* 10, 477–487. doi:10.1016/0883-2927(95)00019-g

King, F. (2005). Evolution of environmental conditions in a deep geological repository in the sedimentary rock of the Michigan Basin, Ontario. *Ontario Power Generation Nuclear Waste Management Division Report 06819-REP-01300-10102-R00*.

King, F. (2006). "Review and gap analysis of the corrosion of copper containers under unsaturated conditions, Ontario Power Generation," in *Nuclear Waste Management Division Report 06819-REP-01300-10124-R00*.

King, F. (2008a). "Corrosion of carbon steel under anaerobic conditions in a repository for SF and HLW in Opalinus Clay," in *Nagra Technical Report 08-12* (Wettingen, Switzerland: Nagra).

King, F. (2008b). "Mixed-Potential Modelling of the Corrosion of Copper in the Presence of Sulphide," in *Working Report 2007-63* (Finland: Posiva Oy).

King, F. (2013a). Container materials for the storage and disposal of nuclear waste. *Corrosion* 69, 986–1011. doi:10.5006/0894

King, F. (2013b). *A review of the properties of pyrite and the implications for corrosion of the copper canister. TR-13-19*. Sweden: SKB.

King, F. (2014a). *Durability of High Level Waste and Spent Fuel Disposal Containers-an overview of the combined effect of chemical and mechanical degradation mechanisms. Appendix B. 6-Corrosion of Nickel Alloys*. AMEC Nuclear UK Limited.

King, F. (2014b). Predicting the Lifetimes of Nuclear Waste Containers. *J. Mater.* 66, 526–537. doi:10.1007/s11837-014-0869-3

King, F. (2017). "Nuclear waste canister materials: corrosion behaviour and long-term performance in geological repository systems," in *Chapter in: Geological Repository Systems for Safe Disposal of Spent Nuclear Fuels and Radioactive Waste*. Editors M.J. Apted and J. Ahn (Elsevier Ltd), 365–408.

King, F. (2020). "Canister Materials for the Disposal of Nuclear Waste," in *Comprehensive Nuclear Materials*. 2nd Edition (Elsevier).

King, F., and Behazin, M. (2021). A Review of the Effect of Irradiation on the Corrosion of Copper-Coated Used Fuel Containers. *Corros. Mater. Degrad.* 2, 678–707. doi:10.3390/cmd2040037

King, F., and Kolář, M. (2000). *The copper container corrosion model used in AECL's second case study. 06819-REP-01200-10041-R00. Ontario Power Generation*. Nuclear Waste Management Division.

King, F., and Kolář, M. (2006). *Consequences of microbial activity for corrosion of copper used fuel containers–analyses using the CCM-MIC. OPG 06819-REP-1300-10120-R00*. Toronto, Canada: Ontario Power Generation.

King, F., and Kolář, M. (2019). *Copper Sulphide Model (CSM). Model improvements, sensitivity analyses, and results from the Integrated Sulphide Project inter-model comparison exercise*. Sweden: SKB. TR-18-08.

King, F., and LeNeveu, D. (1992). "Prediction of the lifetimes of copper nuclear waste containers," in *Proceedings of the Topical Meeting on Nuclear Waste Packaging, Focus '91. Las Vegas: La Grange Park* (American Nuclear Society), 253–261.

King, F., and Lilja, C. (2014). Localised corrosion of copper canisters. *Corros. Eng. Sci. Technol.* 49, 420–424. doi:10.1179/1743278214y.0000000182

King, F., and Padovani, C. (2011). Review of the corrosion performance of selected canister materials for disposal of UK HLW and/or spent fuel. *Corros. Eng. Sci. Technol.* 46, 82–90. doi:10.1179/1743278211y.0000000005

King, F., Litke, C.D., and Ryan, S.R. (1992). A Mechanistic Study of The Uniform Corrosion of Copper In Compacted Na-Montmorillonite/Sand Mixtures. *Corros. Sci.* 33, 1979–1995. doi:10.1016/0010-938x(92)90196-a

King, F., Kolář, M., and Maak, P. (2008). Reactive-transport model for the prediction of the uniform corrosion behaviour of copper used fuel containers. *J. Nucl. Mater.* 379, 133–141. doi:10.1016/j.jnucmat.2008.06.017

King, F., Lilja, C., Pedersen, K., Pitkänen, P., and Vähänen, M. (2010). *An Update of the State-of-the-Art Report on the Corrosion of Copper Under Expected Conditions in a Deep Geologic Repository*. Swedish Nuclear Fuel and Waste Management Co. Report, Technical Report TR-10-67 and Posiva Oy Report, POSIVA 2011-01.

King, F., Kolář, M., Vähänen, M., and Lilja, C. (2011). Modelling long term corrosion behaviour of copper canisters in KBS-3 repository. *Corros. Eng. Sci. Technol.* 46, 217–222. doi:10.1179/18211y.0000000004

King, F., Kolář, M., and Keech, P.G. (2014). Simulations of long-term anaerobic corrosion of carbon steel containers in Canadian deep geological repository. *Corros. Eng. Sci. Technol.* 49, 455–459. doi:10.1179/1743278214y.0000000187

King, F., Sanderson, D., and Watson, S. (2016). *Durability of High-Level Waste and Spent Fuel Disposal Containers – an overview of the combined effect of chemical and mechanical degradation mechanisms*. AMEC Report 17697/TR/03.

King, F., Hall, D.S., and Keech, P.G. (2017a). Nature of the nearfield environment in a deep geological repository and the implications for the corrosion behaviour of the container. *Corros. Eng. Sci. Technol.* 52, 25–30. doi:10.1080/1478422x.2017.1330736

King, F., Chen, J., Qin, Z., Shoesmith, D., and Lilja, C. (2017b). Sulphide-transport control of the corrosion of copper canisters. *Corros. Eng. Sci. Technol.* 52, 210–216. doi:10.1080/1478422x.2017.1300363

King, F., Kolář, M., Puigdomenech, I., Pitkänen, P., and Lilja, C. (2021). Modeling microbial sulfate reduction and the consequences for corrosion of copper canisters. *Mater. Corros.* 72, 339–347. doi:10.1002/maco.202011770

Knorr, J., Lippmann, W., Reinecke, A-M., Wolf, R., Kerber, A., and Wolter, A. (2008). SiC encapsulation of (V)HTR components and waste by laser beam joining of ceramics. *Nucl. Eng. Des.* 238, 3129–3135. doi:10.1016/j.nucengdes.2008.01.022

Koivuluoto, H., and Vuoristo, P. (2010). Structural analysis of cold-sprayed nickel-based metallic and metallic ceramic coatings. *J. Therm. Spray Technol.* 19, 975–989. doi:10.1007/s11666-010-9481-4

Kojima, Y., Hioki, T., and Tsujikawa, S. (1995). Simulation of The State of Carbon Steel *n* Years After Disposal with *n* Years of Corrosion Product on its Surface in a Bentonite Environment. *Materials Research Society Symposium Proceedings* 353, 711–718. doi:10.1557/proc-353-711

Konovalova, V. (2021). The Effect of Temperature on the Corrosion Rate of Iron-Carbon Alloys. *Materials Today: Proceedings* 38, 1326–29. doi:10.1016/j.matpr.2020.08.094

Kottemann, M., Kish, A., Iloanusi, C., Bjork, S., and DiRuggiero, J. (2005). Physiological responses of the halophilic archaeon Halobacterium sp. strain NRC1 to desiccation and gamma irradiation. *Extremophiles* 9, 219–227. doi:10.1007/s00792-005-0437-4

Kotelnikova, S., and Pedersen, K. (1998). Distribution and activity of methanogens and homoacetogens in deep granitic aquifers at Aspo Hard Rock Laboratory, Sweden. *FEMS Microbiology Ecology* 26 (Issue 2), 121–134. doi:10.1016/S0168-6496(98)00028-2

Kumpalainen, S., Kiviranta, L., and Korkeakoski, P. (2016). Long-term effects of an iron heater and Äspö groundwater on smectite clays: Chemical and hydromechanical results from the *in situ* alternative buffer material (ABM) test package 2. *Clay Miner* 51, 129–144. doi:10.1180/claymin.2016.051.2.02

Kursten, B., MacDonald, D.D., Smart, N.R., and Gaggiano, R. (2017). Corrosion Issues of Carbon Steel Radioactive Waste Packages Exposed to Cementitious Materials with Respect to the Belgian Supercontainer Concept. *Corros. Eng. Sci. Technol.* 52, 11–16. doi:10.1080/1478422x.2017.1292345

Kursten, B., Smailos, E., Azkarate, I., Werme, L., Smart, N.R., and Santarini, G. (2003). COBECOMA State-of-the-Art Document on the Corrosion Behaviour of Container Materials. *EUROPEAN COMMISSION 5th EURATOM FRAMEWORK PROGRAMME 1998-2002*.

Kwong, G.M. (2011). *Status of Corrosion Studies for Copper Used Fuel Containers Under Low Salinity Conditions*. Nuclear Waste Management Organization. NWMO TR-2011-14.

Landolt, D., Davenport, A., Payer, A., and Shoesmith, D. (2009). A review of materials and corrosion issues regarding canisters for disposal of spent fuel and high-level waste in Opalinus clay. *NAGRA Technical Report 09-02*.

Lapuerta, S., Moncoffre, N., Millard-Pinard, N., Jaffrézic, H., Bérerd, H., and Crusset, D. (2006). Role of proton irradiation and relative air humidity on iron corrosion. *J. Nucl. Mater.* 352, 174–181. doi:10.1016/j.jnucmat.2006.02.051

Lapuerta, S., Bérerd, N., Moncoffre, N., Millard-Pinard, N., Jaffrézic, H., Crusset, D., and Féron, D. (2008). The Influence of Relative Humidity on Iron Corrosion under Proton Irradiation. *J. Nucl. Mater.* 375, 80–85. doi:10.1016/j.jnucmat.2007.10.011

Larker, H. (1980). *Method of containing spent nuclear fuel or high-level nuclear fuel waste*. Patent US4209420, United States.

Lee, M.S, Choi, H. J., Choi, J. W., and Kim, H. J. (2011). Application of Cold Spray Technique to the underground disposal copper canister and its corrosion properties. *Nucl. Eng. Technol.* 43, 557–566. doi:10.5516/net.2011.43.6.557

Lee, S., and Staehle, R.W. (1997). Adsorption of water on copper, nickel and iron. *Corrosion* 53, 33–42. doi:10.5006/1.3280431

Lee, Y.T.R., Ashrafizadeh, H., Fisher, G., and McDonald, A. (2017). Effect of type of reinforcing particles on the deposition efficiency and wear resistance of low-pressure cold-sprayed metal matrix composite coatings. *Surf. Coat. Technol.* 324, 190–200. doi:10.1016/j.surfcoat.2017.05.057

Legoux, J.G. (2014). Development of cold spray coating for nuclear waste storage container application. *EUCOSS*, 2014. Paris, May 26th.

Li, M., and Zinkle, S. (2012). "Physical and Mechanical Properties of Copper and Copper Alloys," in *Comprehensive Nuclear Materials*. Editor R.J.M. Konings (Amsterdam: Elsevier), 4, 667–690. doi:10.1016/b978-0-08-056033-5.00122-1

Liang, D., Liu, X., Woodard, T. L., Holmes, D. E., Smith, J. A., Nevin, K. P., et al. (2021). Extracellular electron exchange capabilities of Desulfovibrio ferrophilus and Desulfopila corrodens. *Environ. Sci. Tech.* 55, 16195–16203. doi:10.1021/acs.est.1c04071

Litke, C.D., Ryan, S.R., and King, F. (1992). *TA mechanistic study of the uniform corrosion of copper in compacted clay-sand soil*. Atomic Energy of Canada Ltd. AECL-10397, COG-91-304.

Little, B.J., Hinks, J., and Blackwood, D.J. (2020). Microbially influenced corrosion: Towards an interdisciplinary perspective on mechanisms. *Int. Biodeterior. Biodegrad.* 154, 105062. doi:10.1016/j.ibiod.2020.105062

Liu, C., Wang, J., Zhang, Z., and Han, E-H. (2017). Studies on Corrosion Behaviour of Low Carbon Steel Canister with and without γ-Irradiation in China's HLW Disposal Repository. *Corros. Eng. Sci. Technol.* 52, 136–40. doi:10.1080/1478422X.2017.1348762

Lobach, K., Kupriiyanova, Y., Kolodiy, I., Sayenko, S., Shkuropatenko, V., Voyevodin, V., Zykova, A., Bykov, A., Chunyayev, O., and Tovazhnyanskyy, L. (2018). Optimisation of Properties of Silicon Carbide Ceramics with the Use of Different Additives. *Funct. Mater.* 25, 496–504. doi:10.15407/fm25.03.496

Lobach, K.V., Sayenko, S. Y., Shkuropatenko, V. A., Voyevodin, V. M., Zykova, H. V., Zuyok, V. A., et al. (2020). Corrosion Resistance of Ceramics Based on SiC under Hydrothermal Conditions. *Mater. Sci.* 55, 672–682. doi:10.1007/s11003-020-00358-5

Lopez-Fernandez, M., Cherkouk, A., Vilchez-Vargas, R., Jauregui, R., Pieper, D., Boon, N., Sanchez-Castro, I., and Merroun, M.L. (2015). Bacterial Diversity in Bentonites, Engineered Barrier for Deep Geological Disposal of Radioactive Wastes. *Microb. Ecol.* 70, 922–935. doi:10.1007/s00248-015-0630-7

Lousada, C. M., Soroka, I. L., Yagodzinsky, Y., Tarakina, N. V., Todoshchenko, O., Hänninen, H., et al. (2016). Gamma radiation induces hydrogen absorption by copper in water. *Scientific Reports* 6 (1), 24234. doi:10.1038/srep24234

Lu, C., Samper, J., Fritz, B., Clement, A., and Montenegro, L. (2011). Interactions of corrosion products and bentonite: An Extended multicomponent reactive transport model. *Physics and Chemistry of the Earth* 36, 1661–1668. doi:10.1016/j.pce.2011.07.013

Lundgren, K. (2004). *Final disposal of fuel - electron radiation outside copper canister. Technical Report SKB-TR-04-06*. Stockholm, Sweden: Swedish Nuclear Fuel and Waste Management Co.

Lv, M.Y., and Du, M. (2018). A review: microbiologically influenced corrosion and the effect of cathodic polarization on typical bacteria. *Rev. Environ. Sci. Biotechnol.* 17, 431–446. doi:10.1007/s11157-018-9473-2

Maak, P., and King, F. (2006). A Model for Predicting Stress Corrosion Cracking of Copper Containers in A Deep Geologic Repository. *MRS Online proceedings Library* 932, 291. doi:10.1557/proc-932-29.1

Maanoja, S., Lakaniemi, A. M., Lehtinen, L., Salminen, L., Auvinen, H., Kokko, M., et al. (2020). Compacted bentonite as a source of substrates for sulfate-reducing microorganisms in a simulated excavation-damaged zone of a spent nuclear fuel repository. *Appl. Clay Sci.* 196, 105746. doi:10.1016/j.clay.2020.105746

Maanoja, S., Palmroth, M., Salminen, L., Lehtinen, L., Kokko, M., Lakaniemi, A. M., et al. (2021). The effect of compaction and microbial activity on the quantity and release rate of water-soluble organic matter from bentonites. *Appl. Clay Sci.* 211, 106192. doi:10.1016/j.clay.2021.106192

Malmström, M., Banwart, S., Duro, L., Wersin, P., and Bruno, J. (1995). Biotite and chlorite weathering at 25 degrees C: the dependence of pH and (bi)carbonate on weathering kinetics, dissolution stoichiometry, and solubility; and the relation to redox conditions in granitic aquifers-. *SKB Technical Report 95-0.1, Stockholm, Sweden*.

Mand, J, Park, HS, Okoro, C, Lomans, BP, Smith, S, Chiejina, L, and Voordouw, G (2016). Microbial Methane Production Associated with Carbon Steel Corrosion in a Nigerian Oil Field. *Front. Microbiol.* 6, 1538. doi:10.3389/fmicb.2015.01538

Marion (2014). "Modélisation électrochimique de la vitesse de corrosion généralisée du fer en milieu poreux," in *Contribution à un modèle prédictif de la durabilité des aciers non alliés en conditions de stockage géologique* (Université de Bourgogne;2014). PhD Thesis.

Marsh, G.P., and Taylor, K.J. (1988). An Assessment of Carbon Steel Containers for Radioactive Waste Disposal. *Corros. Sci.* 28, 289–320. doi:10.1016/0010-938X(88)90111-4

Marshall, M.H.M., McKelvie, J.R., Simpson, A.J., and Simpson, M.J. (2015). Characterization of natural organic matter in bentonite clays for potential use in deep geological repositories for used nuclear fuel. *Appl. Geochem.* 54, 43–53. doi:10.1016/j.apgeochem.2014.12.013

Marty, N.C.M., Fritz, B., Clément, A., and Michau, N. (2010). Modelling the long-term alteration of the engineered bentonite barrier in an underground radioactive waste repository. *Appl. Clay Sci.* 47, 82–90. doi:10.1016/j.clay.2008.10.002

Masurat, P., Eriksson, S., and Pedersen, K. (2010). Microbial sulphide production in compacted Wyoming bentonite MX-80 under *in situ* conditions relevant to a repository for high-level radioactive waste. *Appl. Clay Sci.* 47, 58–64. doi:10.1016/j.clay.2009.01.004

Matschiavelli, N., Kluge, S., Podlech, C., Standhaft, D., Grathoff, G., Ikeda-Ohno, A., et al. (2019). The Year-Long Development of Microorganisms in Uncompacted Bavarian Bentonite Slurries at 30 and 60 °C. *Environ. Sci. Tech.* 53, 10514–10524. doi:10.1021/acs.est.9b02670

Matts, O., Hammoud, H., Sova, A., Bensaid, Z., Kermouche, G., Klöcker, H., et al. (2019). Influence of Cold Spray Nozzle Displacement Strategy on Microstructure and Mechanical Properties of Cu/SiC Composites Coating. *Key Eng. Mater.* 813, 110–115. doi:10.4028/www.scientific.net/KEM.813.110

Mattson, E. (1980). "Aluminium oxide as the encapsulation material for unreprocessed nuclear fuel waste-evaluation from the viewpoint of corrosion," in *Swedish Corrosion Institute* (Final Report KBS), 80–15.

McNamara, N.P., Black, H.I.J., Beresford, N.A., and Parekh, N.R. (2003). Effects of acute gamma irradiation on chemical, physical and biological properties of soils. *Appl. Soil Ecol.* 24, 117–132. doi:10.1016/s0929-1393(03)00073-8

Mendoza, A. (2017). *Gas generation and migration in clay media as a result of anaerobic steel corrosion*. Prague: SURAO. Technical report No. 187/2017.

Miller, W., Alexander, R., Chapman, N., McKinley, M., and Smellie, J. (1994). *Natural analogue studies in the geological disposal of radioactive wastes*. Sweden: Wettingen. Nagra Technical Report NTB-93-03.

Milodowski, A.E., Styles, M.T., and Hards, V.L. (2000). *A natural analogue for copper waste canisters: The copper-uranium mineralised concretions in the Permian mudrocks of south Devon, SKB Report TR-00-11*.

Milodowski, A.E., Styles, M.T., Horstwood, M.S.A., and Kemp, S.J. (2002). Alteration of uraniferous and native copper concretions in the Permian mudrocks of south Devon, United Kingdom. A natural analogue study of the corrosion of copper canisters and radiolysis effects in a repository for spent nuclear fuel. *SKB Report TR-02-09*.

Milošev, I., and Navinšek, B. (1993). Corrosion properties of selected Cr-based hard and protective coatings. *Surf. Coat. Technol.* 60, 545–548. doi:10.1016/0257-8972(93)90150-m

Milošev, I., Strehblow, H.H., and Navinšek, B. (1997). Comparison of TiN, ZrN and CrN hard nitride coatings: electrochemical and thermal oxidation. *Thin Solid Films* 303, 246–254. doi:10.1016/s0040-6090(97)00069-2

Minhas, B., Dino, S., Zuo, Y., Qian, H., and Zhao, X. (2021). Improvement of Corrosion Resistance of TiO2 Layers in Strong Acidic Solutions by Anodizing and Thermal Oxidation Treatment. *Materials* 14, 1188–13. doi:10.3390/ma14051188

Mironenko, N.V., Alekhina, I.A., Zhdanova, N.N., and Bulat, S.A. (2000). Intraspecific variation in gamma-radiation resistance and genomic structure in the filamentous fungus Alternaria alternata: A case study of strains inhabiting Chernobyl reactor no. 4. *Ecotoxicology and Environmental Safety* 45, 177–187. doi:10.1006/eesa.1999.1848

Mohajerani, M., Delage, P., Sulem, J., Monfared, M., Tang, A.M., and Gatmiri, B. (2012). A laboratory investigation of thermally induced pore pressures in the Callovo-Oxfordian claystone. *International Journal of Rock Mechanics and Mining Sciences* 52, 112–121. doi:10.1016/j.ijrmms.2012.02.012

Mohamed-Said, M., Vuillemin, B., Oltra, R., Marion, A., Trenty, L., and Crusset, D. (2017). "Predictive modelling of the corrosion rate of carbon steel focusing on the effect of the precipitation of corrosion products. Corrosion Engineering," in *Science and Technology 52/sup1*, 178–185.

Mon, A., Samper, J., Montenegro, L., Naves, A., and Fernández, J. (2017). Long-term non-isothermal reactive transport model of compacted bentonite, concrete and corrosion products in a HLW repository in clay. *Journal of Contaminant Hydrology* 197, 1–16. doi:10.1016/j.jconhyd.2016.12.006

Montes-H, G., Marty, N., Fritz, B., Clement, A., and Michau, N. (2005). Modelling of long-term diffusion-reaction in a bentonite barrier for radioactive waste confinement. *Applied Clay Science* 30, 181–198. doi:10.1016/j.clay.2005.07.006

Müller, H.R., Garitte, B., Vogt, T., Köhler, S., Sakaki, T., Weber, H., Spillman, T., Hertrich, M., Becker, J.K., Giroud, N., Cloet, V., Diomidis, N., and Vietor, T. (2017). Implementation of the full-scale emplacement (FE) experiment at the Mont Terri rock laboratory. *Swiss J. Geosci.* 110, 287–306. doi:10.1007/s00015-016-0251-2

Muyzer, G., and Stams, A.J. (2008). The ecology and biotechnology of sulphate-reducing bacteria. *Nat. Rev. Microbiol.* 6, 441–454. doi:10.1038/nrmicro1892

Nagra (2002). *Demonstration of disposal feasibility for spent fuel, vitrified high-level waste and long-lived intermediate-level waste (Entsorgungsnachweis)*. Nagra Technical Report Number 02-05.

Nardi, A., Idiart, A., Trinchero, P., de Vries, L. M., and Molinero, J. (2014). Interface COMSOL-PHREEQC (iCP), an efficient numerical framework for the solution of coupled multiphysics and geochemistry. *Comput. Geosci.* 69, 10–21. doi:10.1016/j.cageo.2014.04.011

Necib, S., Diomidis, N., Keech, P., and Nakayama, M. (2017). Corrosion of carbon steel in clay environments relevant to radioactive waste geological disposals, Mont Terri rock laboratory (Switzerland). *Swiss J. Geosci.* 110, 329–342. doi:10.1007/s00015-016-0259-7

Necib, S., Linard, Y., Crusset, D., Michau, N., Daumas, S., Burger, E., Romaine, A., and Schlegel, M.L. (2016). Corrosion at the carbon steel-clay borehole water and gas interfaces at 85 °C under anoxic and transient acidic conditions. *Corros. Sci.* 111, 242–258. doi:10.1016/j.corsci.2016.04.039

Nelson, J.L., Westerman, R.E., and Gerber, F.S. (1983). Irradiation-Corrosion Evaluation of Metals for Nuclear Waste Package Applications in Grande Ronde Basalt Groundwater. *MRS Proceedings* 26, 121. doi:10.1557/PROC-26-121

Ngo, V.V., Delalande, M., Clément, A., Michau, N., and Fritz, B. (2014). Coupled transport-reaction modeling of the long-term interaction between iron, bentonite and Callovo-Oxfordian claystone in radioactive waste confinement systems. *Applied Clay Science* 101, 430–443. doi:10.1016/j.clay.2014.08.020

Nguyen, T.S., Selvadurai, A.P.S., and Armand, G. (2005). Modelling the FEBEX THM experiment using a state surface approach. *Int. J. Rock Mech. Min. Sci.* 42, 639–651. doi:10.1016/j.ijrmms.2005.03.005

NUMO (2021). *The NUMO Pre-siting SDM-based Safety Case, NUMO-TR-21-01*. Nuclear Waste Management Organization of Japan.

NWMO (2016). *Implementing Adaptive Phased Management 2016 to 2020*. Nuclear Waste Management Organization Report.

Ochs, M., and Talerico, C. (2004). "SR-Can," in *Data and uncertainty assessment. Migration parameters for the bentonite buffer in the KBS-3 concept*. Sweden: SKB. SKB TR-04-18.

Ogawa, K., Ito, K., Ichimura, K., Ichikawa, Y., Ohno, S., and Onda, N. (2008). Characterization of Low-Pressure Cold-Sprayed Aluminum Coatings. *J. Therm. Spray Technol.* 17, 728–735. doi:10.1007/s11666-008-9254-5

Ogwu, MC, Kerfahi, D, Song, H, Dong, K, Seo, H, Lim, S, Srinivasan, S, Kim, MK, Waldman, B, and Adams, JM (2019 May 27). Changes in soil taxonomic and functional diversity resulting from gamma irradiation. *Sci Rep* 9 (1), 7894. doi:10.1038/s41598-019-44441-7

Otte, J.M., Blackwell, N., Soos, V., Rughöft, S., Maisch, M., Kappler, A., Kleindienst, S., and Schmidt, C. (2018). Sterilization impacts on marine sediment - Are we able to inactivate microorganisms in environmental samples? *EMS Microbiol. Ecol.* 94, fiy189. doi:10.1093/femsec/fiy189

Padovani, C., King, F., Lilja, C., Féron, D., Necib, S., Crusset, D., Deydier, V., Diomidis, N., Gaggiano, R., Ahn, T., Keech, P.G., Macdonald, D.D., Asano, H., Smart, N., Hall, D.S., Hänninen, H., Engelberg, D., Noël, J.J., and Shoesmith, D.W. (2017). The Corrosion Behaviour of Candidate Container Materials for the Disposal of High-Level Waste and Spent Fuel – a Summary of the State of the Art and Opportunities for Synergies in Future R&D. *Corr. Eng. Sci. Tech.* 52, 227–31. doi:10.1080/1478422X.2017.1356973

Padovani, C., Pletser, D., Jurkschat, K., Armstrong, D., Dugdale, S., Brunt, D., Faulkner, R., Was, G., and Johansson, A.J. (2019). *Assessment of microstructural changes in copper due to gamma radiation damage*. Report number: SKB TR-19-12.

Parkhurst, D.L., and Appelo, C.A.J. (2013). "Description of input and examples for PHREEQC version 3 – A computer program for speciation, batch-reaction, one-dimensional transport, and inverse geochemical calculations," in *Techniques and Methods 6–A43* (Denver, Colorado: U.S. Geological Survey).

Patel, R., Punshon, C., Nicolas, J., Bastid, P., Zhou, R., Schneider, C., Bagshaw, N., Howse, D., and King, F. (2012). Canister design concepts for disposal of spent fuel and high level waste. *Nagra Technical Report*. NTB 12-06.

Payer, J.H., Finsterle, S., Apps, J.A., and Muller, R.H. (2019). Corrosion Performance of Engineered Barrier System in Deep Horizontal Drillholes. *Energies* 12, 1491. doi:10.3390/en12081491

Pedersen, K. (2010). Analysis of copper corrosion in compacted bentonite clay as a function of clay density and growth conditions for sulfate-reducing bacteria. *J. Appl. Microbiol.* 108, 1094–1104. doi:10.1111/j.1365-2672.2009.04629.x

Pedersen, K. (2017). *MIND deliverable 2.4: Bacterial activity in compacted bentonites*. Available at: https://mind15.eu/deliverables/.

Pedersen, K., Motamedi, M., Karnland, O., and Sandén, T. (2000). Mixing and sulphate-reducing activity of bacteria in swelling, compacted bentonite clay under high-level radioactive waste repository conditions. *J. Appl. Microbiol.* 89, 1038–1047. doi:10.1046/j.1365-2672.2000.01212.x

Pękala, M., Alt-Epping, P., and Wersin, P. (2019). 3D and 1D Dual-Porosity Reactive Transport Simulations - Model Improvements, Sensitivity Analyses, and Results from the Integrated Sulfide Project Inter-Model Comparison Exercise. *Posiva Working Report 2018-31*.

Pekala, M., Wersin, P., Cloet, V., and Diomidis, N. (2019). Reactive transport calculations to evaluate sulphide fluxes in the near-field of a SF/HLW repository in the Opalinus Clay. *Applied geochemistry* 100, 169–180. doi:10.1016/j.apgeochem.2018.11.006

Pekala, M., Smith, P., Wersin, P., Diomidis, N., and Cloet, V. (2020). Comparison of models to evaluate microbial sulphide generation and transport in the near field of a SF/HLW repository in Opalinus Clay. *Journal of contaminant hydrology* 228, 103561. doi:10.1016/j.jconhyd.2019.103561

Peña, J, Torres, E, Turrero, MJ, Escribano, A, and Martín, PL (2008). Kinetic modelling of the attenuation of carbon steel canister corrosion due to diffusive transport through corrosion product layers. *Corrosion Science* 50 (8), 2197–2204. doi:10.1016/j.corsci.2008.06.004

Phillips, R.W., Wiegel, J., Berry, C.J., Fliermans, C., Peacock, A.D., White, D.C., and Shimkets, L.J. (2002). Kineococcus radiotolerans sp. nov., a radiationresistant, Gram-positive bacterium. *Int. J. Syst. Evol. Microbiol.* 52, 933–938. doi:10.1099/00207713-52-3-933

Pignatelli, I., Bourdelle, F., Bartier, D., Mosser-Ruck, R., Truche, L., Mugnaioli, E., and Michau, N. (2014). Iron–clay interactions: Detailed study of the mineralogical transformation of claystone with emphasis on the formation of iron-rich T–O phyllosilicates in a step-by-step cooling experiment from 90 °C to 40 °C. *Chem. Geol.* 387, 1–11. doi:10.1016/j.chemgeo.2014.08.010

Pignatelli, I., Mugnaioli, E., Hybler, J., Mosser-Ruck, R., Cathelineau, M., and Michau, N. (2013). A multi-technique characterization of cronstedtite synthesized by iron-clay interaction in a step-by-step cooling procedure. *Clays and Clay Miner* 61, 277–289. doi:10.1346/ccmn.2013.0610408

Pinnel, M.R., Tompkins, H.G., and Heath, D.E. (1979). Oxidation of copper in controlled clean air and standard laboratory air at 50°C to 150°C. *Appl. Surf. Sci.* 2, 558–577. doi:10.1016/0378-5963(79)90047-3

Poller, A., Mayer, G., Darcis, M., and Smith, P. (2016) "Modelling of gas generation in deep geological repositories after closure," in *Nagra Technical Report NTB 16-04*. Wettingen, Switzerland: Nagra.

Pospiskova, L., Dobrev, D., Kouril, M., Stoulil, J., Novikova, D., Kotnour, P., and Matal, O. (2017). Czech national programme and disposal canister concept. *Corros. Eng. Sci. Technol.* 52, 6–10. doi:10.1080/1478422x.2017.1300379

Posiva (2007). *Expected evolution of a spent nuclear fuel repository at Olkiluoto*. Posiva Report 2006-05.

Posiva (2013). *Safety Case for the Disposal of Spent Nuclear Fuel at Olkiluoto - Models and Data for the Repository System 2012*. Eurajoki: Posiva Oy.

Posiva (2021a). Canister evolution. *Posiva Oy Working Report, WR-2021-06*.

Posiva (2021b). Sulfide fluxes and concentrations in the spent nuclear fuel repository at Olkiluoto – 2021 update. *Posiva Oy Working Report, WR-2021-07*.

Puigdomenech, I., Ambrosi, J.-P., Eisenlohr, L., Lartigue, J.-E., Banwart, S.A., Bateman, K., Milodowski, A.E., West, J.M., Griffault, L., Gustafsson, E., Hama, K., Yoshida, H., Kotelnikova, S., Pedersen, K., Michaud, V., Trotignon, L., Rivas Perez, J., and Tullborg, E.-L. (2001). *O2 depletion in granitic media — the REX project*. Svensk Kärnbränslehantering AB. Report no. TR-01-05.

Pusch, R., Karnland, O., Lajudie, A., and Decarreau, A. (1992). MX 80 Clay Exposed to High Temperatures and Gamma Radiation. *SKB Technical Report* 93–03 (93–03).

Qin, Z., Daljeet, R., Ai, M., Farhangi, N., Noël, J.J., Ramamurthy, S., Shoesmith, D., King, F., and Keech, P. (2017). The active/passive conditions for copper corrosion under nuclear waste repository environment. *Corros. Eng. Sci. Technol.* 52, 45–49. doi:10.1080/1478422x.2016.1274088

Raiko, H., and Salo, J.-K. (1999). *Design report of the disposal canister for twelve fuel assemblies*. Posiva 99-18.

Raikko, H., Sandström, R., Rydén, H., and Johansson, M. (2010). *Design analysis report for the canister*. Stockholm: SKB Report. SKB TR-10-28.

Rajala, P., Carpén, L., Vepsäläinen, M., Raulio, M., Sohlberg, E., and Bomberg, M. (2015). Microbially induced corrosion of carbon steel in deep groundwater environment. *Front. Microbiol.* 6, 647. doi:10.3389/fmicb.2015.00647

Rebata-Landa, V., and Santamarina, J.C. (2006). Mechanical limits to microbial activity in deep sediments. *Geochem. Geophys. Geosystems* 7. doi:10.1029/2006GC001355

Refait, P., Grolleau, A.-M., Jeannin, M., Francois, E., and Sabot, R. (2016). Localized corrosion of carbon steel in marine media: Galvanic coupling and heterogeneity of the corrosion product layer. *Corros. Sci.* 111, 583–595. doi:10.1016/j.corsci.2016.05.043

Riba, O. C., Coene, E., Silva, O., and Duro, L. (2020). Spent fuel alteration model integrating processes of different time-scales. *MRS Advances* 5, 159–166. doi:10.1557/adv.2020.51

Rockhvarger, A.E., and Khizh, A.B. (1999). Process for the preparation of thick-walled ceramic products. *ROKON SYSTEMS INC., Patent US5911941A*.

Rockhvarger, A.E., and Khizh, A.B. (2000). *Processus and apparatus for joining thick-walled ceramic parts*. Patent US6054700.

Rockhvarger, A.E., and Khizh, A.B. (1998). *Large size, thick-walled ceramic containers*. NUCON SYSTEMS INC. Patent WO9844834.

Romaine, A., Jeannin, M., Sabot, R., Necib, S., and Refait, P. (2015). Corrosion processes of carbon steel in argillite: Galvanic effects associated with the heterogeneity of the corrosion product layer. *Electrochim. Acta* 182, 1019–1028. doi:10.1016/j.electacta.2015.10.010

Romanoff, M. (1989). *Underground corrosion*. Houston: NACE International.

Roy, S.K., and Sircar, S.C. (1981). A critical appraisal of the logarithmic rate law in thin-film formation during oxidation of copper and its alloys. *Oxidation of Metals* 15, 9–20. doi:10.1007/bf00603754

Rutqvist, J., and Tsang, C-F. (2008). *Review of SKB´s Work on Coupled THM Processes Within SR-Can: external review contribution in support of SKI´s and SSI´s review of SR-Can*. SKI Report 2008:08.

RWM (2016). *Geological Disposal-Waste Evolution Status Report*. NDA Report DSSC/451/01. Radioactive Waste Management.

Saheb, M., Marsal, F., Matthiesen, H., Neff, D., Dillmann, P., and Pellegrini, D. (2011). Fluctuation of redox conditions in radioactive waste disposal cell: characterisation of corrosion layers formed on archaeological analogues. *Corros. Eng. Sci. Technol.* 46, 199–204. doi:10.1179/1743278210y.0000000006

Samper, J., Lu, C., and Montenegro, L. (2008). Reactive transport model of interactions of corrosion products and bentonite. *Physics and Chemistry of the Earth* 33, S306–S316. doi:10.1016/j.pce.2008.10.009

Samper, J., Naves, A., Montenegro, L., and Mon, A. (2016). Reactive transport modelling of the long-term interactions of corrosion products and compacted bentonite in a HLW repository in granite: Uncertainties and relevance for performance assessment. *Applied Geochemistry* 67, 42–51. doi:10.1016/j.apgeochem.2016.02.001

Sánchez, M., Gens, A., and Olivella, S. (2012). THM analysis of a large-scale heating test incorporating material fabric changes. *Int. J. Numer. Anal. Meth. Geomech.* 36, 391–421. doi:10.1002/nag.1011

Savage, D., Watson, C., Benbow, S., and Wilson, J. (2010). Modelling iron-bentonite interactions. *Applied Clay Science* 47, 91–98. doi:10.1016/j.clay.2008.03.011

Savage, D. (2012). *Prospects for Coupled Modelling. STUK-TR 13. Radiation and Nuclear Safety Authority*. Finland: Helskinki.

Schanz, T. (2016). Transient boundary conditions in the frame of THM-processes at nuclear waste repositories. *E3S Web of Conferences* 9, 03001. doi:10.1051/e3sconf/20160903001

Schlegel, M.L., Necib, S., Daumas, S., Blanc, C., Foy, E., Trcera, N., and Romaine, A. (2016). Microstructural characterization of carbon steel corrosion in clay borehole water under anoxic and transient acidic conditions. *Corros. Sci.* 109, 126–144. doi:10.1016/j.corsci.2016.03.022

Schlegel, M.L., Necib, S., Daumas, S., Labat, M., Blanc, C., Foy, E., and Linard, Y. (2018). Corrosion at the carbon steel-clay borehole water interface under anoxic alkaline and fluctuating temperature conditions. *Corros. Sci.* 136, 70–90. doi:10.1016/j.corsci.2018.02.052

Schutz, R.W. (1996). Ruthenium enhanced titanium alloys: Minor ruthenium additions produce cost effective corrosion resistant commercial titanium alloys. *Platinum Metals Review* 40, 54–61. doi:10.1595/003214096x4025461

Scully, J.R., and Edwards, M. 2013. *Review of the NWMO Copper Corrosion Allowance*. Toronto: NWMO TR-2013-04.

Senior, N.A., Newman, R C., Artymowicz, D., Binns, W.J., Keech, P.G., and Hall, D.S. (2019). Communication—A Method to Measure Extremely Low Corrosion Rates of Copper Metal in Anoxic Aqueous Media. *Journal of The Electrochemical Society* 166 (11), C3015–C3017. doi:10.1149/2.0031911jes

Sharma, A., Gaidamakova, E. K., Grichenko, O., Matrosova, V. Y., Hoeke, V., Klimenkova, P., et al. (2017). Across the tree of life, radiation resistance is governed by antioxidant Mn2+, gauged by paramagnetic resonance. *PNAS* 114, E9253–E9260. doi:10.1073/pnas.1713608114

Sherar, B.W.A., Keech, P.G., and Shoesmith, D.W. (2011). Carbon steel corrosion under anaerobic-aerobic cycling conditions in near-neutral pH saline solutions – Part 1: Long-term corrosion behaviour. *Corros. Sci.* 53, 3636–3642. doi:10.1016/j.corsci.2011.07.015

Schindleholtz, E., Risteen, B.E., and Kelly, R.G. (2014). Effect of Relative Humidity on Corrosion of Steel under Sea Salt Aerosol Proxies: I. NaCl. *J. Electrochem. Soc.* 161, C450–C459. doi:10.1149/2.0221410jes

Shoesmith, D.W., and King, F. (1999). *The effects of gamma radiation on the corrosion of candidate materials for the fabrication of nuclear waste packages*. Atomic Energy of Canada Limited. AECL-11999.

Shoesmith, D.W. (2006). Assessing the corrosion performance of high-level nuclear waste containers. *Corrosion* 62, 703–722. doi:10.5006/1.3278296

Shrestha, R., Černoušek, T., Stoulil, J., Kovářová, H., Sihelská, K., Špánek, R., et al. (2021). Anaerobic microbial corrosion of carbon steel under conditions relevant for deep geological repository of nuclear waste. *Sci. Total Environ.* 800, 149539. doi:10.1016/j.scitotenv.2021.149539

Shuryak, I., Matrosova, V. Y., Gaidamakova, E. K., Tkavc, R., Grichenko, O., Klimenkova, P., et al. (2017). Microbial cells can cooperate to resist high level chronic ionizing radiation. *PloS one* 12, e0189261. doi:10.1371/journal.pone.0189261

SKB (2006a). *Buffer and backfill process report for the safety assessment SR-Can*. SKB Technical Report TR-06-18: 201.

SKB (2006b). Long-term safety for KBS-3 repositories at Forsmark and Laxemar - a first evaluation. *Main report of the SR-Can project, SKB Technical Report TR-06-09. Swedish Nuclear Fuel and Waste Management Company, Stockholm, Sweden*.

SKB (2010a). *Fuel and canister process report for the safety assessment SR-Site*. Updated 2015-06. SKB Technical Report TR-10-46, Stockholm: SKB.

SKB (2010b). Corrosion calculations report for the Safety Assessment SR-site. *SKB Technical report TR-10-66, SKB*.

SKB (2010c). *Design, production and initial state of the buffer*. Stockholm: Svensk Kärnbränslehantering AB.

SKB (2011). *Long-term safety for the final repository for spent nuclear fuel at Forsmark, Main report of the SR-Site project*. Stockholm: Svensk Kärnbränslehantering AB.

SKB (2019). *Supplementary information on canister integrity issues*. SKB TR, 19–15.

Smart, N.R., Blackwood, D.J., and Werme, L.O. (2001a). "The anaerobic corrosion of carbon steel and cast iron in artificial groundwaters," in *SKB Technical Report TR-99-06* (Stockholm: Swedish Nuclear Fuel and Waste Management Co.).

Smart, N.R., Blackwood, D.J., and Werme, L. (2001b). *The anaerobic corrosion of carbon steel and cast iron in artificial groundwaters*. Stockholm, Sweden: Swedish Nuclear Fuel and Waste Management Co. Technical Report SKB-TR-01-22.

Smart, N.R., Blackwood, D.J., and Werme, L. (2002a). Anaerobic corrosion of carbon steel and cast iron in artificial groundwaters: Part 2 – Gas generation. *Corrosion* 58, 627–637. doi:10.5006/1.3287691

Smart, N.R., Blackwood, D.J., and Werme, L. (2002b). Anaerobic corrosion of carbon steel and cast iron in artificial groundwaters: Part 1 – Electrochemical aspects. *Corrosion* 58, 547–559. doi:10.5006/1.3277646

Smart, N.R., Rance, A.P., Fennell, P., and Werme, L. (2003a), Expansion Due To Anaerobic Corrosion of Steel and Cast Iron: Experimental and Natural Analogue Studies, Presented at International Workshop on Prediction of Long Term Corrosion Behaviour in Nuclear Waste Systems, Cadarache, November 2001, in '*Prediction of Long Term Corrosion Behaviour in Nuclear Waste Systems*' (D. Feron and D.D. Macdonald, eds), EFC Publication No 36, published by Institute of Materials, Minerals and Mining, pg. 280.

Smart, N.R., Adams, R., and Werme, L.O. (2003b), Analogues for the Corrosion-induced Expansion of Iron in HLW Containers, presented at MRS 2003 Kalmar, Sweden, June 15-18, 2003, *Materials Research Society Symposium Proceedings Volume 807, Scientific Basis for Nuclear Waste Management XXVII*, V.M. Oversby and L.O. Werme (eds.), p. 879-884.

Smart, N R, Rance, A P, and Fennell, P A H (2005). *Galvanic corrosion of copper-cast iron couples*. SKB technical report TR-05-06.

Smart, N.R., Fennell, P.A.H., and Rance, A.P. (2006a). Expansion Due to the Anaerobic Corrosion of Iron. *SKB Report TR-06-41*.

Smart, N., Rance, A.P., Carlson, L., and Werme, L.O. (2006b). "Further Studies of the Anaerobic Corrosion of Steel in Bentonite," in *Scientific Basis for Nuclear Waste Management XXIX*.

Smart, N.R., Rance, A.P., and Werme, L.O. (2008). The Effect of Radiation on the Anaerobic Corrosion of Steel. *J. Nucl. Mater.* 379, 97–104. doi:10.1016/j.jnucmat.2008.06.007

Smart, N.R., and Hoch, A.R. (2010). "A Survey of Steel and Zircaloy Corrosion Data for Use in the SMOGG Gas Generation Model," in *Serco Assurance Report SA/ENV 0841 issue 3*.

Smart, N., Rance, A., Reddy, B., Lydmark, S., Pedersen, K., and Lilja, C. (2011). Further studies of*in situ*corrosion testing of miniature copper–cast iron nuclear waste canisters. *Corr. Eng. Sci. Tech.* 46, 142–147. doi:10.1179/1743278210y.0000000020

Smart, N.R., Reddy, B., Rance, A. P., Nixon, D. J., Frutschi, M., Bernier-Latmani, R., et al. (2017). The anaerobic corrosion of carbon steel in compacted bentonite exposed to natural Opalinus Clay porewater containing native microbial populations. *Corros. Eng. Sci. Technol.* 52, 101–112. doi:10.1080/1478422x.2017.1315233

Smith, J.M., Qin, Z., Wren, J.C., and Shoesmith, D.W. (2006). The influence of peroxidation on the corrosion of copper nuclear waste canister in aqueous anoxic sulphide solutions. *MRS Online Proceedings Library* 985, 811.

Soroka, I., Chae, N., and Jonsson, M. (2021). On the mechanism of γ-radiation-induced corrosion of copper in water. *Corros. Sci.* 182, 109279. doi:10.1016/j.corsci.2021.109279

Sova, A., Doubenskaia, M., Grigoriev, S., Okunkova, A., and Smurov, I. (2013a). Parameters of the Gas-Powder Supersonic Jet in Cold Spraying Using a Mask. *J. Therm. Spray Technol.* 22, 551–556. doi:10.1007/s11666-013-9891-1

Sova, A., Klinkov, S., Kosarev, V., Ryashin, N., and Smurov, I. (2013b). Preliminary study on deposition of aluminium and copper powders by cold spray micronozzle using helium. *Surf. Coat. Technol.* 220, 98–101. doi:10.1016/j.surfcoat.2012.09.036

Sova, A., Okunkova, A., Grigoryev, S., and Smurov, I. (2013c). Velocity of the particles accelerated by a cold spray micronozzle: Experimental measurements and numerical simulation. *J. Therm. Spray Technol.* 22, 75–80. doi:10.1007/s11666-012-9846-y

Stroes-Gascoyne, S. (2010). Microbial occurrence in bentonite-based buffer, backfill and sealing materials from large-scale experiments at AECL's Underground Research Laboratory. *Appl. Clay Sci.* 47, 36–42. doi:10.1016/j.clay.2008.07.022

Stroes-Gascoyne, S., Hamon, C.J., Vilks, P., and Gierszewski, P. (2002). Microbial, redox, and organic characteristics of compacted clay-based buffer after 6.5 years of burial at AECL"s Underground Research Laboratory. *Appl. Geochem.* 17, 1287–1303. doi:10.1016/s0883-2927(02)00020-3

Stroes-Gascoyne, S., Hamon, C.J., Dixon, D.A., Kohle, C.L., and Maak, P. (2007). The Effects of Dry Density and Porewater Salinity on the Physical and Microbiological Characteristics of Compacted 100% Bentonite. *MRS Online Proceedings Library* 985, 1302. doi:10.1557/PROC-985-0985-NN13-02

Stroes-Gascoyne, S., Hamon, C.J., and Maak, P. (2011). Limits to the use of highly compacted bentonite as a deterrent for microbiologically influenced corrosion in a nuclear fuel waste repository. *Phys. Chem. Earth, Parts A/B/C* 36, 1630–1638. doi:10.1016/j.pce.2011.07.085

Stroes-Gascoyne, S., Hamon, C.J., Maak, P., and Russell, S. (2010). The effects of the physical properties of highly compacted smectitic clay (bentonite) on the culturability of indigenous microorganisms. *Appl. Clay Sci.* 47, 155–162. doi:10.1016/j.clay.2008.06.010

Stroes-Gascoyne, S., Lucht, L.M., Borsa, J., Delaney, T.L., Haveman, S.A., and Hamon, C.J. (1995). Radiation Resistance of the Natural Microbial Population in Buffer Materials. *MRS Online Proceedings Library Archive* 353, 345–352. doi:10.1557/PROC-353-345

Sudharshan Phani, P., Vishnukanthan, V., and Sundararajan, G. (2007). Effect of heat treatment on properties of cold sprayed nanocrystalline copper alumina coatings. *Acta Mater* 55, 4741–4751. doi:10.1016/j.actamat.2007.04.044

Svensson, D., Sandén, T., Olsson, S., Dueck, A., Eriksson, S., Jägerwall, S., and Hansen, S. (2011). *Alternative buffer material Status of the ongoing laboratory investigation of reference materials and test package 1. SKB TR-11-06: 146*. Stockholm, Sweden: Svensk Kärnbränslehantering AB.

Takase, H. (2004). "Discussion on PA model development for bentonite barriers affected by chemical interaction with concrete: do we have enough evidence to support bentonite stability?," in *International Workshop on Bentonite-Cement Interaction in Repository Environments*. Tokyo, Japan, NUMO-TR 04-05, A3-172 – A3-177; Posiva Report 2004-25: 192.

Taniguchi, N. (2003). "Effect of magnetite as a corrosion product on the corrosion of carbon steel overpack," in *Prediction of Long-Term Corrosion Behaviour in Nuclear Waste Systems* (European Federation of Corrosion), 424–438.

Taxén, C. (2003). Atmospheric corrosion of copper 450 metres underground. Results from three years exposure in the Äspö HRL. *MRS Online Proceedings Library* 807, 423–617. doi:10.1557/proc-807-423

Tay, B.K., Zhao, Z.W., and Chua, D.H.C. (2006). Review of metal oxide films deposited by filtered cathodic vacuum arc technique. *Mater. Sci. Eng.:R.:Rep.* 52, 1–48. doi:10.1016/j.mser.2006.04.003

Terlain, A., Desgranges, C., Gauvain, D., Feron, D., Galtayries, A., and Marcus, P. (2001). *Oxidation of materials for nuclear waste containers under long term conditions, Corrosion/2001*. Houston, TX: NACE International. Paper 01119.

Theodorakopoulos, N., Février, L., Barakat, M., Ortet, P., Christen, R., Piette, L., Levchuk, S., Beaugelin-Seiller, K., Sergeant, C., Berthomieu, C., and Chapon, V. (2017). Soil prokaryotic communities in Chernobyl waste disposal trench T22 are modulated by organic matter and radionuclide contamination. *EMS Microbiol. Ecol.* 93, fix079. doi:10.1093/femsec/fix079

Tournassat, C., Steefel, C.I., Bourg, I.C., and Bergaya, F. (2015). Natural and Engineered Clay Barriers. *Develop. Clay Sci.* 6, 432.

Triantou, K.I., Pantelis, D.I., Guipont, V., and Jeandin, M. (2015). Microstructure and tribological behavior of copper and composite copper+alumina cold sprayed coatings for various alumina contents. *Wear* 336-337, 96–107. doi:10.1016/j.wear.2015.05.003

Trinchero, P., Molinero, J., Román-Ross, G., Berglund, S., and Selroos, J.O. (2014). FASTREACT–An efficient numerical framework for the solution of reactive transport problems. *Appl. Geochem.* 49, 159–167. doi:10.1016/j.apgeochem.2014.04.004

Truche, L., Berger, G., Destrigneville, C., Pages, A., Guillaume, D., Giffaut, E., and Jacquot, E. (2009). Experimental reduction of aqueous sulphate by hydrogen under hydrothermal conditions: Implication for the nuclear waste storage. *Geochim. Cosmochim. Acta* 73, 4824–4835. doi:10.1016/j.gca.2009.05.043

Truche, L., Berger, G., Destrigneville, C., Guillaume, D., and Giffaut, E. (2010). Kinetics of pyrite to pyrrhotite reduction by hydrogen in calcite buffered solutions between 90 and 180°C: Implications for nuclear waste disposal. *Geochim. Cosmochim. Acta* 74, 2894–2914. doi:10.1016/j.gca.2010.02.027

Truche, L., Jodin-Caumon, M.C., Lerouge, C., Berger, G., Mosser-Ruck, R., Giffaut, E., and Michau, N. (2013). Sulphide mineral reactions in clay-rich rock induced by high hydrogen pressure. Application to disturbed or natural settings up to 250 °C and 30 bar. *Chem. Geol.* 351, 217–228. doi:10.1016/j.chemgeo.2013.05.025

Turnbull, A. (2009). *A Review of the Possible Effects of Hydrogen on Lifetime of Carbon Steel Nuclear Waste Canisters*. Wettingen, Switzerland: Nagra. Technical Report 09-04.

Vachon, M.A., Engel, K., Beaver, R. C., Slater, G. F., Binns, W. J., and Neufeld, J. D. (2021). Fifteen shades of clay: distinct microbial community profiles obtained from bentonite samples by cultivation and direct nucleic acid extraction. *Sci. Rep.* 11, 22349. doi:10.1038/s41598-021-01072-1

Van Gerwen, S.J.C., Rombouts, F M., Van´t Riet, K., and Zwietering, M.H. (1999). A Data analysis of the irradiation parameter D10 for bacteria and spores under various conditions. *J. Food Prot.* 62, 1024–1032. doi:10.4315/0362-028x-62.9.1024

Van Loon, L.R., Glaus, M.A., and Müller, W. (2007). Anion exclusion effects in compacted bentonites: towards a better understanding of anion diffusion. *Appl. Geochem.* 22, 2536–2552. doi:10.1016/j.apgeochem.2007.07.008

Vandenborre, J., Crumière, F., Blain, G., Essehli, R., Humbert, B., and Fattahi, M. (2013). Alpha Localized Radiolysis and Corrosion Mechanisms at the Iron/Water Interface: Role of Molecular Species. *J. Nucl. Mater.* 433, 124–31. doi:10.1016/j.jnucmat.2012.09.034

Venzlaff, H., Enning, D., Srinivasan, J., Mayrhofer, K. J., Hassel, A. W., Widdel, F., et al. (2013). Accelerated cathodic reaction in microbial corrosion of iron due to direct electron uptake by sulfate-reducing bacteria. *Corros. Sci.* 66, 88–96. doi:10.1016/j.corsci.2012.09.006

Villar, M. V., and Gómez-Espina, R. (2009). *Report on Thermo-Hydro-Mechanical Laboratory Tests Performed by CIEMAT on Febex Bentonite 2004-2008*. Madrid, Spain: CIEMAT Technical Report 1178.

Villar, M.V., and Lloret, A. (2008). Influence of dry density and water content on the swelling of a compacted bentonite. *Appl. Clay Sci.* 39, 38–49. doi:10.1016/j.clay.2007.04.007

Villar, M.V., Fernández, A.M., Romero, E, Dueck, A., Cuevas, J., Plötze, M., Kaufhold, S., Dohrmann, R., Iglesias, R., Sakaki, T., Voltolini, M., Zheng, L., Kawamoto, K., and Kober, F. (2017). *FEBEX-DP: Post-mortem THM/THC Report. Analysis of Results*. Nagra Working Report NAB 16-017: 147.

Villar, M.V., Armand, G., Conil, N., de Lesquen, Ch., Herold, Ph., Simo, E., Mayor, J.C., Dizier, A., Li, X., Chen, G., Leupin, O., Niskanen, M., Bailey, M., Thompson, S., Svensson, D., Sellin, P., and Hausmannova, L. (2020). *D7.1 HITEC. Initial State-of-the-Art on THM behaviour of i Buffer clay materials and of ii Host clay materials. Deliverable D7.1 HITEC. EURAD Project*. Horizon 2020 No 847593: 214.

Wada, Yoichi, Tachibana, Masahiko, Watanabe, Atsushi, Ishida, Kazushige, Ota, Nobuyuki, Shigenaka, Naoto, Inagaki, Hiromitsu, and Noda, Hiroshi (2016). Effects of seawater components on radiolysis of water at elevated temperature and subsequent integrity of fuel materials. *Journal of Nuclear Science and Technology (Tokyo)* 53 (6), 809–820. doi:10.1080/00223131.2015.1074876

Wang, Y., Normand, B., Mary, N., Yu, M., and Liao, H. (2014). Microstructure and corrosion behavior of cold sprayed SiCp/Al 5056 composite coatings. *Surf. Coat. Technol.* 251, 264–275. doi:10.1016/j.surfcoat.2014.04.036

Wang, L., Fan, S., Sun, H., Ji, B., Zheng, B., Deng, J., Zhang, L., and Cheng, L. (2020). Pressure-less joining of SiC_f/SiC composites by Y_2O_3–Al_2O_3–SiO_2 glass: Microstructure and properties. *Ceramics International* 46, 27046–27056. doi:10.1016/j.ceramint.2020.07.181

Weetjens, E., Marivoet, J., and Govaerts, J. (2012). *Conceptual model description of the reference case, External Report SCK●CEN-ER-215*. Niras/Ondraf.

Wersin, P., Spahiu, K., and Bruno, J. (1994). *Time evolution of dissolved oxygen and redox conditions in a HLW repository*. Sweden: SKB. TR 94-02.

Wersin, P. (2003). Geochemical modelling of bentonite porewater in high-level waste repositories. *J. Contam. Hydrol.* 61, 405–422. doi:10.1016/s0169-7722(02)00119-5

Wersin, P., Curti, E., and Appelo, C.A.J. (2004). Modelling bentonite–water interactions at high solid/liquid ratios: swelling and diffuse double layer effects. *Appl. Clay Sci.* 26, 249–257. doi:10.1016/j.clay.2003.12.010

Wersin, P., Birgersson, M., Olsson, S., Karnland, O., and Snellman, M. (2008a). "Impact of corrosion-derived iron on the bentonite buffer within the KBS-3H disposal concept," in *The Olkiluoto site as case study. – SKB report R-08-34* (Svensk Kärnbränslehantering AB).

Wersin, P., Birgersson, M., Olsson, S., Karnland, O., and Snellman, M. (2008b). *Impact of corrosion-derived iron on the bentonite buffer within the KBS-3H disposal concept: the Olkiluoto site as case study, SKB Report R-08-34*. Stockholm, Sweden: Swedish Nuclear Fuel and Waste Management Company.

Wersin, P., Alt-Epping, P., Pitkänen, P., and Román-Ross, G. (2014). *Sulphide Fluxes and Concentrations in the Spent Nuclear Fuel Repository at Olkiluoto*. Finland: Posiva Oy. Posiva 2014-01.

Wersin, P., Alt-Epping, P., Pekala, M., Pitkänen, P., and Snellman, M. (2017). Modelling sulfide fluxes and Cu canister corrosion rates in the engineered barrier system of a spent fuel repository. *Procedia earth and planetary science* 17, 722–725. doi:10.1016/j.proeps.2016.12.183

Wersin, P., Hadi, J., Jenni, A., Svensson, D., Grenèche, J.-M., Sellin, P., and Leupin, O.X. (2021). Interaction of Corroding Iron with Eight Bentonites in the Alternative Buffer Materials Field Experiment (ABM2). *Minerals* 11, 907. doi:10.3390/min11080907

Westerman, R.E., Nelson, J.L., Pitman, S.G., Kuhn, W.L., Basham, S.J., and Moak, D.P. (1983). Evaluation of Iron-Base Materials for Waste Package Containers in a Salt Repository. *MRS Proceedings* 26, 427. doi:10.1557/PROC-26-427

Wilfinger, K. (1994). *Ceramic Package Fabrication for YMP Nuclear Waste Disposal*. California, US: Lawrence Livermore National Laboratory. Report UCRL-ID-118660.

Wilson, J., Cressey, G., Cressey, B., Cuadros, J., Ragnarsdottir, K.V., Savage, D., and Shibata, M. (2006a). The effect of iron on montmorillonite stability. (II) Experimental investigation. *Geochimica et Cosmochimica Acta* 70, 323–336. doi:10.1016/j.gca.2005.09.023

Wilson, J., Savage, D., Cuadros, J., Shibata, M., and Ragnarsdottir, K.V. (2006b). The effect of iron on montmorillonite stability. (I) Background and thermodynamic considerations. *Geochim. Cosmochim. Acta* 70, 306–322. doi:10.1016/j.gca.2005.10.003

Wilson, J., Savage, D., Bond, A., Watson, S., Pusch, R., and Bennett, D. (2011). Bentonite. A Review of key properties, processes and issues for consideration in the UK context. *Quintesa report QRS-1378ZG-1*, 137.

Wilson, J., Benbow, S., Sasamoto, H., Savage, D., and Watson, C. (2015). Thermodynamic and fully-coupled reactive transport models of a steel–bentonite interface. *Applied Geochemistry* 61, 10–28. doi:10.1016/j.apgeochem.2015.05.005

Winsley, R.J., Smart, N.R., Rance, A.P., Fennell, P.A.H., Reddy, B., and Kursten, B. (2011). Further Studies on the Effect of Irradiation on the Corrosion of Carbon Steel in

Alkaline Media. *Corros. Eng. Sci. Technol.* 46, 111–16. doi:10.1179/1743278210Y.0000000010

Wolfaardt, G.M., and Korber, D.R. (2012). *Near-field microbiological considerations relevant to a deep geological repository for used nuclear fuel - State of science review*. Toronto: Nuclear Waste Management Organization.

Wötting, G., and Martin, W. (2007). "Large sized, complex shaped sintered silicon carbide components with excellent mechanical properties," in *Proceedings of the 10th ECerS Conference, Baden-Baden*, 1067–1070.

Xiong, Y., Wang, Y., Roselle, G., and Kim, S. (2021). Lead/lead-alloy as a corrosion-resistant outer layer packaging material for high level nuclear waste disposal. *Nucl. Eng. Des.* 380, 111294. doi:10.1016/j.nucengdes.2021.111294

Yang, Q., Toijer, E., and Olsson, P. (2019). *Analysis of radiation damage in the KBS-3 canister materials*. Svensk Kärnbränslehantering AB. SKB TR-19-14.

Yin, S., Xie, Y., Cizek, J., Ekoi, E. J., Hussain, T., Dowling, D. P., et al. (2017). Advanced diamond-reinforced metal matrix composites via cold spray: properties and deposition mechanism. *Compos. B. Eng.* 113, 44–54. doi:10.1016/j.compositesb.2017.01.009

Yunker, W.H. (1990). *Corrosion behavior of copper-base materials in a gamma-irradiated environment*. Richland, Washington: Westinghouse Hanford Company. Report WHC-EP-0188.

Yunker, W. H., and Glass, R. S., 1986. Long-term corrosion behavior of copper-base materials in a gamma irradiated environment. In *Scientific basis for nuclear waste management X: symposium held in Boston, Massachusetts, USA, 1–4 December 1986*. J K. Bates and W B. Seefeldt (eds). Materials Research Society: Pittsburgh, PA, 579–590. doi:10.1557/proc-84-579

Zhang, H., and Datta, A.K. (2003). Microwave Power Absorption in Single - and Multiple - Item Foods. *Food Bioprod. Process.* 81, 257–265. doi:10.1205/096030803322438027

Zheng, L., Samper, J., Montenegro, L., and Fernández, A.M. (2011). A coupled THMC model of a heating and hydration laboratory experiment in unsaturated compacted FEBEX bentonite. *J. Hydrol.* 386, 80–94. doi:10.1016/j.jhydrol.2010.03.009

Zheng, L., Rutqvist, J., Birkholzer, J.T., and Liu, H.H. (2015). On the impact of temperatures up to 200 °C in clay repositories with bentonite engineer barrier systems: A study with coupled thermal, hydrological, chemical, and mechanical modeling. *Eng. Geol.* 197, 278–295. doi:10.1016/j.enggeo.2015.08.026

Zheng, L., Xu, H., Ruqvist, J., Reagan, M., Birkholzer, J., Villar, M.V., and Fernández, A.M. (2020). The hydration of bentonite buffer material revealed by modeling analysis of a long-term *in situ* test. *Appl. Clay Sci.* 185, 105360. doi:10.1016/j.clay.2019.105360

Zhou, H. (2012). Titanium and Titanium alloy Coatings for Corrosion Protection. *Proceedings of the 12th World Conference on Titanium* 3, 1906–1910.

Zhujing, Y., Changqing, L., Li, Y., and Weitao, W. (1991). Corrosion performance of ion-plated titanium and yttrium modified TiN coatings. *Surface and Coatings Technology* 46, 307–315. doi:10.1016/0257-8972(91)90173-t

Zymelka, D (2013). *Suivi par méthode optique du frittage micro-ondes d''oxydes céramiques. École Nationale Supérieure des Mines de Saint-Etienne*. PhD Thesis.